Ph.D. dissertation

Modeling and Control for Representation of Pseudo Force Sensation Using Functional Electrical Stimulation

(機能的電気刺激を用いた疑似力覚呈示のためのモデル化と制御)

March 2021

Course in Mathematics, Electronics, and Informatics,
Programs in Science and Engineering,
Graduate School of Science and Engineering,

Saitama University

Supervised by Dr. Yasuyoshi Kaneko

Dr. Sho Sakaino

Tomoya Kitamura

Contents

Chapter 1 Introduction

1.1 Background

1.1.1 Touch Sense Presentation Technology

Humans perceive the outside world using the five senses: sight, hearing, smell, taste, and touch senses. These senses' information can be communicated, and humans can perceive information at a distant location as if they were in the same place. In particular, information technologies related to vision and hearing have been established from the 19th century, as represented by TV and telephone. These technologies have eliminated the notion of distance from people, allowing them to feel closer to distant persons and objects.

On the other hand, touch sense communication technology has not yet become widespread in our daily lives. Touch sensations can be divided into force, pressure, heat, and pain. Prattichizzo *et al.* and Pacchierotti *et al.* demonstrated the pressure sensation by tilting a plate placed on a fingertip[1], [2]. Osawa *et al.* used a Peltier device to present the heat sensation[3]. Mizuhara *et al.* used mechanical and electrical stimulation to present natural pain sensation[4]. These devices can be made wearable, and as their accuracy improves, these devices are expected to become more prevalent in our daily lives.

However, there has been no progress in making wearable force sensation presentation devices. "Force senssation" here refers to the sensation that a person feels through deep receptors inside the body, such as muscle spindles, tendons, and joints, and refers to the weight and reaction force from contacting objects. Although this sensation is also called a "deep sensation" , it is referred to as force sensation in this dissertation.

1.1.2 Force Sense Presentation Technology

In this dissertation, the force sensation presentation technology is the focus. Prattichizzo *et al.* showed that presenting force and pressure sensations reduced a remotely controlled robot's working time in a peg-in-hole task[1]. In addition, Ramsamy *et al.* reported that force-presentation techniques improved the immersion in VR space[5]. Therefore, transmitting the force sensation will increase the sense of realism in communication with remote locations and improve the workability and safety of the work.

One of the force presentation techniques is bilateral control[6]–[10]. Fig. 1.1 presents a schematic diagram for bilateral control. Bilateral control is a type of master-slave system to transmit the

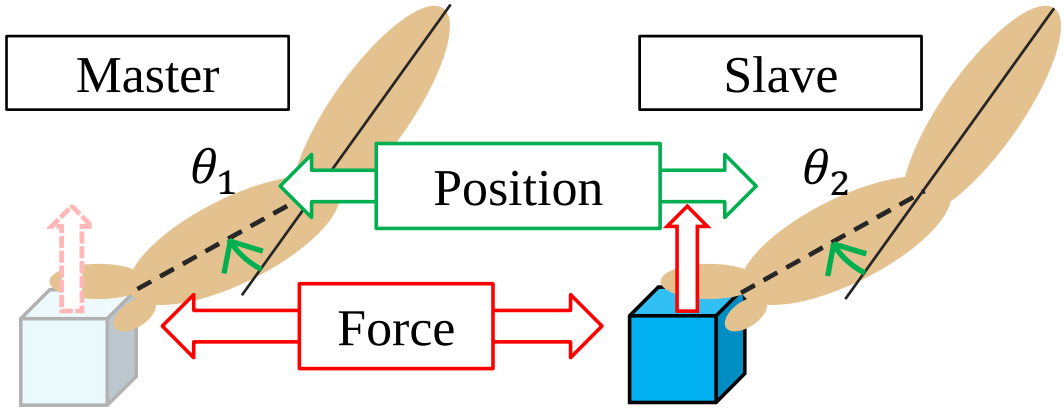

Fig. 1.1 Conceptual diagram of bilateral control

force sense. Bilateral control is expected to be useful in the medical field[8], at disaster sites[9], and in space[10]. However, these studies' force presentation devices can only be used for specific tasks because the devices are tailored to the task. Besides, wearing the device increases the user's discomfort, and the device is too large to be used daily.

On the other hand, Tanabe *et al.* proposed that a pseudo-force sensation could be presented using a vibrating speaker[11]. Honda *et al.* showed that vibration stimulation of muscles could present pseudo-force sense to humans[12]. In conventional research, the approach that reproduces the human brain's perception, rather than faithfully reproducing the presented stimulus, is called "pseudo"[13]. This paper uses the term "pseudo force" because the method mentioned above [11], [12] does not stimulate sensory receptors by applying force to the body.

Functional Electrical Stimulation (FES) is a method of presenting a sense of force to a human. In FES, only small electrode pads are on the human, therefore, freeing the human from a sense of restraint. Also, the stimulator can be small, which prevents the equipment from becoming too large. In FES, an external device does not reproduce the force generated but instead presents force internally, so this dissertation defines the presentation of force sensation by FES as "pseudo force".

Besides, several studies have shown that FES can be used to transmit pseudo-force sensations to humans[14]–[19]. In particular, Lopes *et al.* proposed a system that uses FES to transmit pseudo-force sensations in VR space[14]. In the results, the participants reported that they felt the reaction force more clearly with the electrical stimulation, and this result was statistically superior.

Therefore, by constructing a bilateral control system using FES, a new pseudo-force transmission system can be realized that overcomes conventional bilateral control problems.

However, in some conventional methods[18], [19], the performance of force sensation presentation

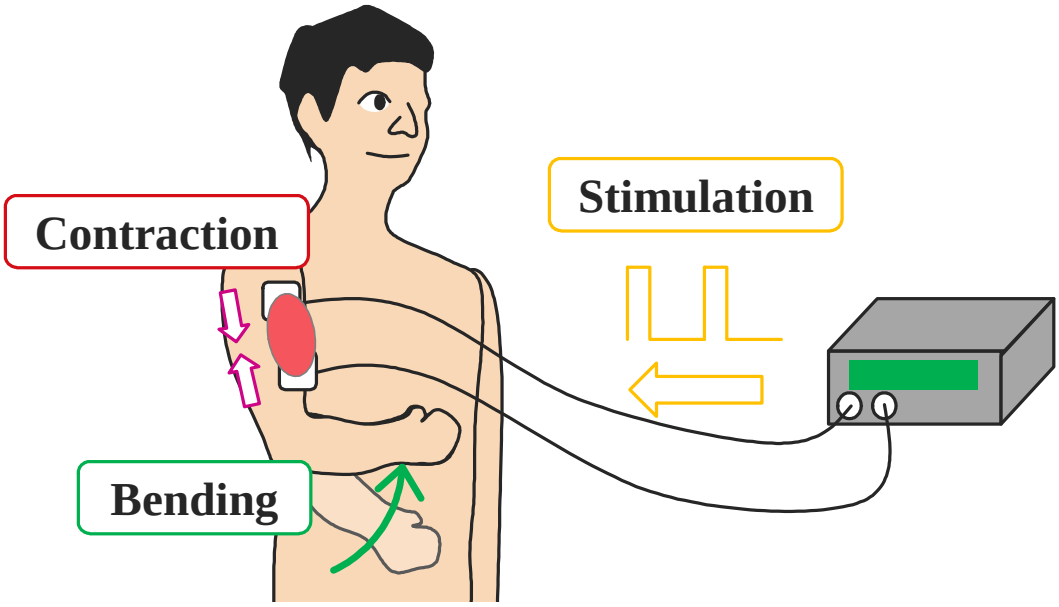

Fig. 1.2 Conceptual diagram of FES

using FES has been verified while the person is stationary. Therefore, the performance of presentation during voluntary movement has not been verified. Besides, in the study of presenting force sensation by FES during voluntary movement[14]–[17], the control system to reproduce the force sensation has not been constructed.

1.1.3 FES

Fig. 1.2 presents a schematic diagram for FES. FES is a method to drive a joint and display force by inducing muscle contraction by stimulating muscles with pulse current.

FES has been studied since the 1960s for rehabilitation[20], [21]. The FES has already been used to help paralyzed patients to walk, to grasp a cup [22]–[24]. Tamaki *et al.* used the FES for healthy people applications and showed that 24 small pads attached to the forearm of the FES improved Japanese harp performance during experiments[25]. Kurosawa *et al.* showed that feedback error learning controller could improve the accuracy and decrease the dead time [26].

However, the control performance using FES is poor; therefore, clear force sensation presentation is difficult. One of the reasons is the nonlinearity of the body's dynamic characteristics. The dynamic characteristic is the relationship between the stimulus amount and the exerted force (torque). In FES, the dynamic characteristics are represented by a nonlinear function. Besides, the difficulty of control increases because the system includes dead time.

Therefore, estimation of dynamic characteristics and good angular control performance are necessary

to improve the force sensing presentation performance when using FES. Then, if a good force sensation presentation technology using FES can be constructed, a force sensation transmission system that overcomes the conventional shortcomings can be achieved using bilateral control.

1.2 Purpose of This Dissertation

The purpose of this dissertation is to improve the performance of a pseudo-force presentation system using FES based on modeling and control performance improvement methods. Therefore, the following issues are discussed in this dissertation.

The first is the modeling of dynamic properties. There are two methods for modeling dynamic properties in the FES: using chemical reaction equations and muscle potential, but it is difficult to create an inverse model. Therefore, I should discuss a simple modeling method that can create an inverse model.

The second is the improvement of angle control performance. In building bilateral control systems, angular control is generally necessary. Although angular control and force control are generally used for force presentation to the master, some reports use only force control. However, synchronization of the slave with the master's motion is basically achieved by the angular control. In the angular control methods using FES, time-varying control systems using neural networks, fuzzy control, and adaptive control have shown excellent control performance. However, these methods are computationally intensive and require large computers. It is not desirable for a force presentation system using FES to lead to colossal equipment size. Therefore, a discussion on a less computationally intensive and robust control system is needed.

The third is the multi-degrees-of-freedom (multi-DOFs) joint control technique. Most of the tasks that people perform are those that use multiple joints. Therefore, it is necessary to control multiple joints when we perform force presentation. The electrical interference in the multi-DOFs joint control technique using FES is discussed. In addition. methods to generate motion patterns by stimulating multiple electrodes and methods to generate desired motions using the principle of superposition are reported. However, mechanical interferences such as inertial forces and coupled oscillations should also be discussed.

Finally, I validate a bilateral control system that integrates the methods to solve the problems mentioned above and confirm that a pseudo-force presentation system using FES is improved. Finally, the bilateral control system using FES that integrates methods to solve the above problems was validated, and confirm that a pseudo-force presentation system using FES is improved.

Conventional researches for each issue are described in each section.

1.3 Construction of This Dissertation

The structure of this dissertation is shown in Fig. 1.3. Some of the content has already been published by the author in his master's thesis. However, as the content is relevant to this thesis, it is included in this dissertation.

Chapter 2 discusses the modeling of the body's dynamic characteristic when using FES. Modeling the dynamic characteristic is an essential point in the aspects of position and force control. In this dissertation, a model is attempted by measuring the frequency characteristics using the Fourier transform. The results show that the relationship between the stimulus current and the exerted force can be approximated by a first-order lag system that includes the dead time.

Chapter 3 discusses the body's angle control using FES; the degradation of control performance due to the delay time has been a problem in angle control using FES. Therefore, this dissertation discusses a method using Smith compensator and sliding mode control using amplitude-frequency modulation. It is shown that the method using Smith compensator improves angular tracking. However, the master's autonomous motion in bilateral control and the slave's contact motion are considered disturbances in control. Smith compensator has been shown to have degraded control performance for systems that are participant to disturbances. Therefore, the control performance was degraded in experiments with bilateral control. Sliding mode control using amplitude-frequency modulation was found to suppress chattering, which is a high-frequency vibration. The proposed method's converge at the origin in the sliding surface, while oscillations of the conventional method occurs near the origin.

Chapter 4 discusses multi-DOFs control using FES. Most of the motions performed by humans are multi-DOFs motions. Therefore, controlling multiple joints in conjunction with each other is a necessary condition for FES-based applications. The first is two joint control of the shoulder and elbow joints. It has been shown that frequency modulation can improve control performance when controlling the shoulder joint. The results showed that the control performance was improved when controlling the shoulder joint by modulating the frequency according to the participant and the stimulation location. Secondly, a two-joint control of the elbow and wrist joints was used; the problem with the simple system of angular control was that the inertial forces generated by the elbow joint's motion deteriorated the control performance of the wrist joint. Therefore, in this dissertation, a control system is proposed that uses antagonistic muscle stimulation to strengthen the wrist joint's stiffness to suppress the disturbance generated by the elbow joint. These results are also discussed in Chapter

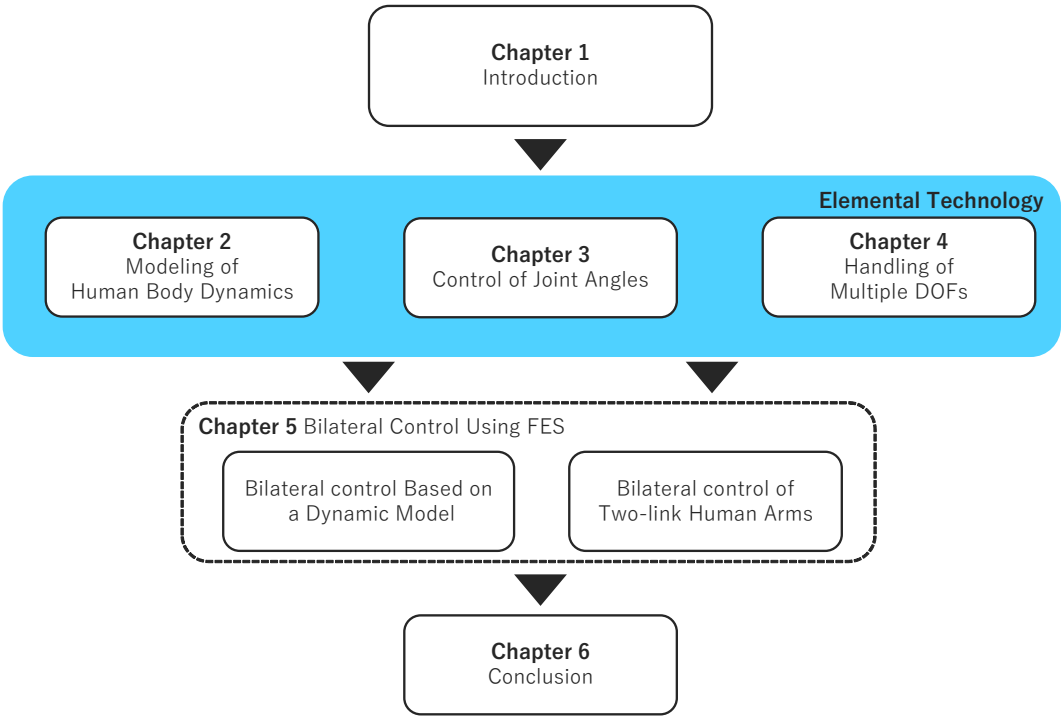

Fig. 1.3 Chapters constructed in this dissertation.

5.

Chapter 5 discusses bilateral control using FES. Firstly, the two-joint bilateral control of the elbow and wrist joints. It is shown that the method above using antagonistic muscle stimulation improves control performance and enables bilateral control with multi-DOFs. Secondly, the method using a dynamic model of 4ch bilateral control was validated. 4ch bilateral control is a type of bilateral control system. The control goal is to achieve both synchronization of position and the action-reaction of force. The results showed that approximating with a dynamic model improves the reaction force estimation's performance. Secondly, it was shown that the proposed method is most viable for the control goals of general bilateral control: position synchronization and force action-reaction.

Finally, this dissertation is concluded in Chapter 6.

Chapter 2 Modeling of Human Body Dynamics

In this chapter, the description of the modeling of the FES dynamic characteristics is described. The relationship between the input variables and the output torque is hereinafter referred to as the *model*. In using FES control, the model uncertainly is a factor that causes control performance degradation. Then, position control and force control become easier to construct when the model is identified.

2.1 Background

The representative model for the formulation of muscle characteristics is the Hill-type model [27], which can be described using two differential equations according to Zajac *et al.* [28], [29]. Several studies applying this model to the FES dynamic characteristic modeling have already been published. Ding *et al.* examined a mathematical model that describes the dynamic characteristics under conditions in which fatigue occurs [30]–[32]. By adding the transition of calcium troponin in the formula, Ding *et al.* considered the effect of fatigue during electrical stimulation. In addition, Hmed *et al.* showed that the muscle strength can be estimated at different stimulus strengths by adding an expression for the current intensity [33], [34]. Berniker *et al.* proposed modeling based on the probability theory for the uncertainty of electrical command and muscle output when using FES [35], [36]. Good results were obtained in experiments to estimate the exerted force by mouse using electrical stimulation. At the time of identification using FES, the force-induced damping occurs because of the noise caused by voluntary contraction or muscle fatigue. Therefore, the method of selecting the value with the highest probability possibility is effective.

Li *et al.* showed that the modeling of the target muscle and the exercise torque can be performed using evoked electromyogram (eEMG) [37], [38]. A random voltage was input in their first modeling step. After which, the eEMG and the current torque were measured. In the second step, the relationship between the eEMG and the exerted torque was estimated using the nonlinear autoregressive exogenous (NARX) model [37] or the recurrent NN (RNN)-NARX [38] model. This method obtained an error of approximately 10% and a good torque estimation. The study did not touch upon the relationship between the value of the stimulus and the eEMG; however, its estimation may influence the improvement of the control performance. The participants used in the study were both healthy and non-healthy volunteers, but no difference was found in the results for the two groups.

Ferrarin *et al.* modeled the dynamic characteristics based on the equation of motion [39] by using

the moment of inertia, as well as the length and weight of the lower limbs. The authors initially determined the rigidity and the viscosity of the limbs by performing a pendulum experiment. The relationship between the voltage and the torque were derived once the electrical stimuli were applied. Yassin *et al.* used the NARX model [40] and the cascade forward neural network (CFNN)-NARX model [41] to estimate the muscle activity characteristics. The NARX model allows for the rough forces and fine errors to be estimated by using an NN.

2.2 Issue

As described in Chapter 2, a simple design is preferred for systems using FES. The reason is that the device should be small for use in daily life. Besides, in using EMG methods, the number of electrodes required increases, which reduces convenience for the user and gives a sense of restraint.

Therefore, this chapter discusses the estimation of dynamic characteristics using the Fourier-transform-based frequency characteristic estimation method. If this method can correctly estimate the dynamic characteristics, it is expected to realize a computationally inexpensive system and does not require large equipment.

2.3 Estimation of Relationship between Stimulation Current and Force Exerted during Isometric Contraction

In this section, the relationship between stimulus value and exerted force is examined. Firstly, the relationship between applied voltage and inflow current is investigated. Secondly, it is confirmed that the force determined by the inflow current value. Thirdly, the inflow current is gradually increased, and the threshold current to drive the joint is measured. Next, the transfer function of the current and force are estimated using the transfer function estimation method with fast Fourier transform (FFT). As a result, the relationship between current and force can be represented by a first-order lag system with dead time was confirmed. Finally, parameters are fitted by multiple regression analysis, and the proposed model is validated.

2.3.1 FES

In this section, the basic FES stimulation method in this dissertation is described. FES is a technique that induces muscle contraction and drives joints by applying electrical stimulation to muscles.

The stimulus position and stimulus waveform for controlling the elbow joint in this section have been followed in the experiments in the other chapters and sections.

Here, how to control a human's elbow joint is described. To begin, the participants' biceps brachii

muscle and the triceps brachii muscle were stimulated. When the biceps brachii muscle is stimulated, the elbow joint flexes. Moreover, when the triceps brachii muscle is stimulated, the elbow joint extends. Fig. 2.1 indicates the location of the pads.

[1]Triceps brachii muscle (Extensor muscle)

[2]Biceps brachii muscle (Flexor muscle)

Fig. 2.1 Stimulus location

In these experiment, a pulse wave was used because it is most frequently used conventionally. The stimulating parameters were a pulse width of 0.2 ms and a frequency of 50 Hz. The stimulation waveform is shown in Fig. 2.2. In this dissertation, control was performed by adjusting the voltage amplitude with the maximum set to 40 V. The circuit was configured to conform to the Japanese Industrial Standard (JIS). Therefore, the current flowing through the human body did not exceed 20 mA.

2.3.2 Methods

2.3.2.1 Estimation of Transfer Function using FFT

In this section, a transfer function estimation method using FFT is described. The Fourier transform is expressed by the following equation:

$$U(f) = \int_{-\infty}^{\infty} u(t)e^{-jft}dt, \tag{1}$$

where $u(t)$ represents the time domain, and $U(f)$ represents the frequency domain. Discrete Fourier Transform (DFT) and FFT are generally used for Fourier transformation; in this dissertation, FFT, which can shorten calculation time, was adopted. The transfer function $H(f)$ represents the relation-

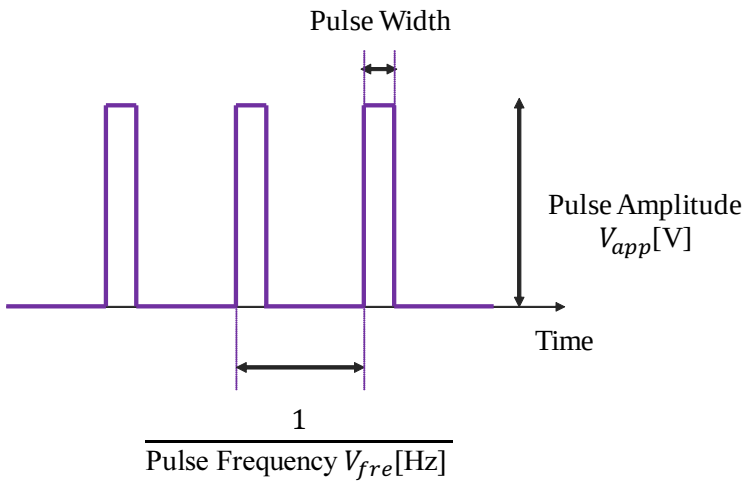

Fig. 2.2 Outline of stimulation the pulse and variable parameters

ship between the input $X(f)$ and the output $Y(f)$. In the frequency domain,

$$H(f) = \frac{Y(f)}{X(f)}. \tag{2}$$

However, noise is included in the actual measurement. Therefore, we rewrite (2) as follows:

$$H(f) = \frac{Y(f) \cdot X(f)^*}{X(f) \cdot X(f)^*}, \tag{3}$$

where the superscript $*$ represents the complex conjugate of the complex spectrum obtained using the Fourier transform. The denominator in (3) is called the auto power spectrum, and the numerator is called the cross spectrum. By using (3), the influence of noise on the output side can be reduced. By confirming the gain margin and the phase margin of the obtained $H(f)$, it is possible to estimate the transfer function.

2.3.3 Experimental Methods and Results

In this section, the procedures and the results of the experiment for modeling the current and the exerted force are described sequentially. Two healthy participants (referred to as A and B) were used to test the proposed system. In this dissertation, I will henceforth refer to the participants by the letters beginning with A. These participants may not be the same person in common. This rule is because the data were anonymized at the time of data collection, making it difficult to link them together. In addition, assigning a new number to a participant could seriously compromise the readability of this dissertation. Therefore, in other experiments, I will call the participants starting with A. Informed consent was obtained from the participants, and the study was approved by Ethics

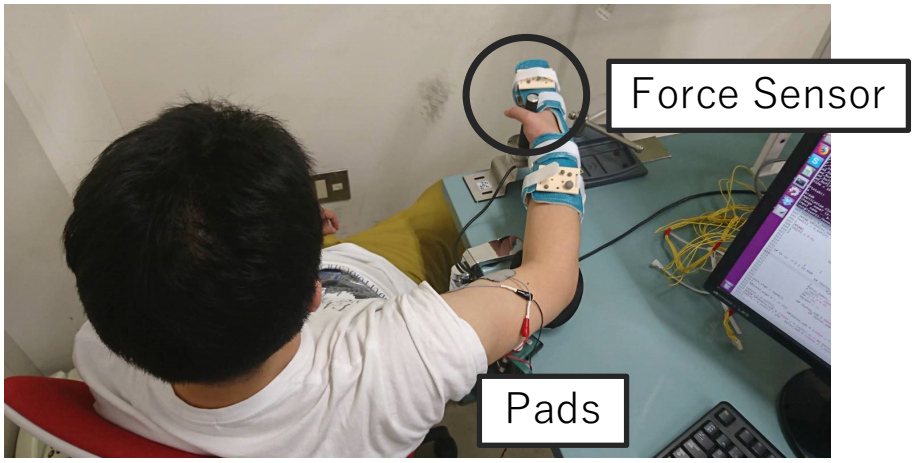

Fig. 2.3 Scene of Experiment

Committee of Saitama University. The experimental setup is indicated in Fig. 2.3. Participants sat on the chair so that their arms were level with the floor. The hands of the participants are fixed with Gibbs. Therefore, the wrist joint cannot exert a force. The participants were made to allow the hands to hit the force sensor. The force sensor was used by PFS055YA251U6 ("Leptrino, Japan").

2.3.3.1 Relationship between Applied Voltage and Inflow Current

In the experiment conducted herein, the stimulators, pads, and resistors were placed as shown in Fig. 2.4. Assuming the voltage applied to a person is V^{app} and the current flowing in the body is I^{flo}, the relationship with the voltage V_n applied across the resistor R_n can be written as follows:

$$\begin{aligned} V^{app} &= V_1 \cdot \frac{R_1 + R_2}{R_1} - V_3 \\ I^{flo} &= \frac{V_3}{R_3}. \end{aligned} \tag{4}$$

In this dissertation, the resistances $R_1 = 0.2M\Omega$, $R_2 = 1.8M\Omega$, and $R_3 = 100\ \Omega$ were used. Therefore, (4) can be rewritten as follows:

$$\begin{aligned} V^{app} &= 10V_1 - V_3 \\ I^{flo} &= \frac{V_3}{100}. \end{aligned} \tag{5}$$

We measured V_1 and V_3 by using an oscilloscope with a sampling period of 1.0 μsec. Therefore, the sampling frequency was 1.0 MHz. The applied voltage V^{app} and the actual inflow current I^{flo} in this experiment are shown in Fig. 2.5. As shown in Fig. 2.5, the input voltage is an M-series signal that changes randomly at +10 or -10 V at a carrier frequency of 10 kHz. The relationship between the applied voltage and the inflow current was calculated using multiple regression analysis. As a result,

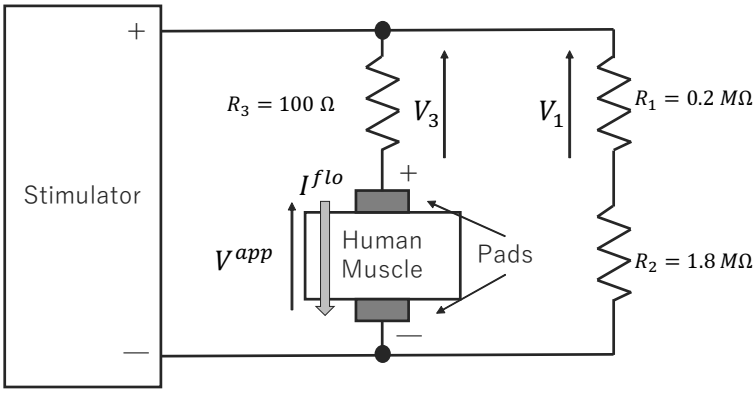

Fig. 2.4 Placement of stimulator, pad, and resistor

the mathematical formula represented by the (6) has the highest correlation value.

$$G_{VI}(s) = \frac{I(s)}{V(s)} = \frac{d_1 s}{c_2 s^2 + c_1 s + 1}, \tag{6}$$

where, c_2, c_1, and d_1 are constants. These three values were estimated using multiple regression analysis. The fixed values and resonance frequency of each participant are listed in Table 2.1. In addition, the gain margin in the participant A is shown in Fig. 2.6. The results showed that the resonance frequency of $G_{VI}(s)$ is high frequency. Therefore, $G_{VI}(s)$ is represented by one differentiation in the low frequency range.

Table 2.1 Values of parameter concerning $G_{VI}(s)$ and resonance frequency

	Participant A	Participant B
c_2	8.0×10^{-10}	1.2×10^{-9}
c_1	2.2×10^{-5}	4.6×10^{-5}
d_1	1.9×10^{-7}	1.4×10^{-7}
Resonance frequency [kHz]	5.6	4.6

2.3.3.2 Stimulus with Long Pulse Width

Next, it was verified whether the applied voltage or the incoming current was related to the applied force. The participants were given electrical stimulation with a pulse width of 500 ms and amplitude of 20 V. Fig. 2.7 shows the results of normalizing the maximum value, inflow current, and exerted force of the applied voltage of participant A with 1. Three points can be confirmed from the result.

- A dead time of about 20 ms passed until the force was generated after the flow of current.
- The exerted force was generated with a short dead time after the flow of current. In addition, no current flowed for about 100-400 ms, and no force is generated at the time of voltage application. Therefore, the force was determined by the inflow current.

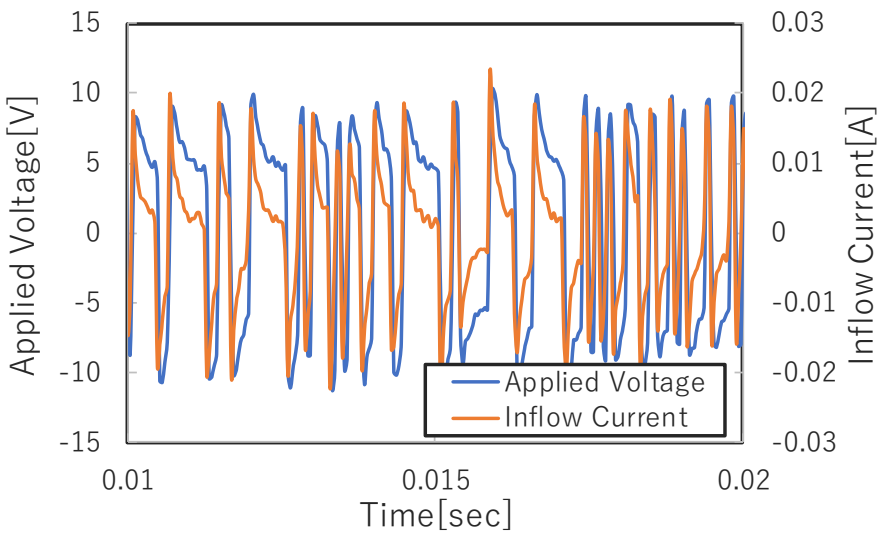

Fig. 2.5 Applied voltage and inflow current of participant A

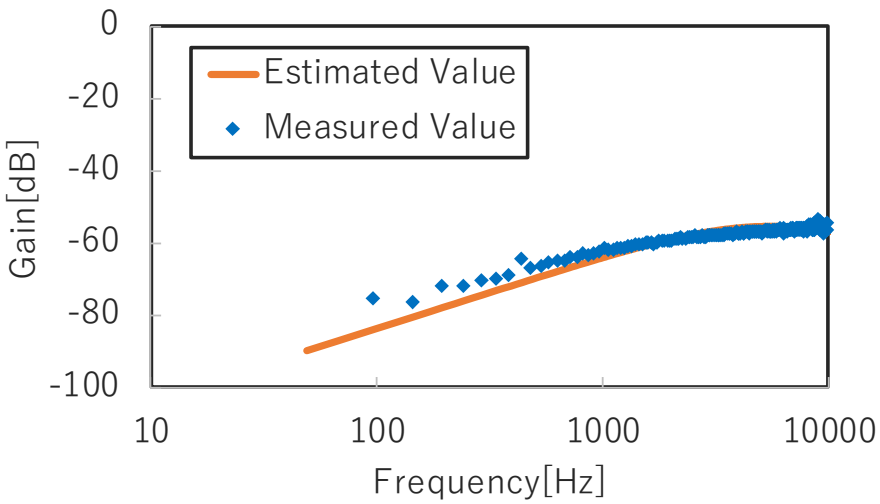

Fig. 2.6 Gain margin of current and voltage of participant A

- Forces were generated by the positive current and the negative current, and the characteristics of the exerted forces were different from each other.

The dead time of each participant was estimated from this experiment. The average of five experimental results was defined as the dead time of each participant. Table 2.2 shows the dead times of each participant. The subscripts + and − denote positive and negative currents.

Table 2.2 Values of Dead Time t_d

	Participant A	Participant B
$t_{d+}[s]$	0.023	0.021
$t_{d-}[s]$	0.025	0.028

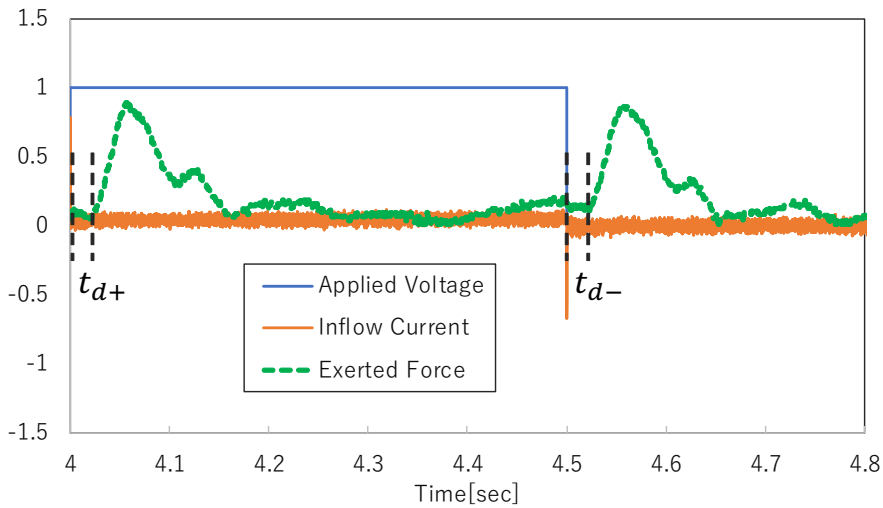

Fig. 2.7 Applied voltage, inflow current, and exerted force (normalized to a maximum value of one) after stimulation of flexor muscle of participant A

2.3.3.3 Measurement of Threshold Current

Next, the current flowing into the subjects was measured and the threshold current required to drive the joint was investigated. In the experiment, the voltage corresponding to the stimulation waveform shown in Fig. 2.8 was applied. The reason for using this shape is that the negative current can be reduced by the waveform shown in Fig. 2.8, and only the force generated by the positive current can be measured. In addition, by exchanging the positive and negative sides of the stimulation waveform of Fig. 2.8, only the force due to the negative current can be measured. The stimulation frequency was set to 10 pps (pulses per second), stimulation was performed for 1 sec, and a 1 sec break was set. The initial voltage was 6 V, and it was increased in steps of 2 V. The results of participant B are shown in Fig. 2.9. There exists a threshold current at which the participant's joints exert their forces. When the direction of the current changed, the same result was obtained in the experiment, even with a different participant. The threshold current I_{th} values of each participant are listed in Table 2.3.

Table 2.3 Values of Threshold Current t_d

	Participant A	Participant B
$I_{th+}[mA]$	14.4	15.1
$I_{th-}[mA]$	8.32	12.3

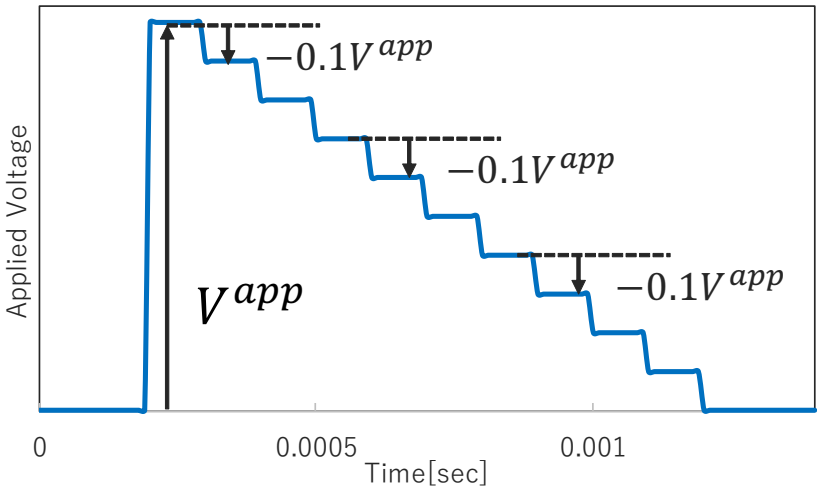

Fig. 2.8 Shape of stimulation waveform that can check the effect of only one side current

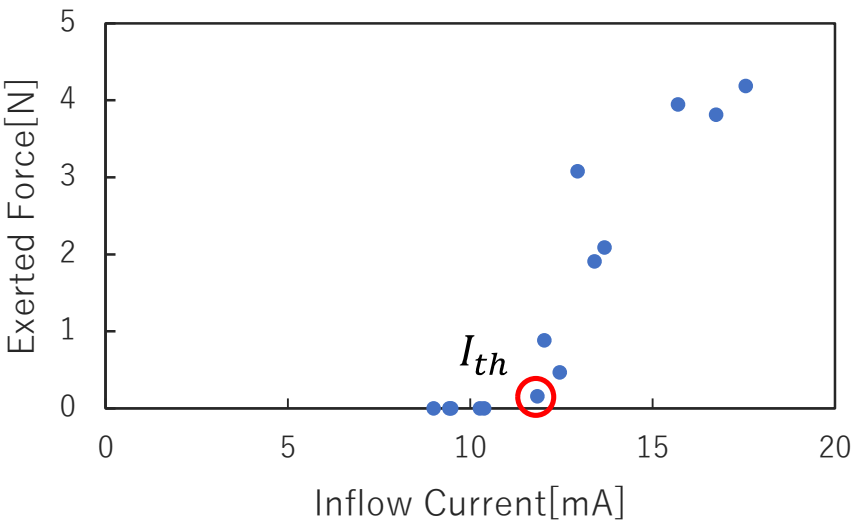

Fig. 2.9 Experimental results of temporal change in electric current and exerted force of participant B

2.3.3.4 Relationship between Inflow Current and Exert Force

For the two participants, an experiment was conducted in which the stimulation waveform shown in Fig. 2.8 was randomly applied at intervals of 1 ms. The timing of applying the stimulus was 1000 pps, but the probability of applying the stimulus was 1/2. Therefore, a pseudo M-sequence signal

was generated. The maximum amplitude of the voltage was 20 V for both participants. The inflow current I^{flo} and the exerted force f^{ext} were acquired with a sampling period of 0.1 ms. There after that, decimation was performed to limit the sampling period to 5.0 ms. The transfer function $G_{IF}(s)$ is estimated using the method described in Section III with the 512 pieces of data obtained. The current I used in the verification is expressed as follows:

$$I = \begin{cases} I^{flo} - I_{th} & (I^{flo} > I_{th}) \\ 0 & (I^{flo} \leq I_{th}). \end{cases} \tag{7}$$

The gain margin in the cases of a positive current applied to participant A and B are shown in Figs. 2.10, and 2.11, respectively. The results shows that the gain margin changes from a certain point at -20 dB/dec. Therefore, it is inferred that the inflow current and the exerted force constitute a first-order lag system. The transfer function $G_{IF+}(s)$ is written with the constants C_1, D_0:

$$G_{IF+}(s) = \frac{F_+(s)}{I_+(s)} = \frac{D_0}{C_1 s + 1}, \tag{8}$$

These two values were estimated using multiple regression analysis. The fixed values of each participant are shown in Table 2.4.

Table 2.4 Values of parameter concerning $G_{IF}(s)$

	Participant A	Participant B
C_{1+}	0.1889	0.5789
D_{0+}	32207	4888.2
C_{1-}	0.2476	0.4325
D_{0-}	13796	7331.5

The outline of the transfer function obtained using the values listed in Table 2.4 and (8) is shown by the solid line in Figs. 2.10, and 2.11. It was confirmed that the relationship between the inflow current and the exerted force agrees with the result obtained using FFT. In this measurement environment, it was difficult to suppress the mechanical interference (characteristics caused by dampers and spring elements) between the force sensor and the contacting devices and between the force sensor and biological tissues (skin, muscle, fat, etc.). It is very difficult to suppress the interference because it requires a surgical operation. In this experiment, the results were verified at low frequencies (below 5Hz) without using high frequency results that would be caused by interference. From the results, it can be inferred that the relationship between the inflow current and the exerted force is a first-order lag system.

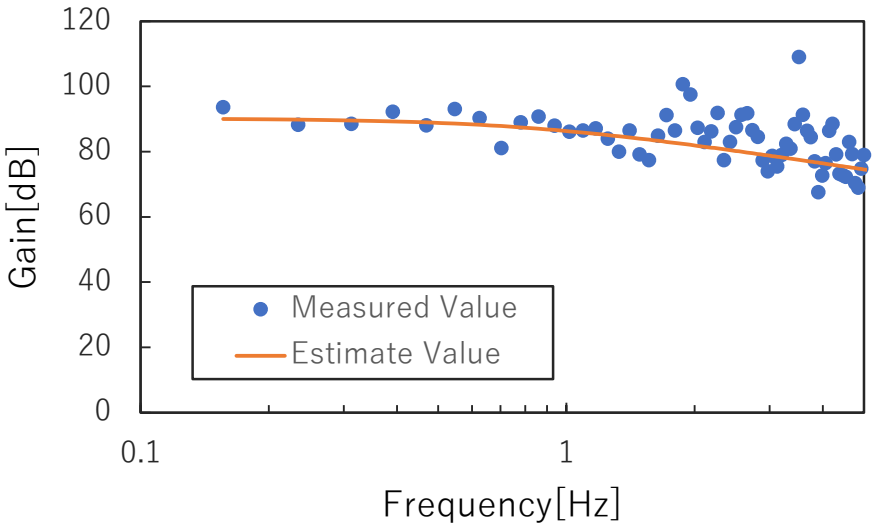

Fig. 2.10 Gain margin of positive current of participant A

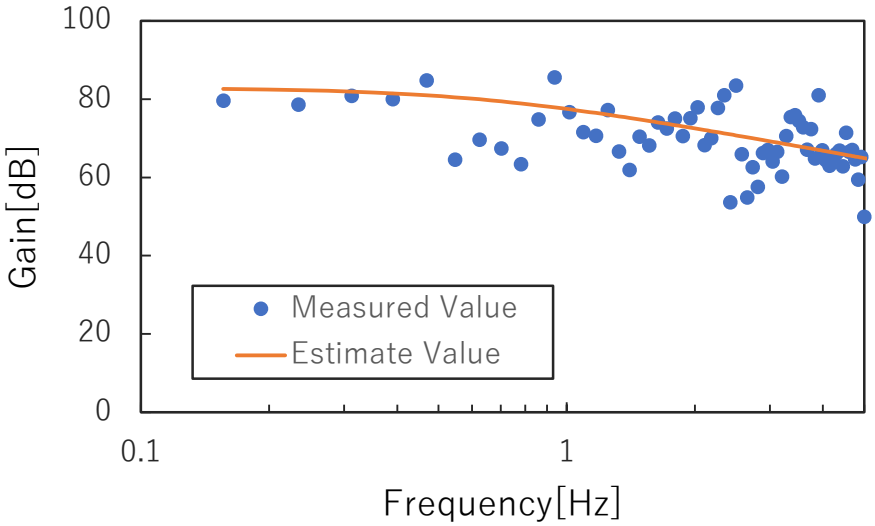

Fig. 2.11 Gain margin of positive current of participant B

2.3.4 Verification

In this section, the accuracy of the force estimation is verified by employing a stimulation pattern different from the one used in the previous section. From the results in Fig. 2.7, the positive current and negative current exert power independently. Therefore, the model of human muscle (i.e, the relationship between current and force) is defined in Fig. 2.12. The stimulus pattern used for verification was an M-sequence signal that changed at +15 V and –15 V at 1000 pps.

The measured and estimated values of the exerted force are shown in Figs. 2.13 and 2.14. In addition,

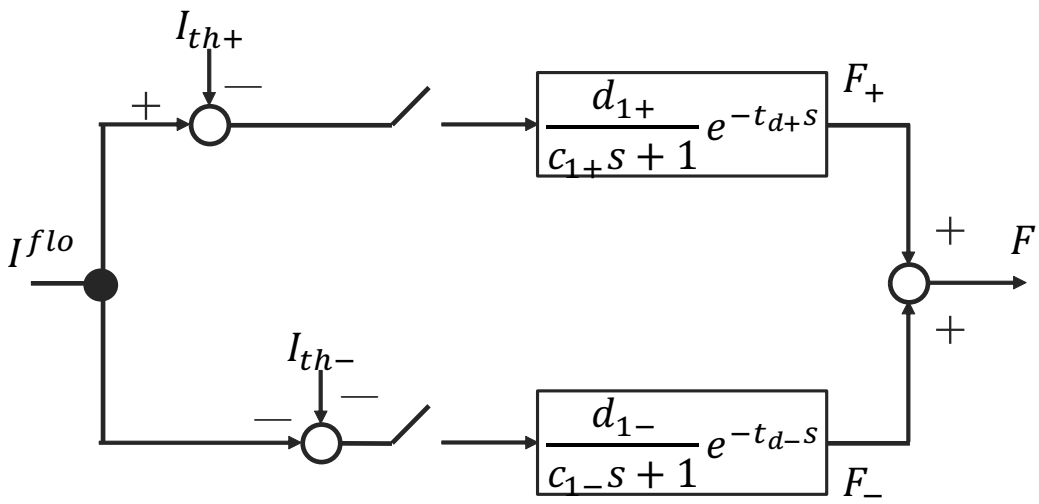

Fig. 2.12 Structure of model of human muscle

the current and the exerted force are passed through a low-pass filter with a cutoff frequency of 100 Hz.

From the results, it is clear that the error is large from the start to about 0.5 sec, but thereafter, the two values agree reasonably. One of the factors that caused errors after starting was incorrect modeling of the transient response. Because the data used to create the model in the proposed method were related to stationary response, there is a high possibility that the model cannot handle transient responses. The goal is to improve the estimation accuracy for transient response in the future.

2.3.5 Summary

In this section, the method modeling the relationship between current and exerted force when using FES was proposed. First, it is revealed that the exerted force is determined by the inflow current. Next, the relationship between the inflow current and exerted force can be formulated as a first-order lag system including dead time. As a result, the proposed method can be used to estimate the exerted force under steady state response.

2.4 Summary of Chapter 2

In this chapter, the model of the stimulus current and the exerted force was estimated using a frequency response measurement technique using the FFT. As a result, it is shown that the relationship between the stimulus current and the exerting force can be approximated by a first-order delay system, including the dead time.

This result is expected to contribute to the improvement of angular control and force control using

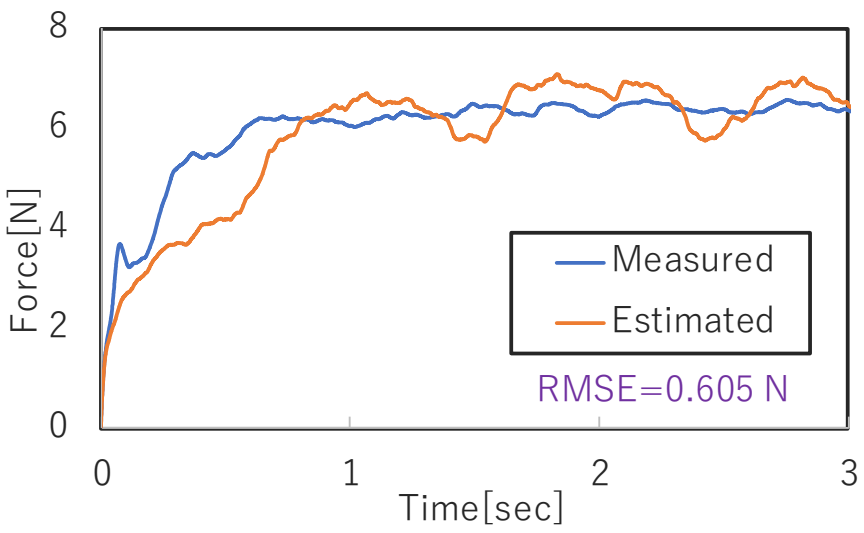

Fig. 2.13 Actual measured value and estimated value of participant A

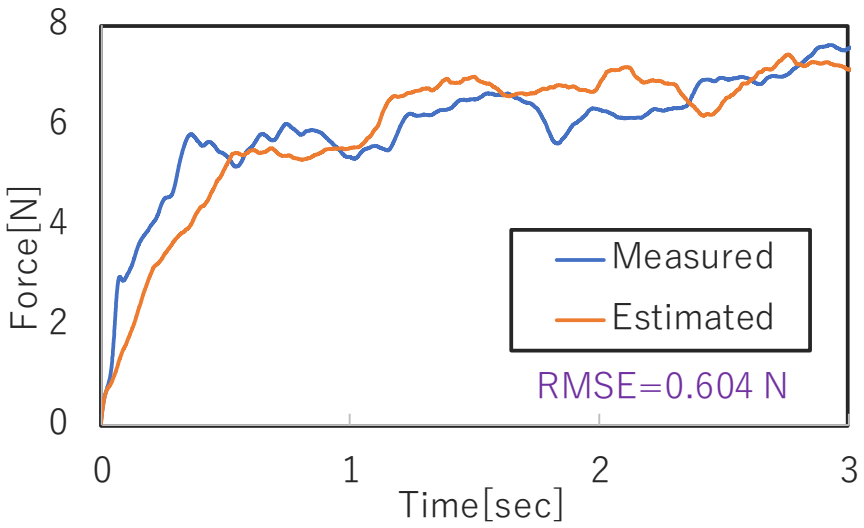

Fig. 2.14 Actual measured value and estimated value of participant B

the FES. However, it is necessary to develop a stimulator that outputs the desired current and an adaptation mechanism to deal with muscle fatigue and modeling errors.

In this chapter and Fig. 2.7, it was shown that the current is determined by the derivative of the voltage. The experiment in Fig. 1 shows the results when a voltage is applied for a long time. However, a square wave with a short pulse width is generally used in FES, and a pulse width of 0.2 ms is used in this dissertation. Therefore, both the current and voltage have comparable pulse widths. In other words, when the pulse width of the voltage is short, it is possible to control the exerted torque by modulating the voltage amplitude. Therefore, in the following chapters, the control and modeling is

done using voltage amplitude modulation.

Chapter 3 Control of Joint Angles

In this chapter, the FES angle control methods applied to the human body is described. The control methods that use a feedback controller have been studied since the 1990s. Since then, a controller that involves the successive estimation of constants by using a neural network (NN) or adaptive controller has reached a good level of efficiency and become mainstream. However, the nonlinear properties of the human body and the insufficient precision of the used sensors are causing a delay in the feedback controller development. This section provides a description of the mechanisms used to implement the feedback controller using two methods: a control method with a robust controller and a control method with a learning-based controller.

3.1 Background

3.1.1 Robust Controller

Gollee *et al.* succeeded in realizing an upright motion using an H∞ controller or a linear quadratic Gaussian controller [42], [43]. Even though the experimental results of their studies showed that small perturbations can be suppressed, the disturbances that occurred because of a large force cannot be suppressed, implying that the method cannot yet be used in a realistic setting. Bô *et al.* proposed a control system in which disturbances are suppressed by the method of antagonistic muscle stimulation [44]. Their experimental results showed that the proposed method provides a better suppression of disturbances than when only a single stimulus is used. However, the procedure used to set the relevant parameters was proven difficult, and the error was not eliminated in all cases.

Farhoud *et al.* proposed a method that combines a higher-order sliding mode (HOSM) controller providing robust control and a fuzzy controller used to compensate for the lowering output that occurs because of muscle fatigue [45]. In the experimental result of the study, a cycling operation with a length of 900 sec was reported to have been successfully realized. This device used not only electrical stimulation to the muscles, but also a motor to move the pedals.

3.1.2 Learning-based Controller

Chang *et al.* and Kurosawa *et al.* both proposed a controller that uses a proportional-integral-differential controller and an NN [46], [47]. In the method presented by Chang *et al.*, the NN was given the following input values: current voltage, angle, and angular velocity, as well as the values recorded at up to two previous steps. In comparison, the method described by Kurosawa *et al.* uses the current values of the angle, angular velocity, and angular acceleration, as well as their values

in up to five previous steps as input for the NN. In both experimental studies, the tracking error decreased because of the muscle fatigue being addressed using the NNs. However, their disturbance suppression characteristics have not yet been verified. Ajoudani *et al.* proposed a control system that combines an NN and a sliding mode control (SMC), which provides a robustness against disturbance and modeling error [48]. In addition, the chattering on the slip plane, which is one disadvantage of the SMC, is suppressed by the NN [49]. The experimental results showed that the average tracking error decreased to 3.76 deg; however, a task-based verification has not yet been accomplished. Sharma *et al.* proposed a control system that combines an NN and a base control that uses the robust integral of the sign of the error [50]. The experimental results showed a increase in the disturbance suppression characteristics when a weight of 10 lbs was added, as well as a decrease in the average tracking error to 2.96 deg.

Kobravi *et al.* designed a control system by combining a fuzzy-based SMC and adaptive control [51]. Most of the control in the system was performed by using the fuzzy-based sliding mode controller. The modeling error was suppressed by using an adaptive nonlinear compensator. The control system was designed individually for the flexor and the extensor muscles. The disturbance suppression was performed by antagonistic muscle stimulation. In addition, Nekoukar *et al.* proposed an adaptive fuzzy terminal controller with a sliding mode [52]. In this method, the dynamic characteristics were estimated using an adaptive algorithm and fuzzy logic in addition to including a terminal sliding mode controller with a high tracking performance. In the experiment that investigated the control of the ankle joint angle, the average tracking error was reduced to 1.17 deg. The walking motion was realized using the method in [53].

Ferrarin *et al.* designed an inverse dynamics model of the quadriceps muscle and proposed a method to adjust its variable parameters by combining adaptive mechanisms [54]. They demonstrated an improvement in control performance accomplished by combining the feedback control with their model. Kirsch *et al.* proposed the application of a nonlinear predictive control model to the FES knee joint control [55]. Model sampling was performed with a 100 Hz frequency. The performed experiment presented an error of 1.71 deg and confirmed the disturbance suppression characteristics of the model.

3.2 Issue

As mentioned above, control systems with adaptive mechanisms such as NNs have shown excellent control performance. However, these methods are not suitable for using FES in daily life because of the learning time required. Moreover, the current performance of the PC is not sufficient for high-

frequency calculation. Therefore, in the using NNs control method, the angular target is set to a low frequency motion.

There are three problems with angle control using FES.

- The nonlinearity of the body.
- Changes in dynamic properties due to muscle fatigue.
- Dead time from stimulus onset to joint drive.

The HOSM controller mentioned above have been reported to be highly robust to modeling errors and disturbances. In other words, it is highly robust to the nonlinearity of the dynamic properties and to time variation. Therefore, in this dissertation, a control to suppress the effect of dead time is proposed.

3.3 Chattering Reduction of FES with the Smith Compensator

Firstly, reducing chattering in FES with Smith compensator is proposed[56]. By using the Smith compensator, control that is not affected by dead time is realized. I also verify the performance of the control system using the Smith compensator. In addition, when the Smith compensator is used, a model to be controlled is required. However, it is difficult to estimate the dynamic characteristic model when using FES. Therefore, in this dissertation, the dynamic characteristic model is estimated using the autoregressive (AR) model, and the conventional linear approximation method and the AR modeling method was compared.

3.3.1 Bilateral Control

Bilateral control is a type of master-slave system in which the positions of the master and slave are synchronized by the system. In addition, the master can experience the reaction force received by the slave from walls, grasps, etc. A conceptual diagram of bilateral control is presented in Fig. 1.1. Two types of bilateral control systems were used in the present study, *i.e.*, position-symmetric bilateral control and 4ch bilateral control.

3.3.1.1 Position-symmetric Bilateral Control

In this dissertation, position-symmetric bilateral control is often used because

- force sensors are not required,
- configuration is easy, and

- the control system thus becomes stable.

For these reasons, position symmetric bilateral control is used. The goal of position-symmetric bilateral control is to synchronize the positions of the master and slave. The control goal is realized by setting both deviations to 0 as follows:

$$\theta_m - \theta_s = 0, \tag{9}$$

where θ is the angle, and the subscripts m and s represent the master and slave, respectively. Position-symmetric bilateral control has no force feedback; hence, it can only transmit force information when there is a proportional relationship between the position deviation and the force.

4ch bilateral control will be discussed in Chapter 5.

3.3.2 Methods

3.3.2.1 HOSM Controller

The control target in the sliding mode controller is that the state variable x converges to the target value x_d without getting affected by the model's uncertainty and disturbance. The sliding mode controller goal is defined as follows:

$$S(x,t) = (\frac{d}{dt} + \lambda)^{n-1} e(t) = 0, \tag{10}$$

where λ is a positive constant and $e(t)$ denote the difference between the target value x^{cmd} and the measured value x^{res}. Therefore, the error $e(t)$ can be defined as follows:

$$e(t) = x^{cmd} - x^{res}. \tag{11}$$

In addition, n is the number of input variables. In this dissertation, the angle and the velocity were the input; so $n = 2$.

However, in such classical sliding mode control, when $S = 0$, a high-frequency vibration called chattering occurs because the input's positive and negative signals are switched in high speeds. Therefore, in this study, the high-order sliding mode (HOSM) controller was used. The control target of the HOSM controller can be described through (12) using the sliding variable s given in (10).

$$S = \dot{S} = \ddot{S} = \cdots = S^{r-1} = 0. \tag{12}$$

With the HOSM controller, chattering can be suppressed by applying a control so that the high-order element of S, which is supposed to increase when chattering occurs, converges to zero.

In this dissertation, the super-twisting algorithm to implement the HOSM controller is used [45], [57]. In the super-twisting algorithm, the control input u is determined based on the control law

represented by (13),

$$\begin{cases} u = -\lambda \cdot |S|^{\rho} \cdot \mathrm{sgn}(S) + u_a \\ \dot{u}_a = -W \cdot \mathrm{sgn}(S), \end{cases} \tag{13}$$

where W, ρ, and λ are positive constants and ρ is preferably 0.5 when $n = 2$ [57]. Although W and λ are values related to the parameter of the controlled object, in this study, them to $W = 0.2$ and $\lambda = 2.0$ is used by trial and error. These parameter values were used for all experiments and participants.

3.3.2.2 Smith Compensator

The structure of the Smith compensator is shown in Fig. 3.1. Here, $r(t)$, $u(t)$, and $y(t)$ denote target values, inputs, and outputs to the controlled object, respectively. In addition, $G(t)$, $G_c(t)$, and $G_m(t)$ denote transfer functions in the time domain of controlled objects, controllers, and models of the controlled objects, respectively. Dead time is denoted by t_0. The transfer function from input $r(t)$ to the output $y(t)$ results in

$$\frac{y(t)}{r(t)} = \frac{G_c(t)G(t-t_0)}{1 + G_c(t)\{G(t-t_0) - G_m(t-t_0) - G_m(t)\}}. \tag{14}$$

Therefore, when $G(t)$ and $G_m(t)$ are equal, the characteristic equation does not include a dead time element. This allows control that is not affected by dead time. However, to use this method we need to exactly estimate $G_m(t)$.

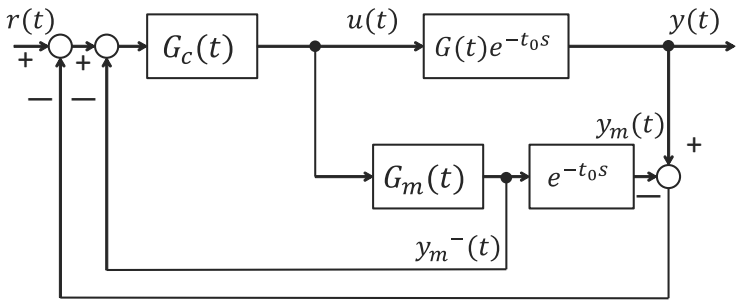

Fig. 3.1 Structure of the Smith compensator

3.3.2.3 Modeling

In my conventional approach, the dynamics of the muscle is modeled using a linear approximation. The voltage-torque relationship obtained after the flexor muscle of participant was stimulated as shown in Fig. 5.6. The parameter V_{th} is defined as the voltage at which the torque first exceeds 0 Nm. In addition, the parameter K_{vt} was obtained by the least-squares method from the point at which the torque exceeded 0 N. Therefore, the torque τ^l exerted when the voltage V^{app} is applied results in

$$\tau^l = (V^{app} - V_{th})e^{-t_d s}/K_{vt}, \tag{15}$$

where t_d denotes the dead time from when a voltage is applied until the torque is exerted. However, the exerted torque is nonlinear and therefore, (15) should actually be more complicated.

In this section, using the AR model is proposed to model the relationship between voltage and angle . The structure of AR modeling is indicated in Fig. 3.3. The output $y(t)$ can be expressed by (16) using the input $x(t)$ and the output $y(t)$. Unit time delay is denoted by t_s.

$$\begin{aligned} &y(t) + a_1 y(t-1) + \cdots + a_{n_a} y(t-n_a) \\ &= b_1 x(t-1) + b_2 x(t-2) + \cdots + b_{n_b} x(t-n_b). \end{aligned} \tag{16}$$

Here,

$$A(s) = 1 + a_1 e^{-t_s s} + \cdots + a_{n_a} e^{-n_a t_s s} \tag{17}$$

$$B(s) = b_1 e^{-t_s s} + b_2 e^{-2t_s s} + \cdots + b_{n_b} e^{-n_b t_s s}, \tag{18}$$

Equation (16) can be rewritten as

$$A(s)y(t) = B(s)x(t). \tag{19}$$

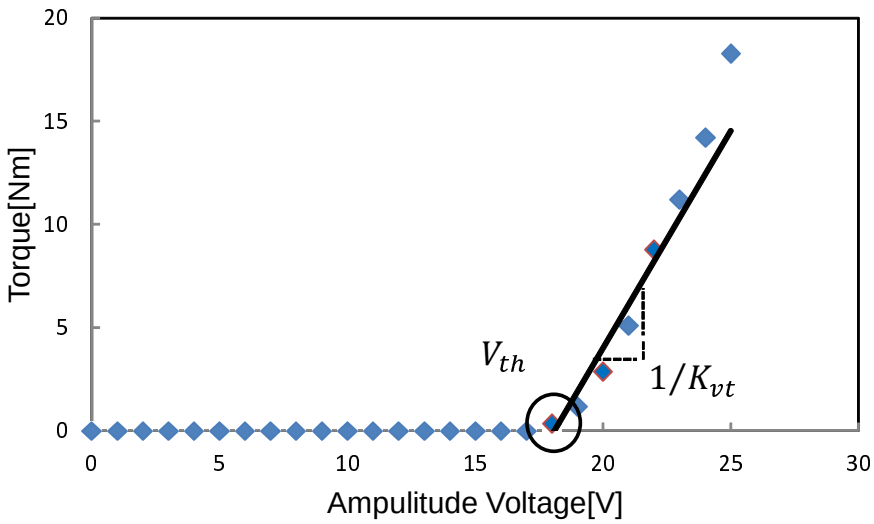

Fig. 3.2 Participant's voltage-torque relationship

3.3.2.4 Proposed System

Fig. 3.4 displays the proposed control method. In this method, the HOSM controller with the Smith compensator was used. Camacho *et al.* simulated a control system using the Smith compensator with the sliding mode controller, which indicated good performance [58], [59].

Although it is the proposal of this dissertation to model the dynamic characteristics using the AR model and implement it in the Smith compensator, the control system is based on previous studies[58].

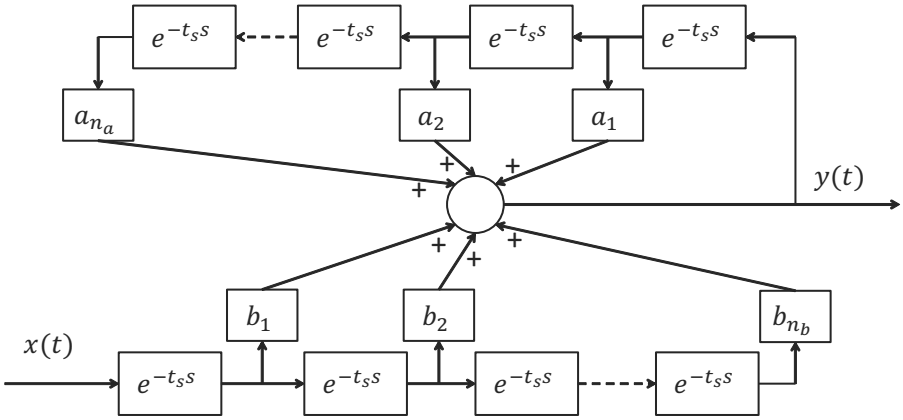

Fig. 3.3 Structure of the AR modeling

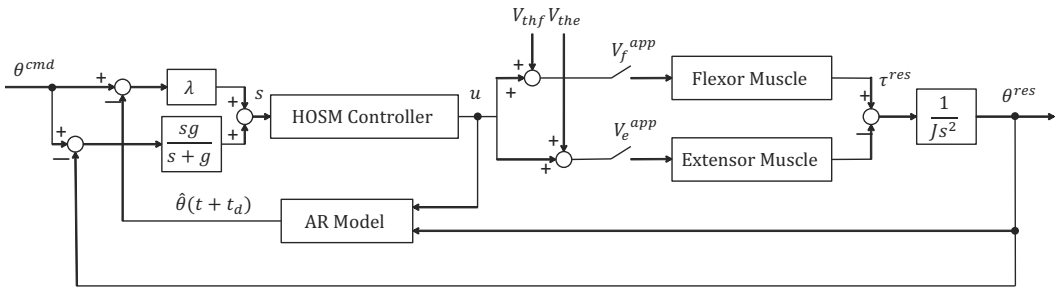

Fig. 3.4 Block diagram of the proposed method

The sliding surface is defined as follows:

$$\begin{aligned} S(t,\theta) &= \lambda e_m^-(t) \\ &\quad + \frac{d}{dt}\{[\theta_d(t) - \theta_m(t)] + [\theta_m(t) - \theta^{res}(t)]\} \\ &= \lambda e_m^-(t) + \frac{d}{dt}e(t) \end{aligned} \tag{20}$$

$$e_m^-(t) = \theta_d(t) - \theta_m^-(t) \tag{21}$$

$$e(t) = \theta_d(t) - \theta^{res}(t), \tag{22}$$

where $\theta_m(t)$, $\theta_m(t)$, $\theta_m^-(t)$, and $\theta^{res}(t)$ denote the target value, model output with dead time element, model output without dead time element, and the response value. The control target is $\theta_d - \theta_m(t)$=0. In addition, $\theta_m(t) - \theta^{res}$ indicates the modeling error, and it is preferable to have a control system so as to eliminate the influence of error. The control input u is determined by substituting S as defined here into (13).

The value of $\theta_m^-(t)$ is estimated $\hat{\theta}(t+t_d)$ using the AR model. $\hat{\theta}(t+t_d)$ is the estimated value of the output after t_d [s] is obtained from the current input and output, which is equal to the response without dead time. Therefore, $\theta_m^-(t)$ and $\hat{\theta}(t+t_d)$ are synonymous. Using input $u(t)$, output $\theta(t)$,

and dead time t_d, (16) can be rewritten as

$$\begin{aligned}\theta(t) = b_1 u(t-1-t_d) + b_2 u(t-2-t_d) + b_3 u(t-3-t_d) \\ -a_1\theta(t-1-t_d) - a_2\theta(t-2-t_d).\end{aligned} \tag{23}$$

Therefore,

$$\begin{aligned}\hat{\theta}(t+t_d) = b_1 u(t-1) + b_2 u(t-2) + b_3 u(t-3) \\ -a_1\theta(t-1) - a_2\theta(t-2).\end{aligned} \tag{24}$$

In this dissertation, the five constants $(a_1, a_2, \text{and}, b_1 - b_3)$ were determined for each participant using multiple regression analysis. The number of constants was determined by trial and error. In addition, dead time t_d was calculated from the impulse response of the angle value. Therefore, the following stimulation voltage amplitude V^{app} was used.

$$V_f^{app} = \begin{cases} u + V_{thf} & (u > 0) \\ 0 & (u \leq 0), \end{cases} \tag{25}$$

$$V_e^{app} = \begin{cases} 0 & (u \geq 0) \\ -u + V_{the} & (u < 0), \end{cases} \tag{26}$$

where subscripts f, e represent the flexor muscle and the extensor muscle, respectively.

3.3.3 Experiments

In this section, the methods and results of these experiments are described. Four healthy participants (referred to as A-D) were used to test the using Smith compensator controller. Informed consent was obtained from the participants, and the study was approved by Saitama University's Ethics Committee. The angle at which the elbow joint was held was measured using an angle measuring device (Fig. 3.5) composed of a frame and a rotary encoder. The measuring device for the elbow joint's angle was fixed to the arm by three belts. Therefore, the measurement device had little effect on articulation. The angular velocity was obtained by pseudo-differentiating the angle, and the cutoff frequency was set to 1.0 Hz. Since this study is an initial study on using the Smith compensator, therefore, participant's movements is set to the horizontal direction so as to reduce the disturbance caused by gravity. The experimental setup is indicated in Fig. 3.6.

3.3.4 Modeling

In this dissertation, the constants in (24) were estimated by multiple regression analysis. Electrical stimulation was applied to the participants, and the voltage and angle values at that time were

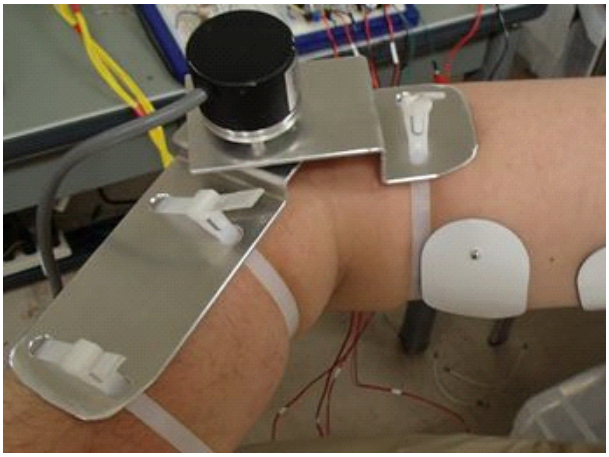

Fig. 3.5 Angle measurement device (elbow joint)

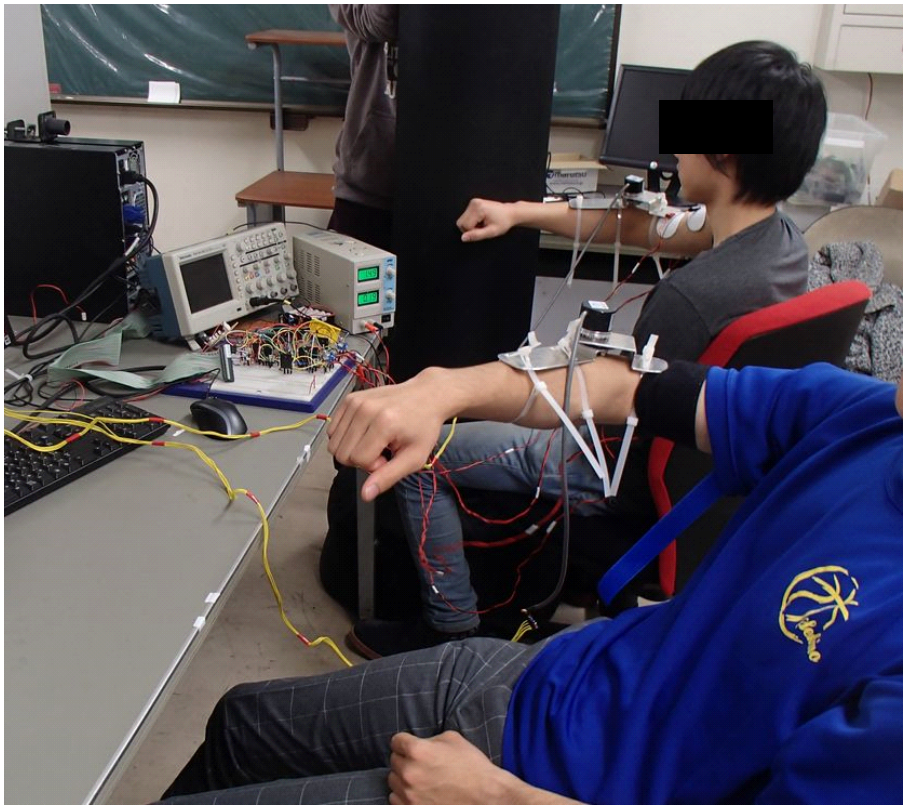

Fig. 3.6 Scene of experiment

recorded. The applied voltage V^{app} in this experiment is

$$\begin{aligned} V^{app} &= 3.0\sin(0.5\pi t) + 3.0\sin(0.33\pi t) \\ &+3.0\sin(0.25\pi t) + 3.0\sin(0.16\pi t) \end{aligned} \tag{27}$$

$$V_f^{app} = \begin{cases} V^{app} + V_{thf} & (V^{app} > 0) \\ 0 & (V^{app} \leq 0), \end{cases} \tag{28}$$

$$V_e^{app} = \begin{cases} 0 & (V^{app} \geq 0) \\ -V^{app} + V_{the} & (V^{app} < 0), \end{cases} \tag{29}$$

The motion frequency of the participant's elbow joint was assumed to be 0.1-1.0 Hz. Therefore, the applied voltage was the sum of voltages, including frequency components in this range. The sampling time was 0.02 s, and data were acquired for 60 s. Data for the first 30 s were used for estimation, and the remaining data were for verification.

The result with participant C is indicated in Fig. 3.7. The solid line is for $\theta(t+t_d)$, the bold dotted line is the estimation result obtained by the proposed method from (24), and the thin dotted line is the estimation result obtained by the conventional method using (15). The error between the true value and the estimated value was calculated using the root mean squared error (RMSE). As a result, the error using the proposed method was 0.0547 rad, and the error using the conventional method was 0.189 rad. Thus, this proves that the modeling using the proposed AR model is better.

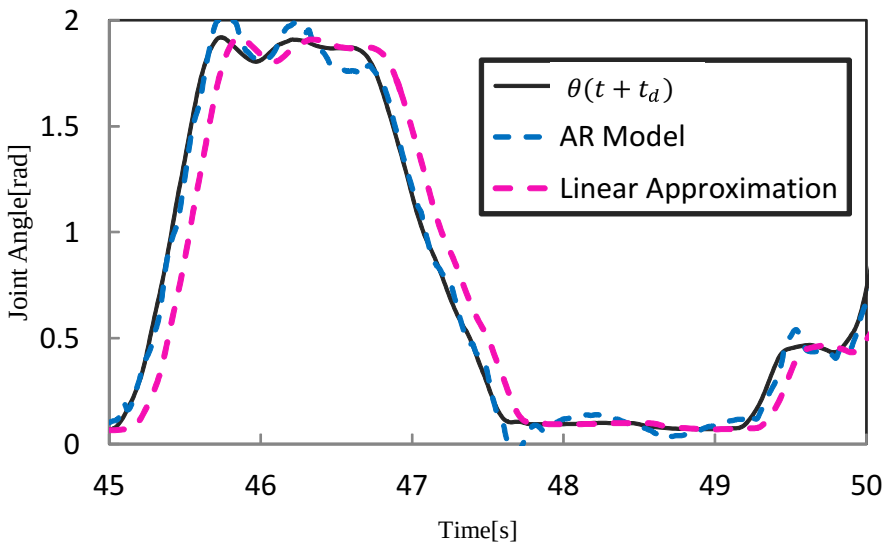

Fig. 3.7 Performance verification of modeling

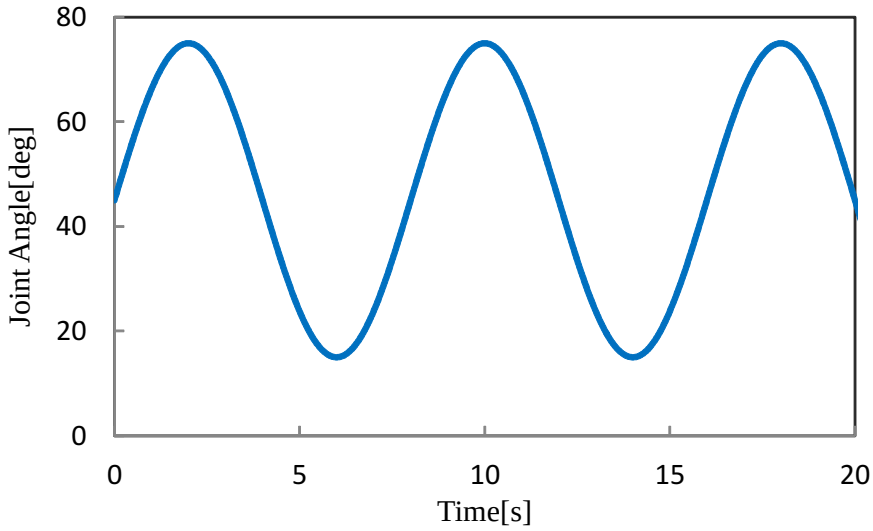

Fig. 3.8 Waveform of target angle

3.3.4.1 Target Value Control

In this experiment, the target value control of the conventional and proposed methods were compared. The applied voltage is obtained from (28), (29). In addition, the sliding surface S in the conventional method was given by (10), and the sliding surface in the proposed method was given by (20). Control using the waveform shown in Fig. 3.8 as a target value was performed by each participant.

The results of participants A and C are indicated in Figs. 3.9 and 3.10, respectively. In addition, the results of the angular velocity values at this time are indicated in Figs. 3.11 and 3.12, respectively. The elbow joint angle using the proposed method is shown by a solid line and that of the conventional method by a dotted line. From the results of Figs. 3.11 and 3.12, the proposed method has smaller angular velocity change. In other words, chattering can be suppressed using the proposed method.

3.3.4.2 Bilateral Control

In this experiment, the performance of the bilateral control with the proposed method was verified. Chairs for the master and the slave were placed back to back, and the master (slave) could not see the movement of the arm of the slave (master). The participants were arranged into two master-slave pairs. One participant of the pair was the master and the other was the slave for 40 s, and then, the participants in the pair exchanged their roles. Placing constraints on the movements of the master may cause the participant to learn the movements, so the master was allowed free movements.

Fig. 3.13 displays the results for the pair master A-slave B, and Fig. 3.14 displays the results for

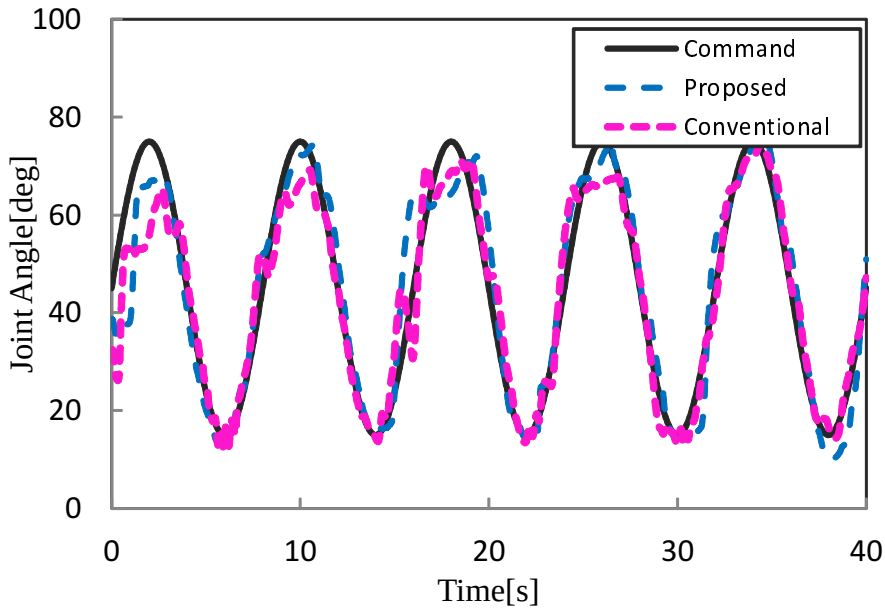

Fig. 3.9 Experimental result of participant A's angular response

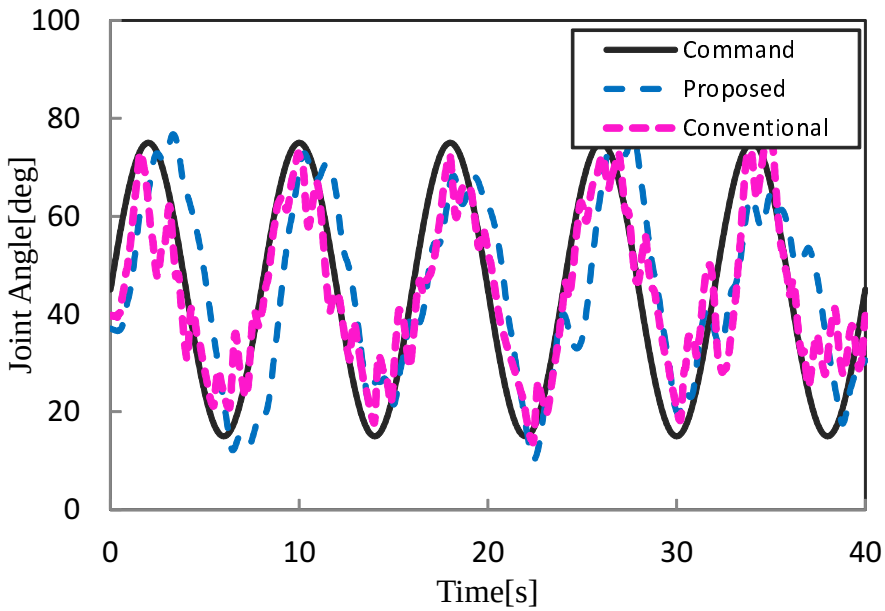

Fig. 3.10 Experimental result of participant C's angular response

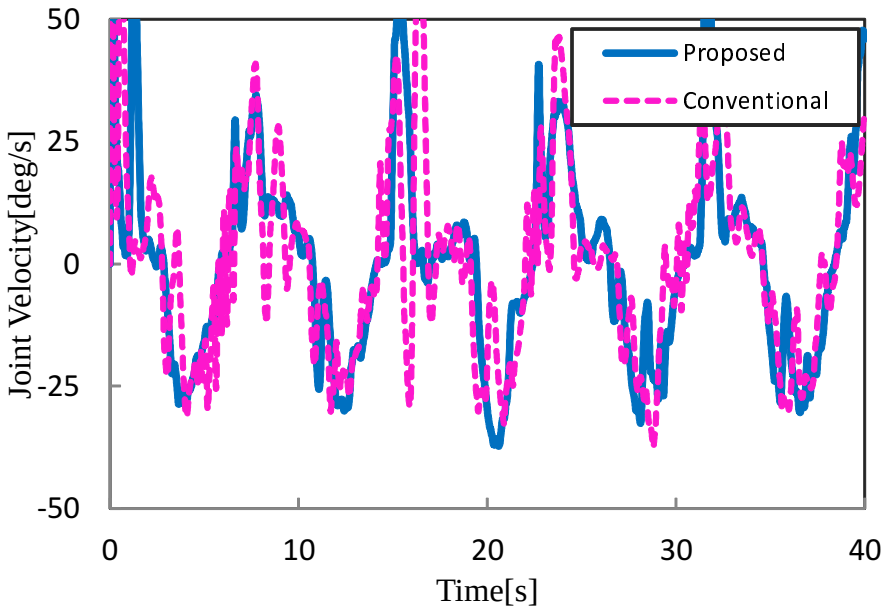

Fig. 3.11 Experimental result of velocity response of participant A

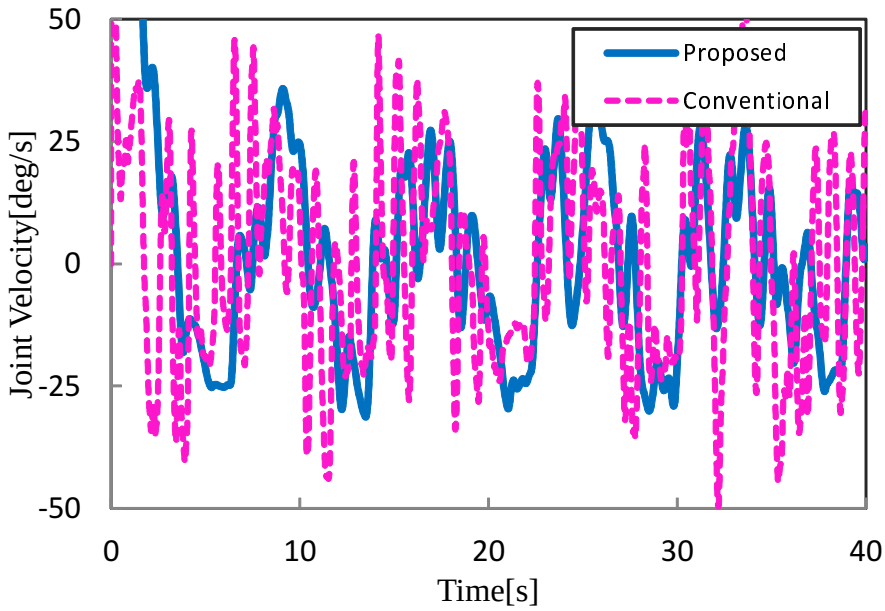

Fig. 3.12 Experimental result of velocity response of participant C

the pair master C-slave D. The elbow joint angle of the master is shown by a solid line and that of the slave by a dotted line. In addition, the color-shaded areas indicate when the slave was in contact with an fixed obstacle.

As a result of free motion, the slave follows the movement of the master. However, the joints of the participants were causing chattering. In this dissertation, the interference of dead time between the master and slave were not considered. It is a future work to construct a control system adapted to bilateral control. As a result of contact motion, the master stopped the arm at the same angle as which the slave stopped the arm. The results suggest that the master could recognize the position of the slave when he made contact with the object.

3.3.5 Summary

In this section, methods that control human bodies using FES with Smith compensator was proposed to deal with the dead time peculiar to FES. Experiments were conducted on four participants. As a result, chattering caused by the dead time was suppressed by the proposed method. However, the master's autonomous motion in bilateral control and the slave's contact motion are considered disturbances in control. Smith compensator has been shown to have degraded control performance for systemsthat including disturbances. Therefore, the control performance was degraded in experiments with bilateral control.

3.4 Control with Adjusted Pulse Frequency and Amplitude in FES

Secondly, a control method to adjust the frequency and amplitude of the stimulation pulse is proposed. In conventional FES control, the pulse amplitude or width is commonly adjusted. However, the exerted torque can also be adjusted by adjusting the frequency. When high-frequency stimulus is used, the exerted torque increases. In addition, muscle fatigue can be alleviated by using low frequency stimulation. Therefore, a control method is proposed that is combining the improvement of responsiveness by high frequency stimulation and suppression of chattering by low-frequency stimulation. As this method involves few parameters, it is suitable for use in daily life.

3.4.1 Methods

3.4.1.1 Conventional Method

Fig. 3.15 shows the block diagram of the proposed system. In the conventional method, the frequency V_{fre} is constant at 50 Hz. As the target value θ^{cmd} in control is an angle, and therefore, (11)

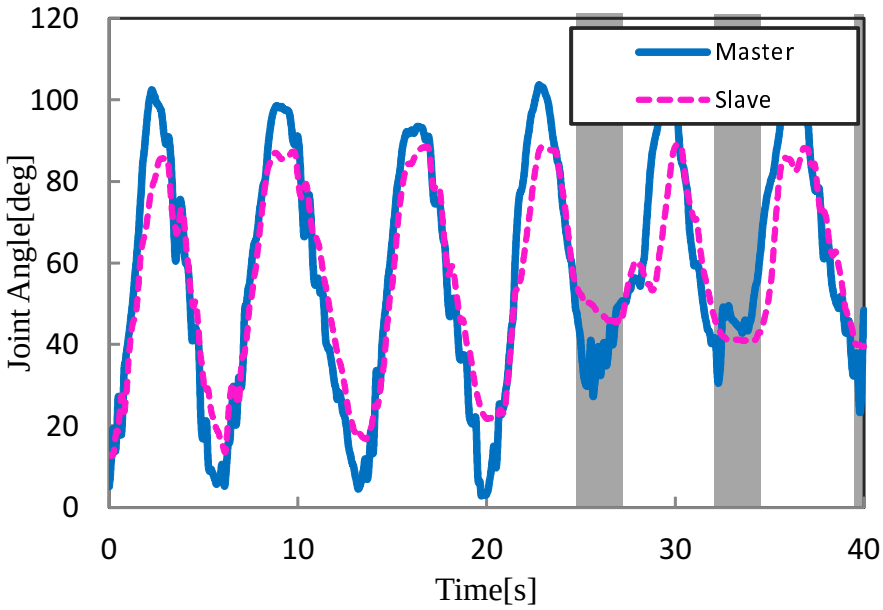

Fig. 3.13 Participant A as master and participant B as slave

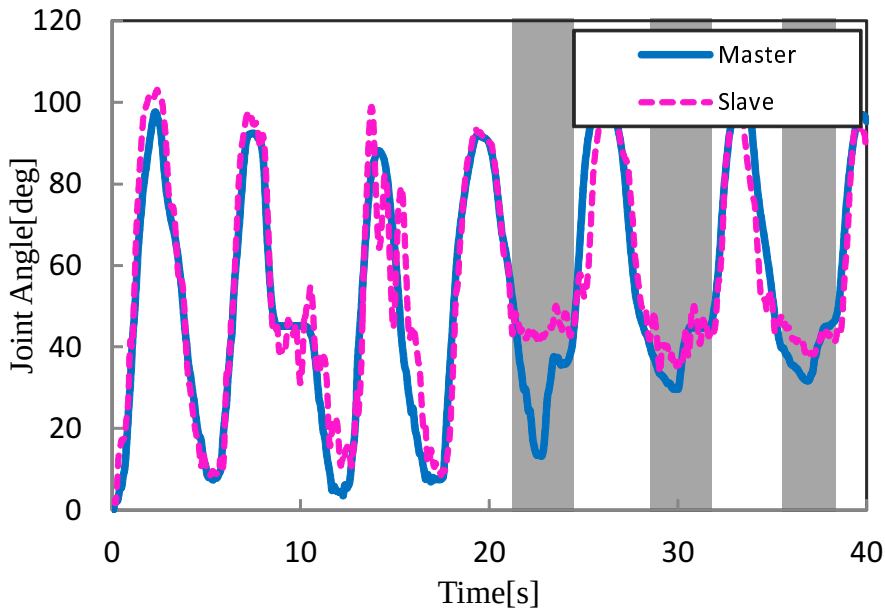

Fig. 3.14 Participant C as master and participant D as slave

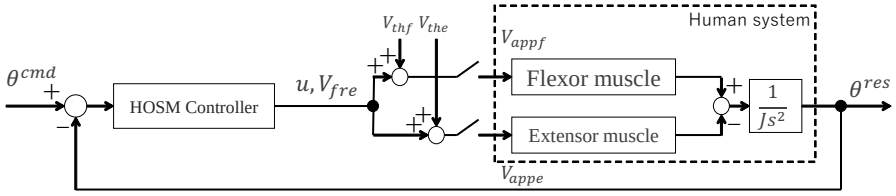

Fig. 3.15 Block diagram of the proposed method

is rewritten as follows;

$$e(t) = \theta^{cmd} - \theta^{res}, \tag{30}$$

$$\dot{e}(t) = \dot{\theta}^{cmd} - \dot{\theta}^{res}. \tag{31}$$

Therefore, the voltage V^{app} applied to the flexor muscle and that applied to the extensor muscle are calculated using (13);

$$V_f^{app} = \begin{cases} u + V_{thf} & (u > 0) \\ 0 & (u \leq 0), \end{cases} \tag{32}$$

$$V_e^{app} = \begin{cases} 0 & (u \geq 0) \\ -u + V_{the} & (u < 0), \end{cases} \tag{33}$$

where subscripts f and e represent the flexor muscle and the extensor muscle, respectively.

3.4.1.2 Proposed Method

In this section, in addition to the pulse amplitude adjustment indicated by equations (32) and (33), pulse frequency adjustment is added. The block diagram of the control system in the proposed method is shown in Fig. 3.15. If the slide variable S is larger than the constant ε, stimulation is performed high-frequency, and when it is smaller, low-frequency is used. In other words, when the error is large, stimulation is performed at high-frequencies, and when the error is small, stimulation is performed at low-frequencies. Therefore, when the error is large, a large torque is generated so that the responsiveness improves, and when the error is small, control is executed by suppressing chattering. Because the increase in torque is reported to stop at around 80 Hz [60] in the conventional research, the high-frequency stimulation was fixed at 80 Hz, and the low-frequency stimulation was conducted at a constant value of 20 Hz. Therefore, the pulse frequency V_{fre} is written as follows;

$$V_{fre} = \begin{cases} 80 & (|S| > \varepsilon) \\ 20 & (|S| \leq \varepsilon). \end{cases} \tag{34}$$

In the present experiment, the constant ε was fixed at 0.3 by trial and error.

3.4.2 Experiments

In this experiments, six healthy male participants (age: 22.8 ± 1.1 years; weight: 68.4 ± 4.6 kg; height: 173.9 ± 4.9 cm, referred as A–F) were used to test the proposed control system. Informed

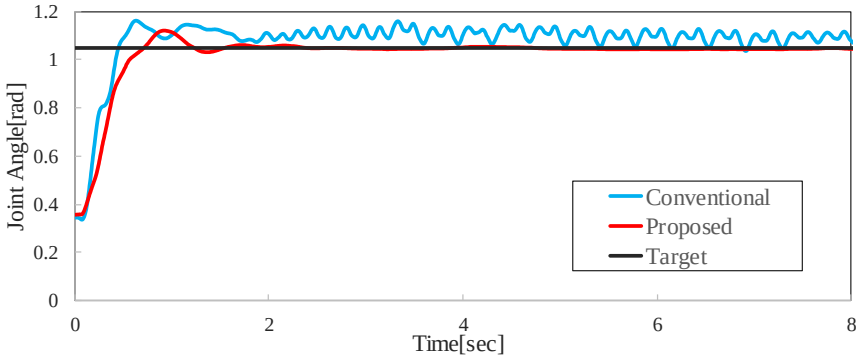

Fig. 3.16 Participant A's angular response

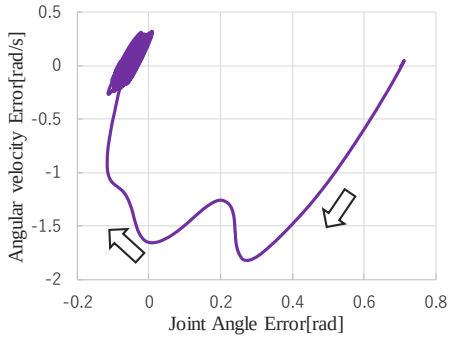

Fig. 3.17 Error of angle and angular velocity in conventional method

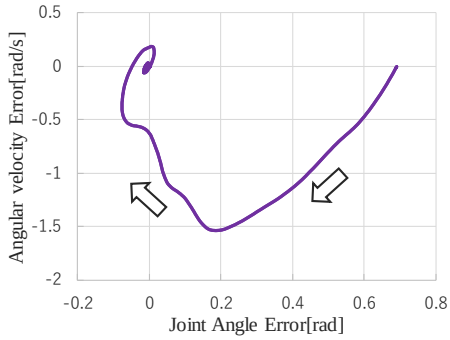

Fig. 3.18 Error of angle and angular velocity in proposed method

consent was obtained from the participants, and the study was approved by Saitama University's Ethics Committee. The angle at which the elbow joint was held was measured using an angle measuring device composed of a frame and a rotary encoder. The angular velocity was obtained by pseudo-differentiating the angle, and the cutoff frequency was set to 1.0 Hz.

3.4.2.1 Stepwise Target Value

Firstly, stepwise target value control was performed for an angle of 1.05 rad. The results for participants A and C are shown in Figs. 3.16–3.21, respectively. Figs. 3.16 and 3.19 show the angular response; Figs. 3.17 and 3.20, the conventional method; and Figs. 3.18 and 3.21, the result of error

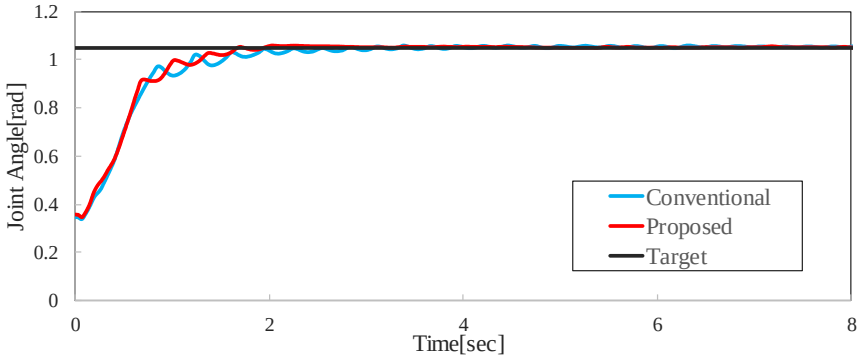

Fig. 3.19 Participant C's angular response

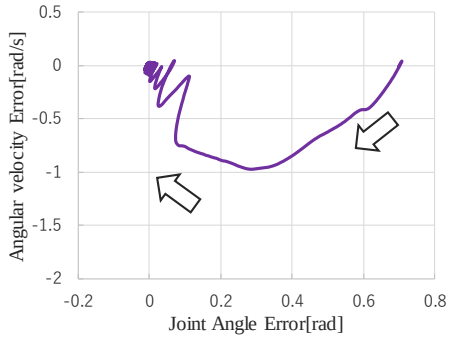

Fig. 3.20 Error of angle and angular velocity in conventional method

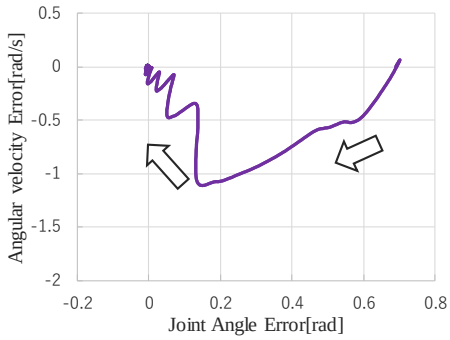

Fig. 3.21 Error of angle and angular velocity in proposed method

when using the proposed method.

These results show that there is no significant difference between the conventional method and the proposed method in terms of the transient response. Even if the frequency is increased, it is inferred that the torque has an upper limit owing the viscosity of the joints and muscles. In the steady state (about 1 sec after the start), chattering occurs near the target value in the conventional method, whereas in the proposed method, it is confirmed that chattering is suppressed. As a result, while the proposed method converges to the origin, it is disorderly near the origin in the conventional method. It is considered that chattering is suppressed because of switching to stimulation at a low-frequency

via the proposed frequency switching, and less torque is generated.

3.4.2.2 Trapezoidal Target Value

Control was performed with the angle on the trapezoid as the target value. Table 3.1 lists the RMSE when using the conventional method and the proposed method in six participants. The results confirmed that the tracking error of angle of participants C, D, and E decreased by using the proposed method. As shown in Fig. 3.22, when the target value varies as a ramp, there is no big difference in angle, but when the target value is stepped and constant, the proposed method shows better performance. In addition, although the follow-up error of participant B greatly decreases when using the conventional method, it is difficult to label the performance as good because it always vibrates as shown in Fig. 3.23. This can also be observed from that the RMSE of the angular velocity increased in the conventional method.

The frequency spectra of each value in Figs. 3.22 and 3.23, obtained using FFT for further confirmation of the chattering phenomenon, are shown in Figs. 3.24 and 3.25. In the conventional method, it was confirmed that the angle response value was larger than the target value at around 5 Hz for both participants. On the other hand, the proposed method resulted in the same frequency component as the target value in the region above 1 Hz. Thus, it was confirmed that the proposed method can suppress chattering.

Table 3.1 Tracking error (RMSE) of each participant

Participant	Angle		Velocity	
	Conventional	Proposed	Conventional	Proposed
A	0.077 rad	0.074 rad	0.12 rad/s	0.10 rad/s
B	0.034 rad	0.067 rad	0.16 rad/s	0.094 rad/s
C	0.090 rad	0.063 rad	0.23 rad/s	0.15 rad/s
D	0.17 rad	0.13 rad	0.14 rad/s	0.12 rad/s
E	0.12 rad	0.074 rad	0.14 rad/s	0.080 rad/s
F	0.082 rad	0.075 rad	0.21 rad/s	0.13 rad/s

3.4.3 Summary

In this section, the FES control performance was improved by combining frequency adjustment with pulse amplitude adjustment, which has been used conventionally. The results show that although the transient characteristics did not change greatly, the steady-state characteristics were good. However, the frequencies when using high frequencies and the value of the constant ε were fixed values.

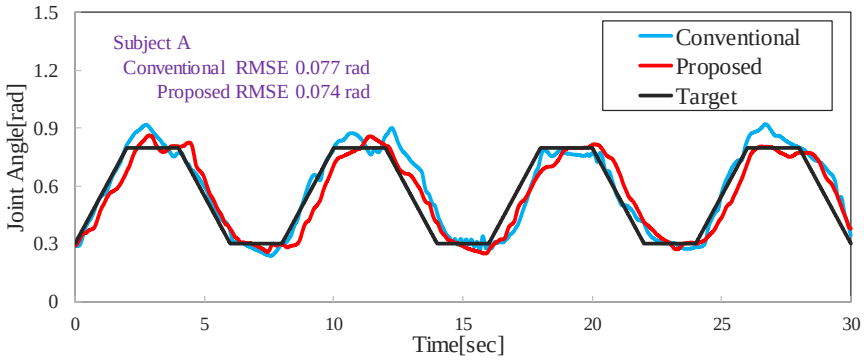

Fig. 3.22 Experimental result of participant A's response

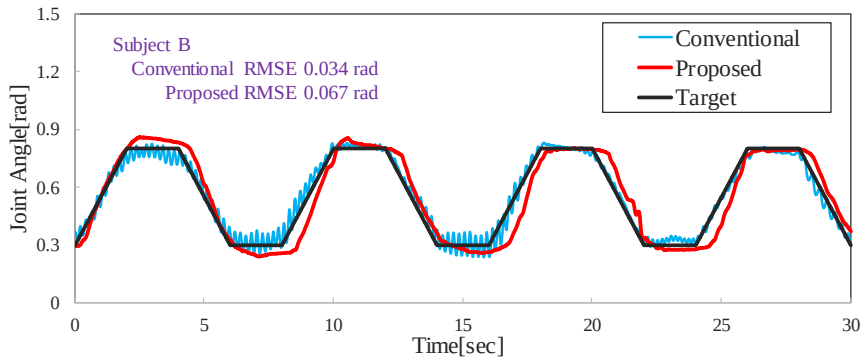

Fig. 3.23 Experimental result of participant B's response

3.5 Summary of Chapter 3

Two angular control methods are discussed in this chapter. The method using a Smith compensator improved the control performance. This method could be a significant contribution in areas such as rehabilitation with FES. However, a disadvantage arose that it cannot be used in bilateral control with autonomous movements and contact actions.

Sliding mode control using amplitude-frequency modulation achieved reasonable angular control with few setting parameters. The small number of setting parameters is a significant contribution to the use of FES. Although the usefulness of the proposed method has already been demonstrated, it is expected that the control performance will be further improved by introducing a mechanism for sequentially updating the constants.

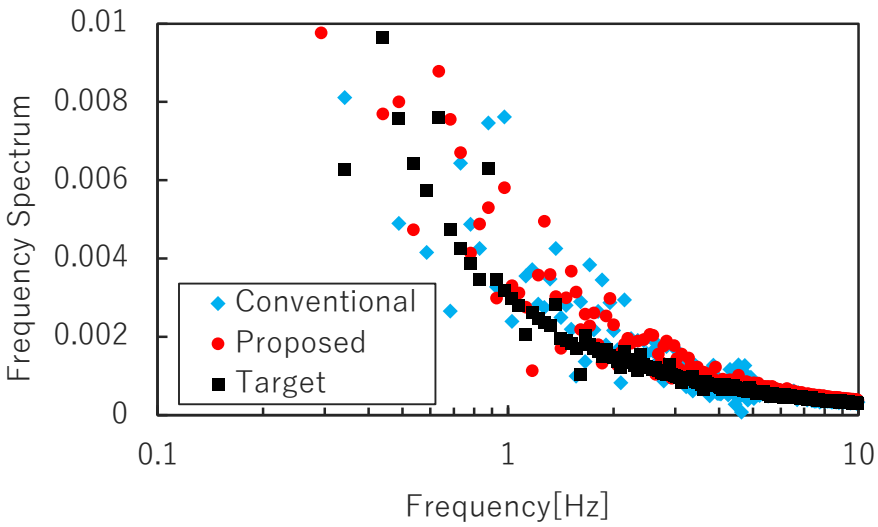

Fig. 3.24 Frequency spectrum of Fig. 3.22 using FFT

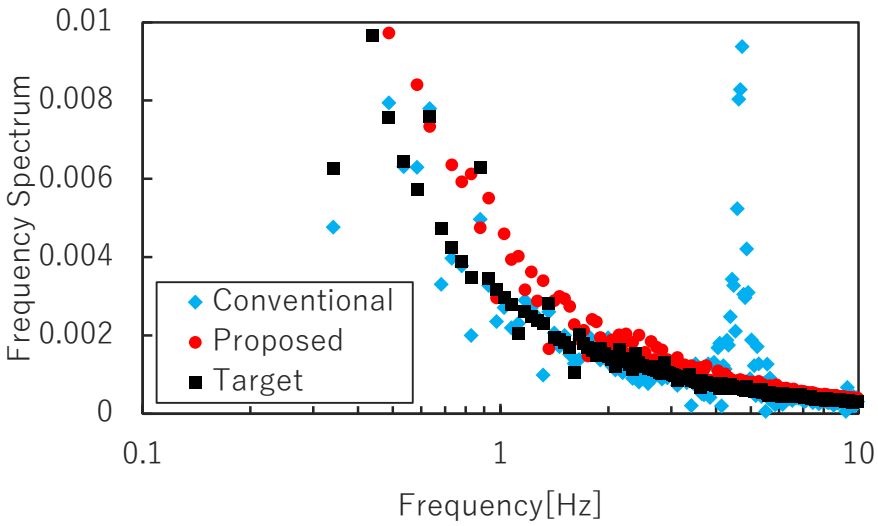

Fig. 3.25 Frequency spectrum of Fig. 3.23 using FFT

Chapter 4 Handling of Multiple DOFs

In this chapter, the control of the multiple DOFs joint is described. In this section, the multiple DOFs control of the lower limbs is not discussed because the pseudo-force feedback was mainly used in upper limbs.

4.1 Background

4.1.1 Hand

A commonly used method for the control of the fingertip joint involved the attachment of numerous (between 10 and 100) electrodes to the forearm. After the motion of the hand is recorded upon the application of random stimuli, the desired motion was realized by relating the position of stimulation to the joint that creates the movement. This setup was used because attaching a pad that covers the forearm was easier than attaching a pair of pads to the small streaks of the forearm.

Tamaki *et al.* developed the PossessedHand and established control of 16 DOF in the hand [23]. Popović *et al.* applied 24 × 2 pads to the forearm, thereby realizing control of the fingertip joint [61]. To achieve the desired operation, the response of each joint to a current applied to each pad was first acquired, after which eight electrodes were selected and stimulated at a time. The participants were recorded to successfully grasp bottles and compact discs (CDs). Bouton *et al.* demonstrated hand control by attaching a total of 160 electrodes to the forearm [62]. They accomplished the control by monitoring the brainwaves, determining the desired behavior of the participant from the date, and realizing the movement using FES. The switching of the anode and the cathode allowed for even more stimulation patterns to be generated. Malešević *et al.* showed different muscles can be stimulated by varying the intensity of the stimulation current [63]. Their experiment showed that the opening and closing of the hand can be performed by feedforward control. In addition, Keller *et al.* proposed a method of placing virtual electrodes at arbitrary locations by simultaneously stimulating multiple electrodes [64]. The simulation presented in their study demonstrated the possibility of generating an arbitrary muscle activity if the distance between the electrodes is less than 2 mm. Their experiment depicted that by adjusting the stimulation position, only the arbitrary muscles can be stimulated, and controlled only single finger.

4.1.2 Shoulder

The muscles that drive the shoulder joint greatly overlap; hence, a few studies on the control of the shoulder joint with surface electrodes have been presented. In this case, the percutaneous electrical

stimulation makes the muscle selection exceedingly difficult. Gibo *et al.* showed that deep muscles can be stimulated by an interference current [65]. However, the exerted torque was small, making the principle unsuitable for use in controlling the shoulder joint.

Schearer *et al.* and Kameyama *et al.* proposed methods to control the shoulder joint with an invasive electrode [66], [67]. When the participant using FES was rehabilitated, the invasive electrode was proven effective, but unsuitable for daily use. Yamaguchi *et al.* and Taniguchi *et al.* showed methods of controlling 1 DOF of the shoulder joint by using a surface electrode [68], [69]. However, these studies used assistance devices to constrain the joint movement; thus, it cannot be said that the tasks were realized by only FES. In addition, Razavian *et al.* proposed reaching control using an elbow joint and a shoulder joint in a two-dimensional (2D) plane [70]. Their control system was constructed based on the movement control model of the body; thus, the joints were controlled using muscle synergy. The result had a position error of approximately 2 cm, and good results were obtained.

4.2 Issue

Interference with other axes is a problem when controlling multiple joints. Interference can be divided into two types: electrical interference (*i.e.*, one stimulus point driving two or more joints) and kinetic interference (*i.e.*, movement of one joint causes movement to an undesired joint). While the former has been studied, the latter has not been discussed.

Therefore, in the first half of this chapter, the two-joint control using antagonistic muscle stimulation is discussed. Antagonist muscle stimulation is a technique that simultaneously stimulates not only the primary mover but also the antagonist muscle when controlling a joint. This technique increases the stiffness of the joint and suppresses the effect of the inertia force.

There are few reports on control of the shoulder joint. It is difficult to selectively stimulate the shoulder joint because it is difficult to stimulate the arranged muscles in an overlapping manner selectively. In previous study, the modulating the frequency can stimulate deep muscles was suggested.

Therefore, in the second half of this chapter, the two-joint control of the shoulder and elbow joints is proposed using frequency modulation.

4.3 Angle Control of Two-Link Human Arms Using Antagonist Muscle Stimulation

In this section, method to increase the rigidity of wrist joints by using antagonist muscle stimulation is proposed to suppress disturbance forces. The proposed method allows us to suppress the influence

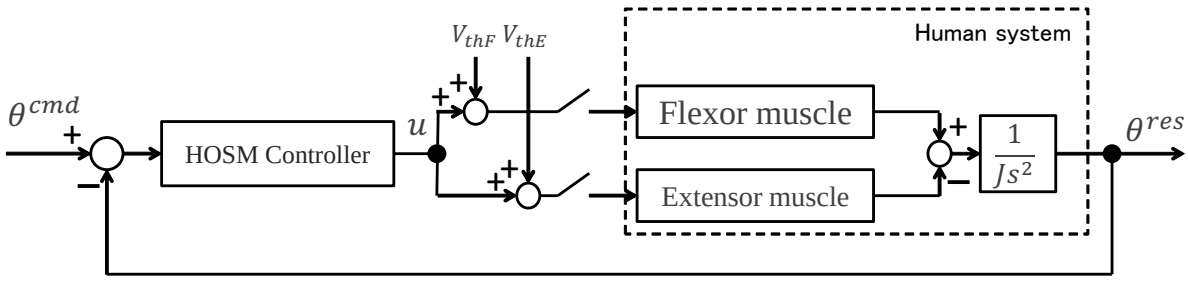

Fig. 4.1 Block diagram of the conventional method

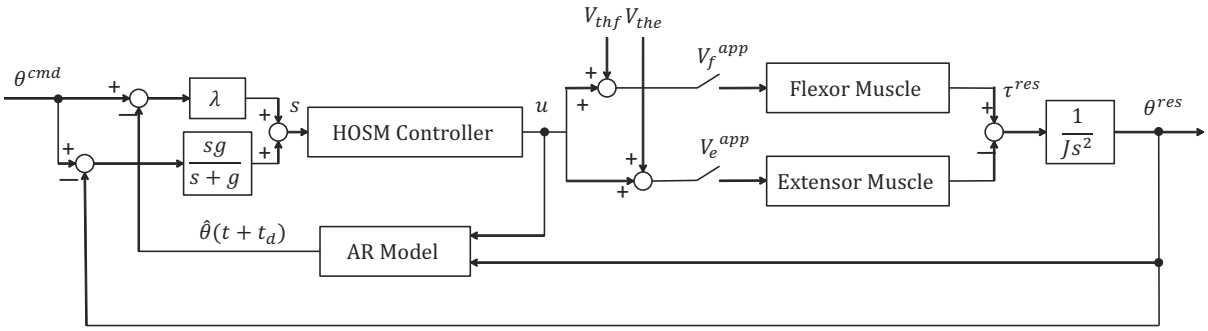

Fig. 4.2 Block diagram of the proposed method

of disturbance by motion of the elbow joints.

4.3.1 Methods

4.3.1.1 Stimulation method

In this study, the triceps brachii muscles were stimulated to extend the elbow joints, whereas the biceps brachii muscles were stimulated to bend the elbow joints. In addition, the extensor carpi radialis longus muscles were stimulated to extend the wrist joints, whereas the flexor carpi radialis muscles were stimulated to bend the wrist joints.

4.3.1.2 Conventional Method

Fig. 4.1 shows the control method in the conventional method using the HOSM controller. The input S to the sliding mode controller is derived from (10) (11) as

$$= \dot{\theta}^{cmd} - \dot{\theta}^{res} + \lambda(\theta^{cmd} - \theta^{res}). \tag{35}$$

In this section, the method of stimulating only the main movable muscle is referred to as the conventional method, “single stimulation”. In the conventional method, single stimulation is used: When the output u, which is the stimulation voltage, is positive, the flexor muscle is stimulated, and when it is negative the extensor muscle is stimulated. In addition, human muscles do not contract unless

a voltage exceeding the threshold voltage V_{th} is applied. Therefore, the following stimulation voltage amplitude V^{app} is used.

$$V_f^{app} = \begin{cases} u + V_{th} & (u > 0) \\ 0 & (u \leq 0), \end{cases} \tag{36}$$

$$V_e^{app} = \begin{cases} 0 & (u \geq 0) \\ -u + V_{th} & (u < 0). \end{cases} \tag{37}$$

4.3.1.3 Proposed Method

Fig. 4.2 shows the proposed control method. As in the conventional method, the control input u is determined using a HOSM controller; however, V_{th} is also applied to the muscles in the direction opposite to the motion. This is because in antagonist muscle stimulation, a voltage is applied to constantly stimulates the flexor muscle and the extensor muscle. Therefore, the stimulation voltage amplitude V^{app} is

$$V_f^{app} = \begin{cases} u + V_{thf} & (u > 0) \\ V_{thf} & (u \leq 0), \end{cases} \tag{38}$$

$$V_e^{app} = \begin{cases} V_{the} & (u \geq 0) \\ -u + V_{the} & (u < 0). \end{cases} \tag{39}$$

However, conventional studies have reported that the antagonizing stimulation voltage has angle dependency [44]. Fig. 4.3 shows the relationship between the voltage applied to the extensor carpi radialis extensor and the wrist joint angles. It is clear that the wrist joint moved less than ±1 deg, that is, antagonizes when 15 V is applied to the radicular carpi radial flexor of the participant for 1 s. From the figure, the relationship between wrist joint angles and antagonist muscle stimulation voltages is identified. This relationship is called "antagonist muscle mapping" in this dissertation and obtained by least squares method. In this dissertation, the threshold voltages of the radial carpi radial flexor muscle V_{thwf} are constant at 15 V, and the threshold voltages of the long radial carpi extensor $V_{thwe}(\theta_w)$ are the voltages obtained by antagonist muscle mapping.

4.3.2 Experiments

This section describes the experimental method and results. Four healthy participants (referred to as A-D) were used to test the proposed and conventional target control systems. The elbow and wrist joint angles were measured using an angle measuring device (Fig. 3.5) composed of a frame and a rotary encoder. The elbow joint angle measuring device was fixed to the arm by three belts, and the wrist joint angle measuring device was fixed the forearm by one belt and the hand gripped a bar in the device as shown in Figs. 3.5 and 4.4. Therefore, both measurement devices had little

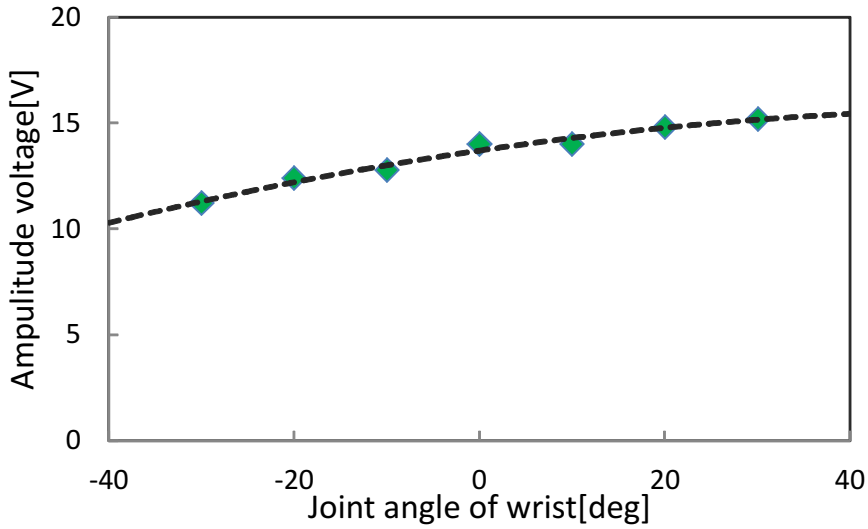

Fig. 4.3 Antagonist mapping

effect on articulation. In addition, by grasping the wrist joint angle measuring device with the hand, movements of the finger joint caused by stimulation to the forearm can be suppressed. The angular velocity was obtained by pseudo-differentiating the angle, and the cutoff frequency was set to 20 Hz. Since this study is an initial study on two-link control,participant's movements was in the horizontal direction for reducing the disturbance caused by gravity. The experimental setup is shown in Fig. 4.5.

In the conventional method, the control system described in Section 4.3.1.2 was used for both the wrist and elbow joints with a constant V_{th} of 15 V. In the proposed method, the control system described in Section 4.3.1.3 was used for the wrist joint and the control system described in Section 4.3.1.2 for the elbow joint, with V_{th} constant at 15 V. Considering fatigue of the participant's muscles and because the elbow joint is closer to the center of the body than the wrist joint, a single stimulation was applied to the elbow joint in the proposed method as well, from the assumption that disturbance due to the inertial force is small.

4.3.3 Target Control

In this experiment, the target control of the conventional and proposed methods were compared. Control using the waveform shown in Fig. 4.6 as a target value was performed by each participant.

The results of the target value control of Participant A using the conventional method and the proposed method are shown in Figs. 4.7 and 4.8, respectively. For the elbow joint, the target and measured values are indicated by a thin solid line and a thin dotted line, respectively. For the wrist joint, the target and measured values are indicated by a thick solid line and a thick dotted line,

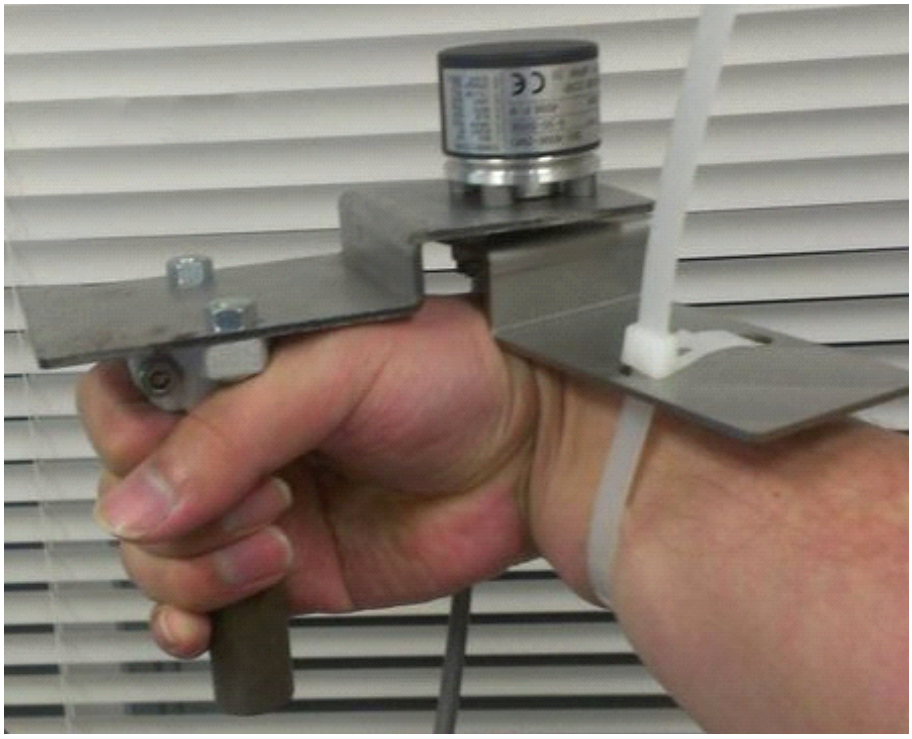

Fig. 4.4 Wrist anglular measurement device (wrist joint)

respectively. For the convenience, I show results only for participant A, but similar results were obtained for participants B-D.

The results of using the conventional method show that the wrist vibrates due to chattering. This is because the wrist joint has a lower rigidity than the elbow joint and because of the delay time peculiar to FES. It has been reported that driving of a joint by FES has a delay time of about 0.3 s [42], which was also observed in my previous research. Because of the delay, the joint is not driven even when the stimulus is applied. This causes the deviation between the target value and the measured value to become large resulting in an excessive voltage to be applied. In addition, since the wrist joints are less rigid than the elbow joints, when a large voltage is applied, the angle exceeds the target value, resulting in chattering.

Using the proposed method, chattering is suppressed by increasing the stiffness of the wrist joint by antagonistic muscle stimulation. However, near 2 s, the wrist joint was bending as the elbow joint was extended, and near 24 s the flexion of the wrist joint was delayedas the elbow joint was flexed. This is considered to be due to insufficient improvement of rigidity by antagonistic muscle stimulation. Previous studies have reported that the joint rigidity increases as the stimulation voltage of both the active and antagonistic muscles increases [44], and the antagonist muscle mapping is suitable for

Fig. 4.5 Scene of experiment

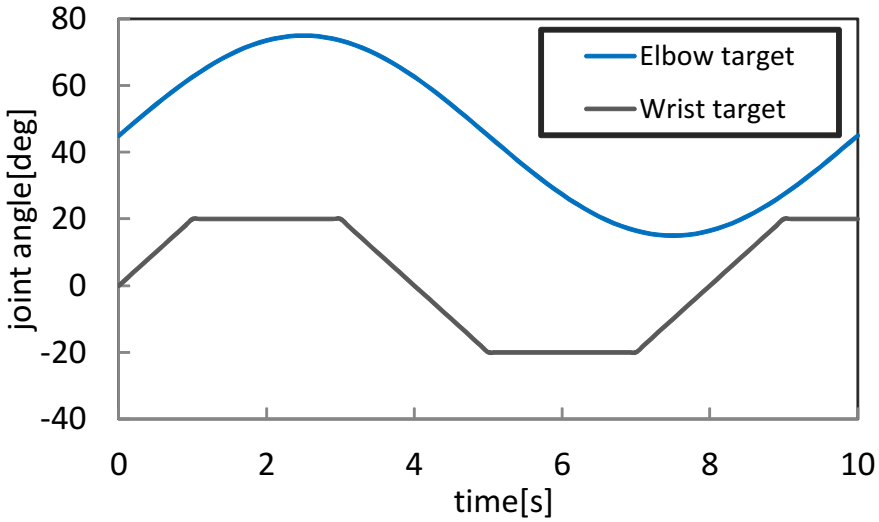

Fig. 4.6 Waveform of target angle

two-link movement.

4.3.4 Summary

In this section,bilateral control of planar 2DoF movement of human arms using antagonist muscle stimulation was verified. The results show that improving the wrist joint rigidity using antagonistic muscle stimulation suppresses disturbance, such as the inertial force exerted by the elbow joint motion on the wrist joint, thereby improving the performance of two-link human arm control.

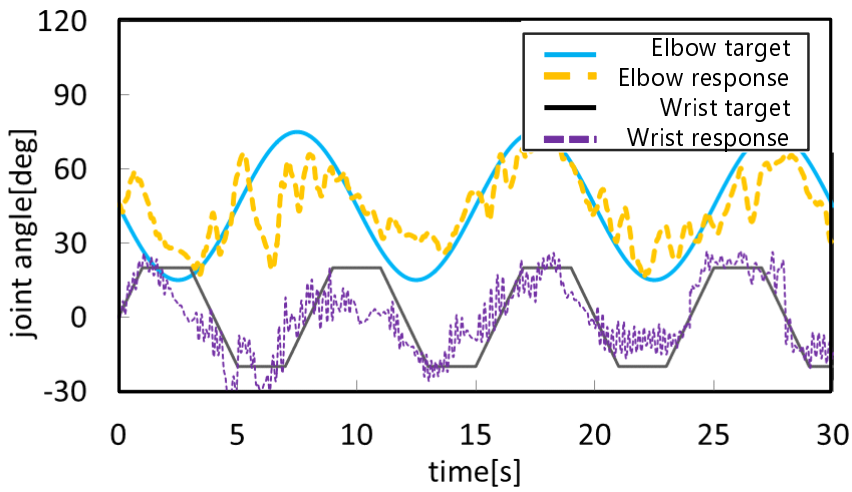

Fig. 4.7 Experimental result of conventional method

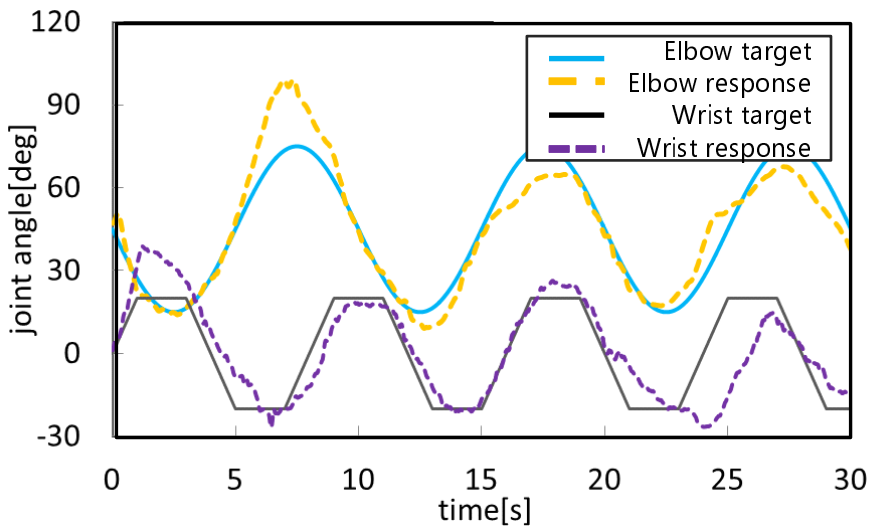

Fig. 4.8 Experimental result of proposed method

4.4 Control of Two Links Between the Shoulder and Elbow using Noninvasive FES

In this section, a method of controlling the elbow joint and shoulder joint using surface electrode is proposed and examined.

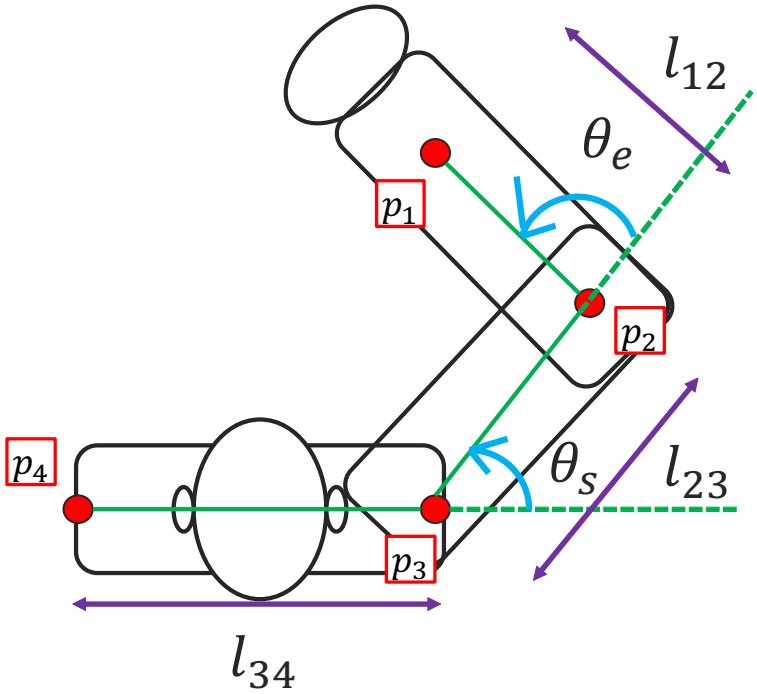

Fig. 4.9 Marker mounting position and the definition of each joint angle

4.4.1 Methods

In these experiments, two healthy participants (referred to as A, and B) were used to test the proposed system. In addition, electrocardiogram measurment and diagnosed from Saitama University Health Center were performed on both patients to ensure they would not be hindered or injured in the experiment.

4.4.1.1 Measure angle

In this experiments, the joint angles were measured using Optitrack (NaturalPoint, USA) which is a three-dimensional position measuring device. The marker mounting position and the definition of each joint angle are shown in Fig. 4.9. The attachment position of the marker is designated as p_n, where n indicates the number of the marker. In addition, e indicates the elbow joint, and the s indicates the shoulder joint. l_{xy} indicates the distance from the measured point x to the point y.

4.4.1.2 Selecting Stimulation Frequency

The relationship between the stimulus frequency for each muscle and the force on the participant was examined. Muscles were stimulated with 20 V and a stimulation frequency ranging from 20-200 Hz in increments of 20 Hz. The experimental setup is presented in Fig. 2.3. Participants were placed

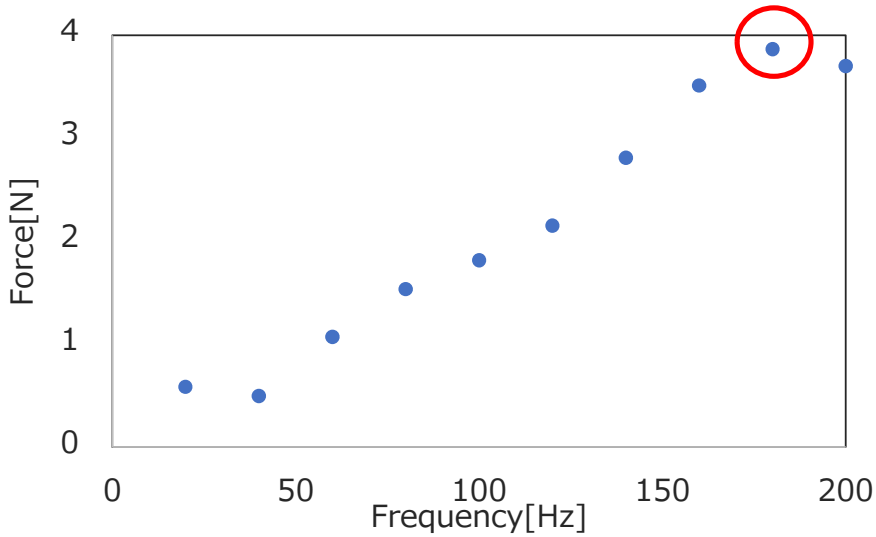

Fig. 4.10 Relationship between stimulation frequency and exerted force [Participant A, deltoid muscle (front)]

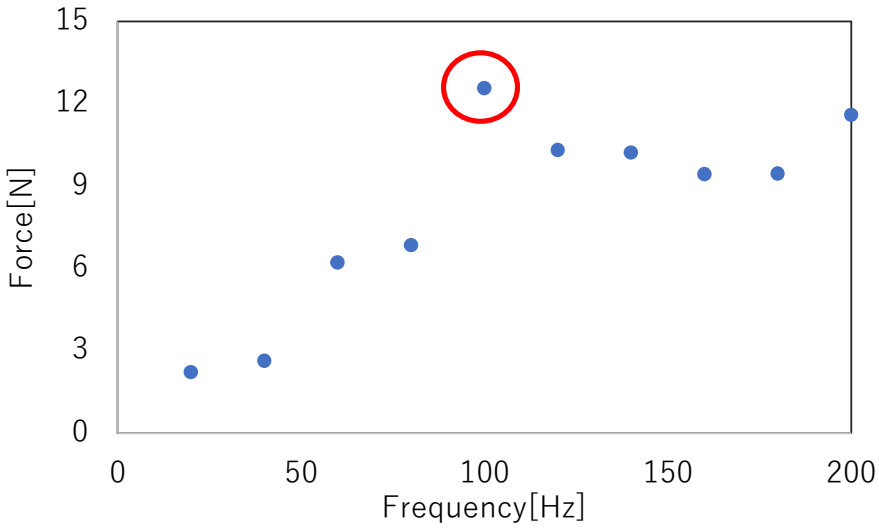

Fig. 4.11 Relationship between stimulation frequency and exerted force [Participant B, deltoid muscle (rear)]

in a chair with their arm parallel with the floor. The hands of the participants were fixed with Gibbs such that the wrist joint could not exert a force. When measuring the force exerted by the shoulder joint, the elbow joint was also fixed with Gibbs. The participants' arms were set up to allow the hands to hit the a force sensor. Figs. 4.10 and 4.11 show the results of stimulation on the deltoid muscle (front) of participant A and the stimulation force applied to the deltoid muscle (rear) of participant B, respectively.

Fig. 4.12 State of the position control experiment

From the results, it was shown that the exerted force saturated/decayed when a certain stimulation frequency was exceeded.

The method for determining the stimulus voltage was similar to the conventional method described in section 2.4.1.

4.4.2 Experiments

The state of the position control experiment is shown in Fig. 4.12. The participants mounted the markers as shown in Fig. 4.9, and the angles were measured. In addition, the stimulus was applied through the attached electrode, and the angle of the joint was controlled. The participant lifted himself so that his upper arm would be parallel to the floor. Consequently, the abduction direction of the shoulder joint was not controlled by the FES, but was raised by the free movements.

In the experiment, the simultaneous control of the elbow joint and shoulder joint was performed. The target value of the angle is shown in Fig. 4.13. To avoid equalizing the periods of the two angle target values, angle target values with different cycles were set.

The results of participant A and B are shown in Figs. 4.14 and 4.15, respectively.

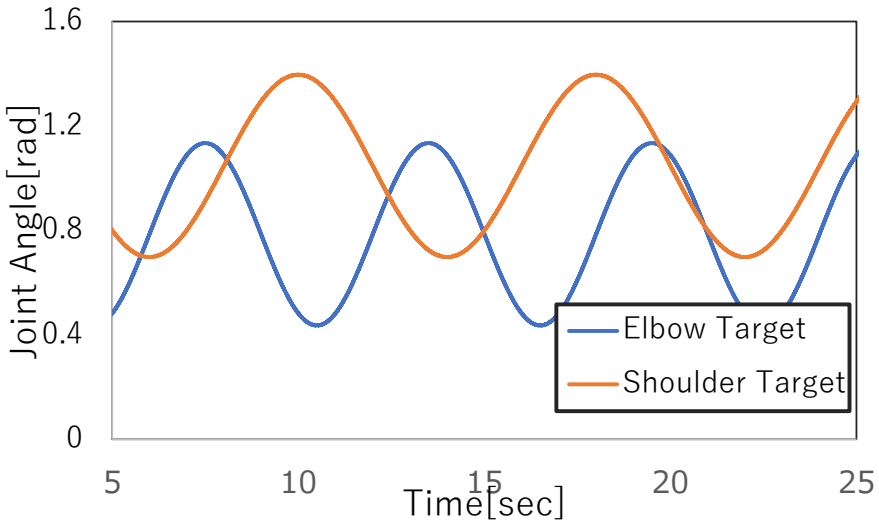

Fig. 4.13 Waveform of the target angles

From the results, it can be seen that the measured values of the two angles generally coincide with the target values. From this result, it was shown that the elbow joint and the shoulder joint can be controlled without using fixtures.

4.4.3 Summary

In this section, control of elbow and shoulder joints using surface electrodes was examined. Good control performance was also obtained as a result of simultaneously controlling the two axes of the elbow joint and the shoulder joint.

4.5 Summary of Chapter 4

This chapter discussed a two-joint control technique using the FES. It was shown that the use of antagonistic muscle stimulation increases the stiffness and allows for control with suppressed inertia forces. It was shown that this method could be applied to other joints as well, so it is expected that the method applied to other joints.

It was shown that the frequency modulation method could control the shoulder joint, which was difficult to control by the conventional method using constant frequency. Since the shoulder joint's motion is essential for the upper limb movements, it is expected that the number of applications using FES will increase.

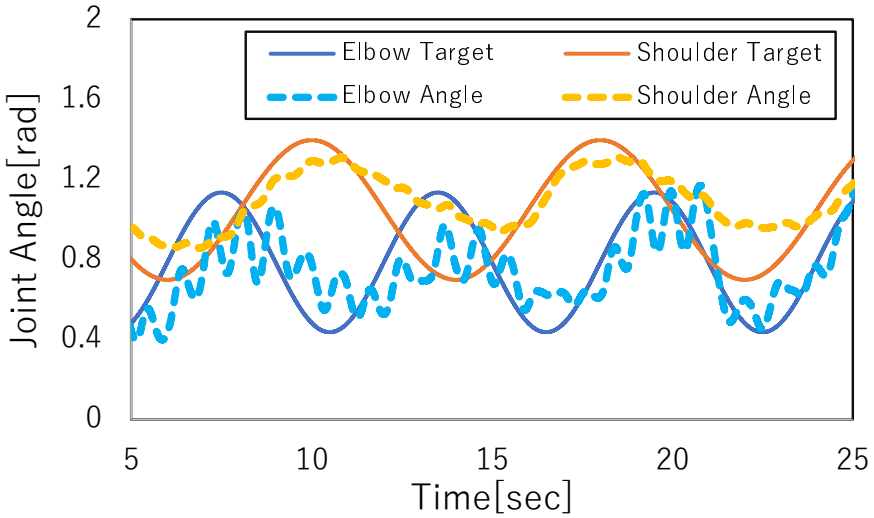

Fig. 4.14 Experimental results of the elbow joint and shoulder joint control for participant A

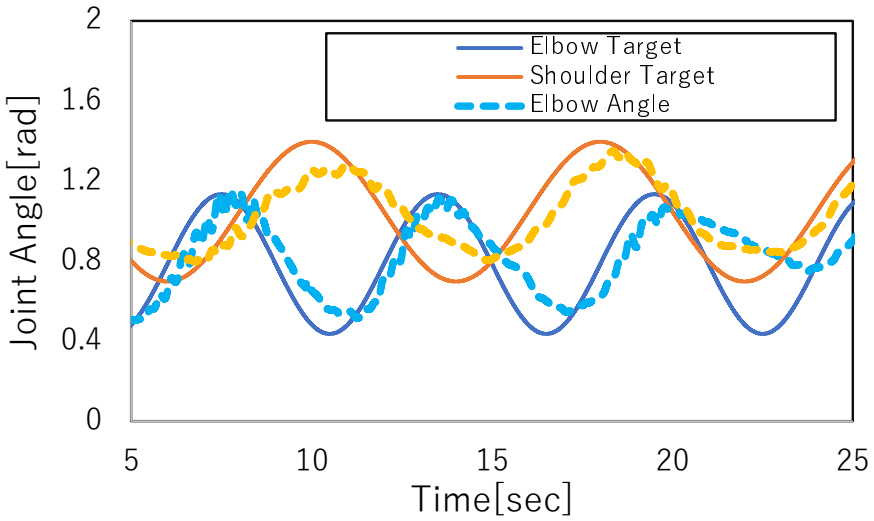

Fig. 4.15 Experimental results of the elbow joint and shoulder joint control for participant B

Chapter 5 Bilateral Control Using FES

In this chapter, bilateral control using FES is described. The purpose of this dissertation is to improve the performance of a pseudo-force presentation system using the FES based on modeling and control performance improvement methods. In this chapter, a bilateral control system that integrates some of the methods mentioned above was validated.

5.1 Bilateral Control of Two-Link Human Arms Using Antagonist Muscle Stimulation

This section describes bilateral control using the two-joint control method with antagonistic muscle stimulation. The controller is the same as in section 4.3.1.3. Here, the angle command value of the master θ_m^{cmd} is the angle response value of the slave θ_s^{res}, and the angle command value of the slave θ_s^{cmd} is the angle response value of the master θ_m^{res}.

5.1.1 Free motion

In this experiment, when position control is performed by the proposed method in a state without disturbance such as obstacles, the slave verifies whether it can follow the movement of the master. Chairs for the master and the slave were placed back to back, and the master (slave) could not see the movement of the arm of the slave (master). The participants were arranged into two master-slave pairs. One participant of the pair was the master and the other was the slave for 30 s, and then the participants in the pair exchanged their roles. Placing constraints on the movements of the master may cause the participant to learn the movements, so the master was allowed free movement.

Fig. 5.1 shows the results for the master A-slave B pair, and Fig. 5.2 shows the results for the master D-slave C pair. The elbow and wrist joint angles of the master are shown by a thin solid line and a thick solid line, respectively. The elbow and wrist joint angles of the slave are shown by a dark dotted line and a thick dotted line, respectively.

In the results shown in Fig. 5.1, the slave's wrist joint fluctuation was small for about 9 s from the start of the experiment, so it cannot follow the master's fast motion. Also, near 20 s or around 25 s, the slave movement was about 1 s behind the master movement when the master was extending and bending the wrist joint. I believe this is because the parameters W, ρ, and λ of the HOSM controller are insufficient and the input u is small and the force cannot be fully exerted in the direction of the target value.

In the results shown in Fig. 5.2, apart from the movement near 6 s, the slave movement of the slave

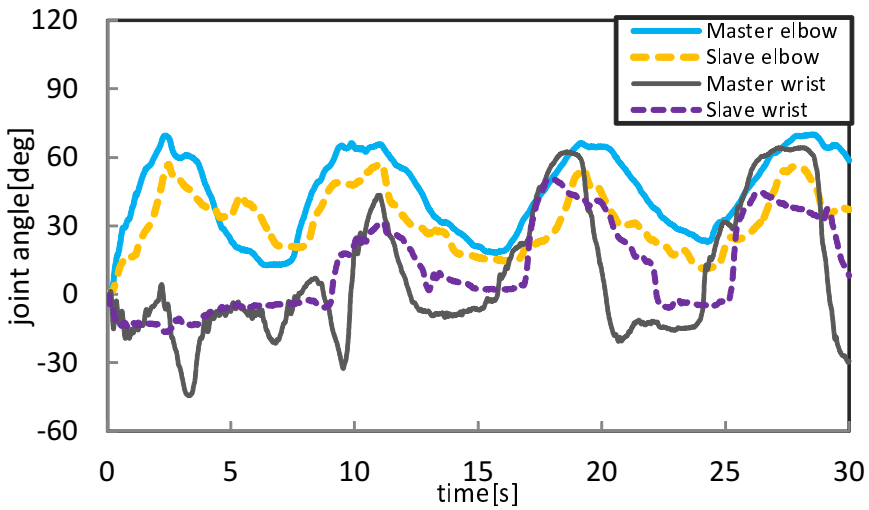

Fig. 5.1 Participant A as master and participant B as slave

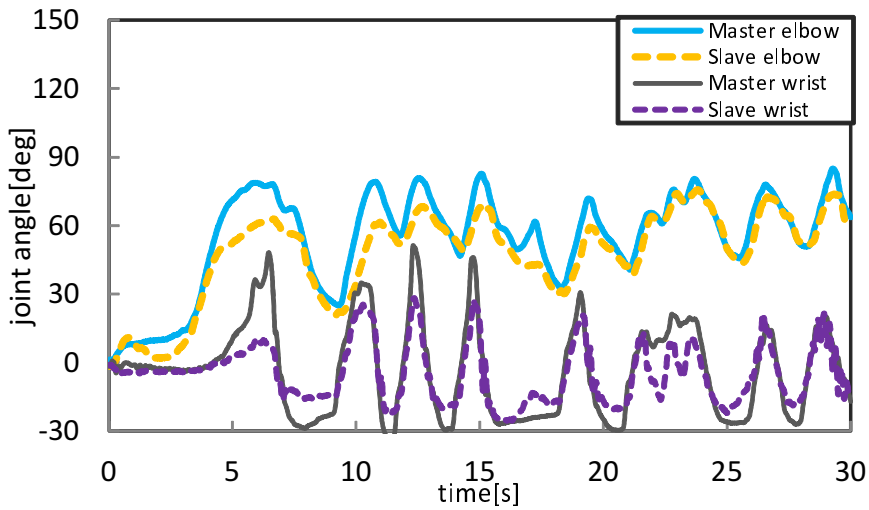

Fig. 5.2 Participant D as master and participant C as slave

followed the master movement. However, around 22 s, the wrist joint of the slave was moving due to the inertial force caused by the fast motion of the elbow joint. The improvement of rigidity given by the antagonistic muscle mapping used in this experiment is not sufficient to remove the effect of the inertial force caused by fast motion.

5.1.2 Contact motion

In this experiment, the slave made contact with an fixed obstacles and the master attempted to recognize the contact position. The two chairs set to back to back as before. An object was placed on the inner forearm or the palm of the slave 5 s. The master then attempted to recognize the contact

Table 5.1 Participant A as master and participant B as slave

contact positions of the slave	response by master
forearm	forearm
palm	palm
forearm	palm
forearm	palm
palm	palm
palm	forearm
accuracy rate	50%

Table 5.2 Participant B as master and participant A as slave

contact positions of the slave	response by master
forearm	forearm
palm	palm
forearm	forearm
forearm	forearm
palm	forearm
palm	palm
accuracy rate	83%

Table 5.3 Participant C as master and participant D as slave

contact positions of the slave	response by master
forearm	forearm
forearm	forearm
palm	palm
forearm	forearm
forearm	forearm
palm	forearm
accuracy rate	83%

Table 5.4 Participant D as master and participant C as slave

contact positions of the slave	response by master
palm	palm
forearm	forearm
forearm	forearm
palm	palm
forearm	forearm
palm	palm
accuracy rate	100%

position. The experiment was conducted six times for each participant with random contact positions. Prior to the experiment, each pair of participants practiced identifying the contact position for 30 s. The slave contact position, the master response, and the correct answer rate for each experiment are given in Tables 5.1-5.4.

In the results given in Tables 5.2-5.4, the correct answer rates are over 80% and the master participants are able to recognize the contact position of the object on the slave. This result shows that it is possible to convey the contact position of the slave to the master in bilateral control using FES, which is a very meaningful result considering practical applications. However, the correct answer rate was only 50% for the experimental result given in Table 5.1. The reason was probably a delay in the movement of the wrist joint when participant B was a slave, as shown in Fig. 5.1. In the position-symmetric-type bilateral controller used in this experiment, the reaction force to the master is determined by the deviation between the positions of the master and the slave; as a result, a delay causes the reaction force to the master to become large. Therefore, even when no object was placed on the slave hand, the reaction force to the master became so large that the master thought that the object was placed on the hand. As mentioned in Section 5.1.1, improvement of the control system is

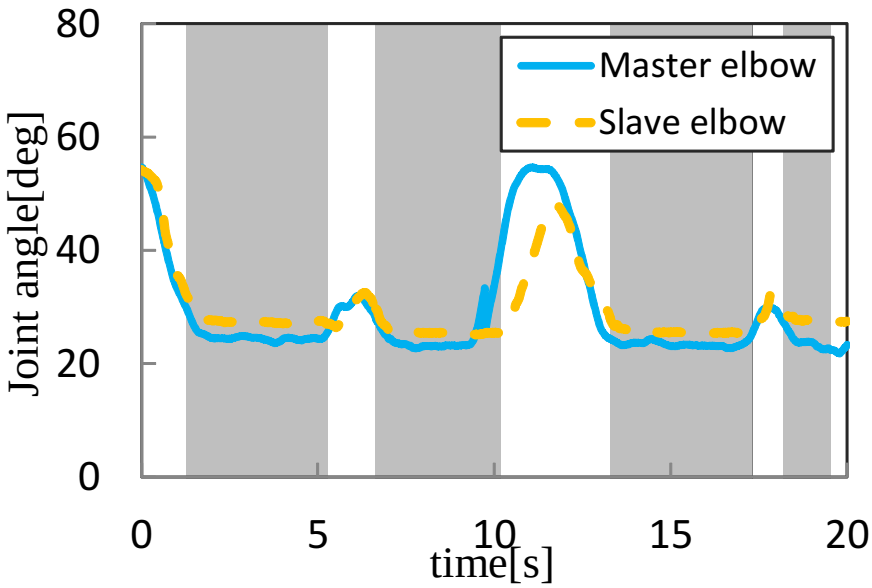

Fig. 5.3 Movement of elbow in contact behavior

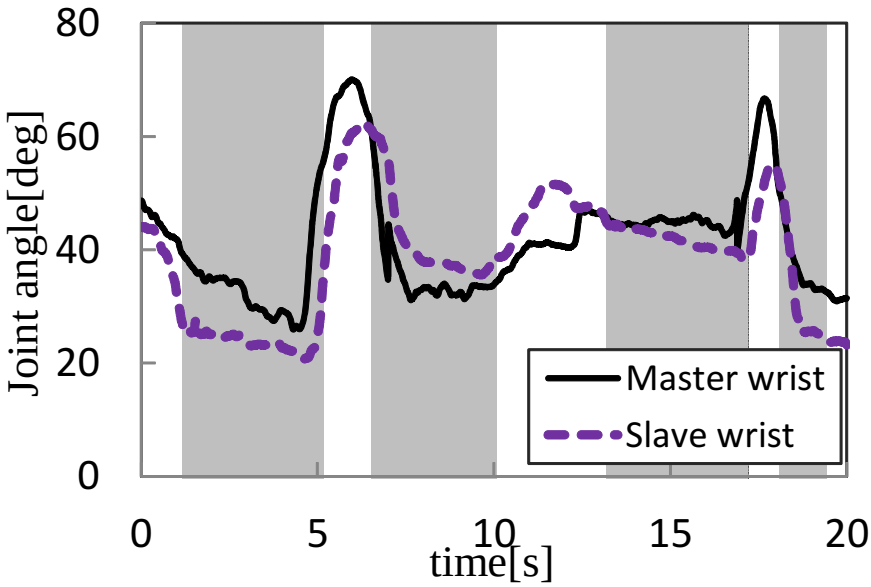

Fig. 5.4 Movement of wrist in contact behavior

necessary to improve the correct answer rate.

Figs 5.3 and 5.4 show results of when the forearm contacts and when the hand tip contacts, respectively. In both cases, participant C is the master and participant D is the slave. These graphs show that about 5 degrees of overshoots occurred, however, the master stopped moving when the slave touched an obstacle. Therefore, it was expected that the master could perceive the position of

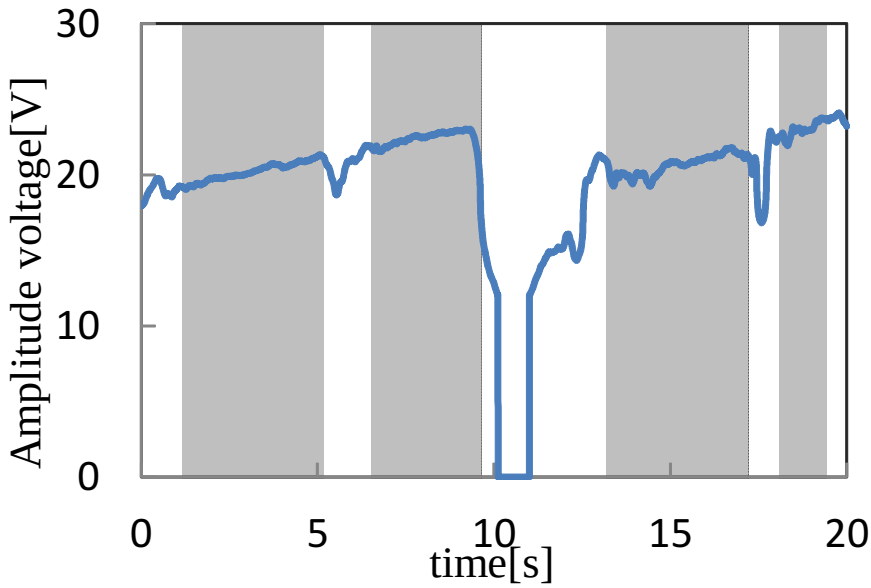

Fig. 5.5 Amplitude voltage to flexor muscle of elbow during experiment shown in Fig. 5.3

obstacle. Fig 5.5 shows voltages applied to flexor muscle of the master during experiment shown in Fig. 5.3. Since the obstacle is placed in front of the slave, the flexor muscle of the master is stimulated when the slave touches. From an increase of voltage when contact occurred in Fig 5.5, it is presumed that the master perceives the position as the reaction force increases. However, the voltage increased while the deviation of positions between the master and the slave has not changed. In other words, the reaction force increased while the values of reaction force should be unchanged. Thus, the reaction force was not transmitted to the master properly.

5.1.3 Summary

In this section, bipartite bilateral control using antagonistic muscle stimulation was discussed. The results show that the proposed antagonist muscle stimulation is also useful in bilateral control.

5.2 Bilateral Control Using FES Based on Dynamic Model Approximation

5.2.1 Background

Generally, in bilateral control, achieving good haptic transmission requires the establishment of force action-reaction, in addition to position synchronization [71][72]. The position-symmetric and force-reflecting type bilateral control methods were proposed. The control goal of position-symmetric

bilateral control is synchronizing the positions of the master and the slave. By contrast, the force-reflecting type bilateral control transmits the slave's reaction force to the master, so that the master's feeling of operation is increased heavily. Moreover, the force action-reaction is not included in the control goal; therefore, a method that makes it a control goal to establish both position synchronization and force action-reaction in bilateral control using FES has not been developed.

One of the reasons owing to which it is difficult to establish both position synchronization and force action-reaction in bilateral control using FES is that the relationship between the stimulus value and the exerted torque in FES is unclear. In a conventional study using force-reflecting type bilateral control, this relationship was approximated through a static model. However, the relationship between the electrical stimulation and the exerted force is likely to be a dynamic system because of the electrochemical reactions that occur inside the body when a muscle is contracted owing to electrical stimulation. Studies have been reported to estimate the exerted force by approximating the chemical reactions inside the body through mathematical expressions[31][33] or using myogenic potential[73][74]. However, inverse models (*i.e.*, models that determine the stimulus value required to exert the desired force), are difficult to create; hence, they cannot be incorporated into force control. It has already been reported that a linear dynamic model[39][75] can approximate the relationship between the stimulus value and the exerted force. Compared to non-linear models, using a linear model makes it easier to create inverse models and incorporate them into the control system.

In this section, 4ch bilateral control using FES based on a dynamic model is proposed. 4ch bilateral control is a method in which the control target is to establish both the synchronization of position and the action-reaction of the force in the master and the slave[71][72]. It should be noted that the purpose of this study is to achieve the control goals of synchronization of positions and establishment of force action-reaction and not to verify the workability and comfort of 4ch bilateral control using FES. Furthermore, it is expected that using the dynamic model will improve the accuracy of the estimation of the reaction force and that of the inverse model, thereby improving the force control performance and the establishment of the action-reaction of the force.

5.2.1.1 Methods

5.2.1.1.1 4ch Bilateral Control

The goal of 4ch bilateral control is not only to synchronize the positions of the master and slave but also to establish the force action-reaction at the master and slave. Therefore, in addition to (1), the control goal includes the following:.

$$f_m + f_s = 0, \tag{40}$$

where f denotes the exerted force and disturbance force. In general, 4ch bilateral control is considered to have the best performance. Therefore, the evaluation in this dissertation was conducted based on whether (1) and (40) were valid or not.

5.2.1.2 Models and Control Systems

5.2.1.2.1 Model Identification

Two models were used in this study to approximate the relationship between applied voltage V^{app} and exerted torque τ^{ext}: a static model and a dynamic model. This section describes each model's overview, identification methods, and the parameters identified for each participant.

5.2.1.2.2 Static Model

The static model was used in the 4ch bilateral control using a static model experiment. The parameters are obtained that is the threshold voltage V_{th} required to drive the participants' joints and the relationship between the voltage and torque K_{vt}. The experiment setup is illustrated in Fig. 2.3. The participants were seated in a chair, and their forearms were fixed to a torque sensor (PFS055YA251U6, "Leptrino, Japan"); moreover, their arms were placed such that they were parallel to the floor. In the experiment, the applied voltage was increased from 6 V to 24 V, with increments of 1 V.

The results obtained when the voltage was applied to the flexor muscle of participant A are plotted in Fig. 5.6, where V_{th} is the voltage immediately before 0 Nm, and K_{vt} is the slope of the straight line approximation of the applied voltage V^{app} and exerted torque τ^{ext}. In addition, it is reported that a delay of approximately 0.1 s occurs from the application of the voltage to the steady-state response. Therefore, exerted torque τ^{ext} can be expressed as (41).

$$\tau^{ext} = \begin{cases} K_{vt}(V^{app} - V_{th})e^{-0.1s} & (V^{app} > V_{th}) \\ 0 & (V^{app} \leq V_{th}). \end{cases} \tag{41}$$

The $\hat{V}_{th}$ and $\hat{K}_{vt}$ values for each participant are detailed in Table 5.5, where the subscripts f and e represent the flexor and extensor muscles, respectively. Moreover, $\hat{\bigcirc}$ represents the estimated values. The value of $\hat{V}_{th}$ was also utilized in the dynamic model described below.

5.2.1.2.3 Dynamic Model

The dynamic model was implemented in the 4ch bilateral control using a dynamic model experiment. As plotted in Fig. 5.7, the transfer function of the applied voltage and exerted torque was determined by measuring the torque response when the sine sweep voltage was applied. A voltage that is more than the threshold voltage is required to start the movement, as described in section 5.1.1. Therefore, a bias voltage that was 10 V greater than V_{th} was added. (The waveform in Fig. 5.7 presents a case

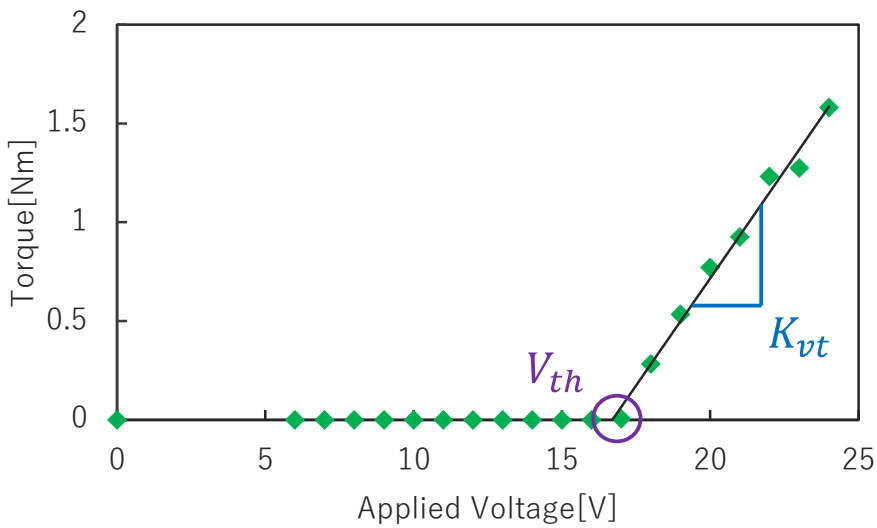

Fig. 5.6 Relationship between the applied voltage and exerted torque (flexor muscle of participant A)

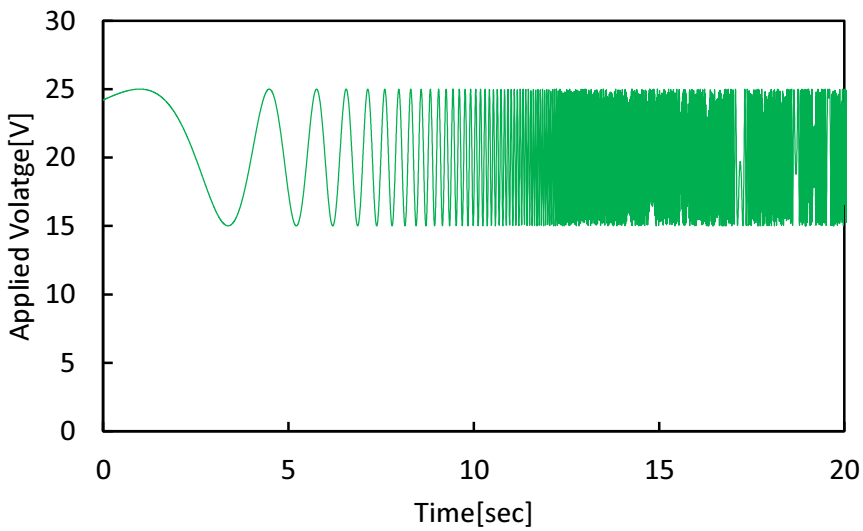

Fig. 5.7 Input voltage for transfer function identification

where the bias voltage was set to 20 V.) Moreover, a sine wave of 5 V amplitude was used with a varying frequency.

The board diagrams of the applied voltage and exerted torque in the flexors of participants B and C are graphed in Figs. 5.8 and 5.9, respectively. Specifically, the decimation was performed at 50 Hz, and these board diagrams were obtained using the fast Fourier transform. The voltage was applied for 10.24 s, and 512 samples of data were obtained. It was observed that the gain characteristic of the first-order lag system decreased by -20 dB/dec from the cutoff frequency. In this study, the relationship between the applied voltage and the applied torque was approximated using a first-order

lag system, as depicted in Figs. 5.8 and 5.9. The phase characteristics could not be utilized in this study for identification and verification because of the noise and the dead time, which reduce the accuracy of measurements. It should be noted that there exists a delay of approximately 0.04 s from the application of voltage to the generation of torque. Moreover, the values of dead time in the static and dynamic models are different. This is because the delay time required to reach the steady-state in the static model and that required to start movement in the dynamic model are the corresponding definitions of dead time in the respective models. The transfer function of the applied voltage and the exerted torque is expressed as (42).

$$G(s) = \frac{\tau^{ext}(s)}{V^{app}(s) - V_{th}} = \frac{B_0}{A_1 s + 1} e^{-0.04s}, \tag{42}$$

where s is a Laplace operator. Moreover, A_1 and B_0 are positive constants, which are calculated through multiple regression analysis. The values of these constants for each participant are provided in Table 5.5.

5.2.1.2.4 Determination of Applied Voltage

In this experiment, the flexor and extensor muscles of the elbow joint were stimulated. Therefore, it was necessary to determine the applied voltage to each muscle from its torque reference value τ^{ref}. The approximate applied voltage and the exerted torque models defined by (41) and (42) includes dead time. When the applied voltage is calculated from the torque reference value, the future torque reference value is used. However, it is not possible in practice. Therefore, the dead time is not included in the approximation for the control plant. In phase of determining the applied voltage, (41) and (42) can be rewritten with $\tau^{ext} = \tau^{ref}$ as follows:

$$\tau^{ref} = \begin{cases} P_{wo}(s)(V^{app} - V_{th}) & (V^{app} > V_{th}) \\ 0 & (V^{app} \leq V_{th}). \end{cases} \tag{43}$$

$$\frac{\tau^{ref}(s)}{V^{app}(s) - V_{th}} = G(s)e^{0.04s} = P_{wo}(s), \tag{44}$$

where, $P_{wo}(s)$ is the relationship between the applied voltage and the exerted torque without dead time, and the values identified for each model were used during the experiments. In the 4ch bilateral control experiment using a static model, the model was set to $P_{wo}(s) = K_{vt}$. By contrast, in the experiments of position-symmetric bilateral control and bilateral control using the dynamic model, the setting was $P_{wo}(s) = \frac{B_0}{A_1 s+1}$. The applied voltage V^{app} is expressed as (45) and (46) using V_{th} and τ^{ref}.

$$V_f^{app} = \begin{cases} \frac{\tau^{ref}}{\hat{P}_{wof}(s)} + \hat{V}_{thf} & (\tau^{ref} > 0) \\ 0 & (\tau^{ref} \leq 0), \end{cases} \tag{45}$$

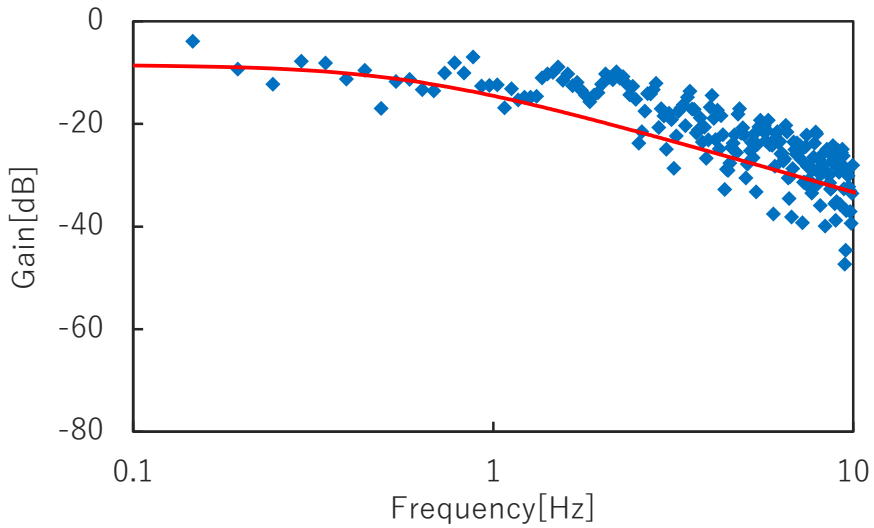

Fig. 5.8 Board diagrams of the applied voltage and exerted torque in the flexors of participant B

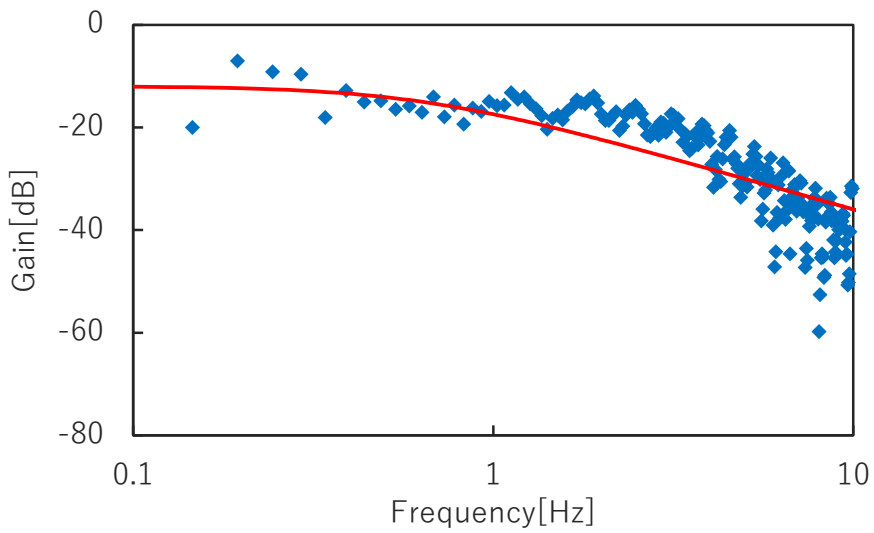

Fig. 5.9 Board diagrams of the applied voltage and exerted torque in the flexors of participant C

$$V_e^{app} = \begin{cases} 0 & (\tau^{ref} \geq 0) \\ -\frac{\tau^{ref}}{\hat{P}_{woe}(s)} + \hat{V}_{the} & (\tau^{ref} < 0). \end{cases} \tag{46}$$

The position-symmetric bilateral control is used to compare the 4ch bilateral control performance using a dynamic model with and without torque control; therefore, the model used for position-symmetric bilateral control is dynamic as well. A block diagram of the relationship between τ^{ref}, V_f^{app}, and V_e^{app} is illustrated in Fig. 5.10.

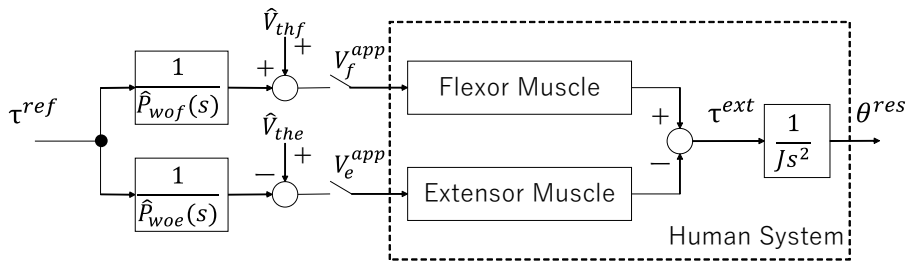

Fig. 5.10 Block diagram of the relationship between torque reference values, applied voltage, and human systems

5.2.1.2.5 RTOB

We estimated the reaction torque using RTOBs [76]. Viscous and elastic friction of human elbow joints have been reported to be small [77]. Therefore, the motion of joints is expressed as follows:

$$J\ddot{\theta} = P_w(s)(V^{app}(s) - V_{th}) - \tau^{dis}, \tag{47}$$

where J, θ, and τ^{dis} are the moment of inertia, joint angle, and disturbance torques, respectively. In addition, $P_w(s)$ is the relationship between the applied voltage and the exerted torque with dead time, and the values identified for each model were used during the experiments. Equations (41) and (42) can be rewritten with $\tau^{ext} = \tau^{ref}$ as follows:

$$\tau^{ref} = \begin{cases} P_w(s)(V^{app} - V_{th}) & (V^{app} > V_{th}) \\ 0 & (V^{app} \leq V_{th}). \end{cases} \tag{48}$$

$$\frac{\tau^{ref}(s)}{V^{app}(s) - V_{th}} = G(s) = P_w(s). \tag{49}$$

The control system was implemented as $P_w(s) = K_{vt}e^{-0.1s}$ in the experiments of 4ch bilateral control using the static model and $P_w(s) = \frac{B_0}{A_1 s+1}e^{-0.04s}$ in 4ch bilateral control experiments using the dynamic model. By contrast, to provide a fair comparison of the torque response values, only those estimated by the dynamic model were used for verification in all experiments.

In this study, the spontaneous torque exerted by a human was also considered as a disturbance. Therefore, disturbance torque is a generic term used for the counter-torque and spontaneously exerted torque from an object in contact. Equation (47) can be rewritten as

$$\tau^{dis} = P_w(s)(V^{app}(s) - V_{th}) - J\ddot{\theta}. \tag{50}$$

τ^{dis} is calculated using $\ddot{\theta}$ and $V^{app}(s)$ via (50). In this study, τ^{dis} is assumed to be the torque response value of human τ^{res}. Equation (50) can be rewritten as (51) using the estimated model

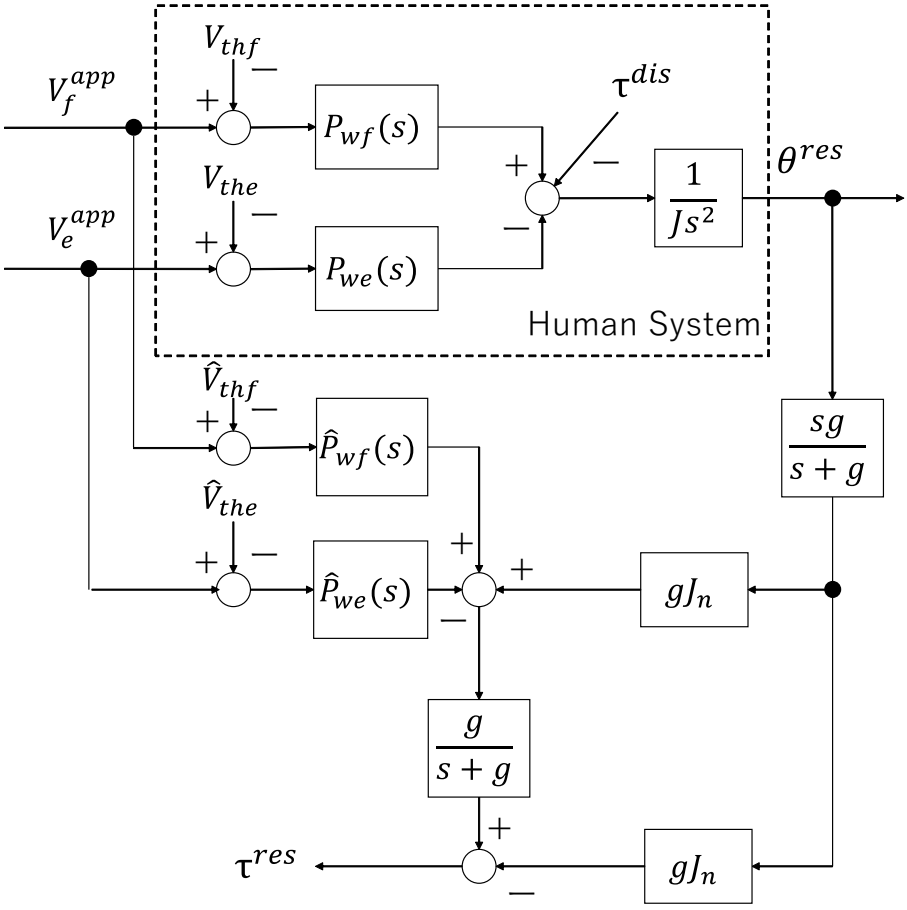

Fig. 5.11 Estimation of the torque response value

parameters.

$$\tau^{res} = -\hat{P}_{wf}(s)(V_f^{app}(s) - \hat{V}_{thf}) + \hat{P}_{we}(s)(V_e^{app}(s) - \hat{V}_{the}) - J_n\ddot{\theta}. \tag{51}$$

The nominal value of the moment of inertia of the elbow joint, J_n, of the participants was set at 0.043 kg·m^2 for all participants, with reference to previous studies[77]. The block diagram constructed to estimate τ^{res} is illustrated in Fig. 5.11.

5.2.2 Experiments

The participants were five healthy men and one healthy woman in their twenties. They are referred to as A-F in this dissertation. The length from the elbow joint to the tip of the hand and the arm circumference of the forearm for each participant are provided in Table 5.5. To protect their personal information, their age, gender, and weight are not listed. The experiment was approved by the Ethics Committee of University of Tsukuba. Prior to conducting the experiment, the participants were

briefed about the experiment, and informed consent was obtained from them.

Table 5.5 Participants' physical information and identified parameters

			Flexor muscle				Extensor muscle			
Participant	Length from the elbow joint to the tip of the hand [m]	Length of the forearm's arm circumference [m]	Threshold voltage $\hat{V}_{thf}$[V]	Slope of voltage-torque $\hat{K}_{vtf}$[Nm/V]	Gain $\hat{B}_{0f}$[Nm/V]	Time constant $\hat{A}_{1f}$[sec]	Threshold voltage $\hat{V}_{the}$[V]	Slope of voltage-torque $\hat{V}_{vte}$[Nm/V]	Gain $\hat{B}_{0e}$[Nm/V]	Time constant $\hat{A}_{1e}$[sec]
A	0.4	0.21	16.6	0.26	0.13	0.053	17.5	0.29	0.095	0.025
B	0.45	0.23	11.0	0.27	0.093	0.015	15.2	0.24	0.029	0.029
C	0.45	0.28	9.8	0.66	0.33	0.052	8.2	0.3	0.1	0.041
D	0.43	0.31	8.3	0.28	0.17	0.021	12.8	0.16	0.066	0.037
E	0.42	0.25	10.2	0.44	0.23	0.032	13.6	0.22	0.1	0.036
F	0.42	0.28	11.2	0.56	0.31	0.046	9.2	0.41	0.24	0.028

In this study, experiments were conducted using three bilateral control systems: two systems that employed comparative methods and one that implemented the proposed method.

- position-symmetric type (Symmetric),
- 4ch type using a static model (4ch static),
- 4ch type using a dynamic model (4ch dynamic).

The purpose of this study is to verify whether the 4ch bilateral control using a dynamic model establishes position synchronization and force action-reaction. The two comparative methods are relatively easy to construct. Therefore, it is preferable to employ them in the control systems if the objective can be achieved using these methods as well.

It is unfair to compare the results of different master motions in bilateral control; however, it is also unfair to determine the master's motion in advance because the participant can predict it. Therefore, I first performed bilateral control with a virtual human, which numerically simulates human motion and a participant (hereafter referred to as bilateral control of virtual human–human). Further, by unifying the exerted force of the virtual human, the experimental results obtained for the same movement. Subsequently, bilateral control was done between the participant and participant, and the results of the experiment between people were verified (hereinafter referred to as bilateral control of human–human).

5.2.2.1 Bilateral Control

5.2.2.1.1 Position-symmetric Bilateral Control

The conceptual diagram of the position-symmetric bilateral control is illustrated in Fig. 5.12. In position-symmetric bilateral control, position control is implemented in both the master and the slave. In this study, a high-order sliding mode (HOSM) controller was used as an angle controller. The control target in the sliding mode controller was that the angle response value θ^{res} should converge to target angle value θ^{cmd} without being affected by the uncertainty and disturbance of the model. Accordingly, the control goal of the sliding mode controller is defined as follows:

$$S(x,t) = (\frac{d}{dt} + \lambda)^{n-1} e(t) = 0, \tag{52}$$

where λ is a positive constant, and $e(t)$ denotes the difference between target value θ^{cmd} and measured value θ^{res}. Therefore, error $e(t)$ can be defined as follows:

$$e(t) = \theta^{cmd} - \theta^{res}. \tag{53}$$

Consequently, the control system was designed such that the value of sliding variable S was zero, and the control goal would be achieved when S became zero. In addition, n is the number of input variables. In this study, the angle and velocity were the inputs; hence, $n = 2$. Equation (52) can be rewritten using subscripts m and s as follows:

$$\begin{cases} S_m = (\dot{\theta}_s - \dot{\theta}_m) + \lambda(\theta_s - \theta_m), \\ S_s = (\dot{\theta}_m - \dot{\theta}_s) + \lambda(\theta_m - \theta_s). \end{cases} \tag{54}$$

I also utilized the super-twisting algorithm to implement the HOSM controller. In this algorithm, control input u_θ is determined based on the control law represented by (55) and (56).

$$\begin{cases} u_{\theta m} = -\lambda \cdot |S_m|^\rho \cdot \mathrm{sgn}(S_m) + u_{am} \\ \dot{u}_{am} = -W \cdot \mathrm{sgn}(S_m), \end{cases} \tag{55}$$

$$\begin{cases} u_{\theta s} = -\lambda \cdot |S_s|^\rho \cdot \mathrm{sgn}(S_s) + u_{as} \\ \dot{u}_{as} = -W \cdot \mathrm{sgn}(S_s), \end{cases} \tag{56}$$

where W, ρ, and λ are positive constants, and ρ is preferably 0.5 when $n = 2$. Even though the values of W and λ are related to the parameter of the controlled object, $W = 0.3$ and $\lambda = 3.0$ through trial and error is set. These parameter values were used for all the experiments and participants. The relationship between the HOSM controller output u_θ and the applied voltage V^{app} was defined as follows:

$$V^{app} = u_\theta + \hat{V}_{th}. \tag{57}$$

Therefore, when $V_{th} = \hat{V}_{th}$ is assumed, the torque reference value is given by (58) and (59) using (44) and (57).

$$\tau_m^{ref} = \begin{cases} \hat{G}_{fm}(s)e^{0.04s}u_{\theta m} & (u_{\theta m} > 0) \\ \hat{G}_{em}(s)e^{0.04s}u_{\theta m} & (u_{\theta m} \leq 0), \end{cases} \tag{58}$$

$$\tau_s^{ref} = \begin{cases} \hat{G}_{fs}(s)e^{0.04s}u_{\theta s} & (u_{\theta s} > 0) \\ \hat{G}_{es}(s)e^{0.04s}u_{\theta s} & (u_{\theta s} \leq 0). \end{cases} \tag{59}$$

5.2.2.1.2 4ch Bilateral Control

The conceptual diagram of the 4ch bilateral control is illustrated in Fig. 5.13. As mentioned earlier, angle control and torque control are both implemented in this method. Furthermore, in this study, a proportional controller was used for torque control. The relationship between target torque value τ^{cmd}, measured torque value τ^{res}, and the reference torque value set by the torque controller τ_τ^{ref} is as follows:

$$\tau_\tau^{ref} = -K_f(\tau^{cmd} + \tau^{res}), \tag{60}$$

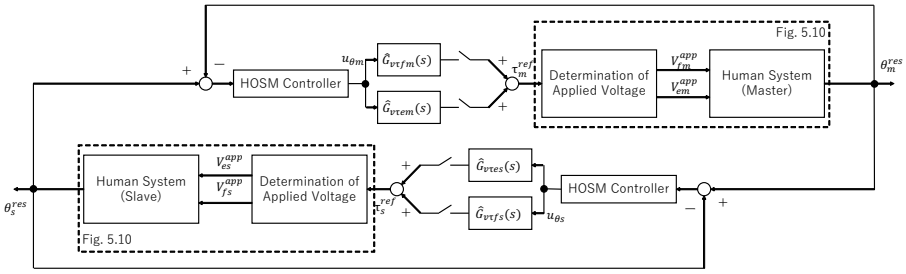

Fig. 5.12 Block diagram of position-symmetric bilateral control

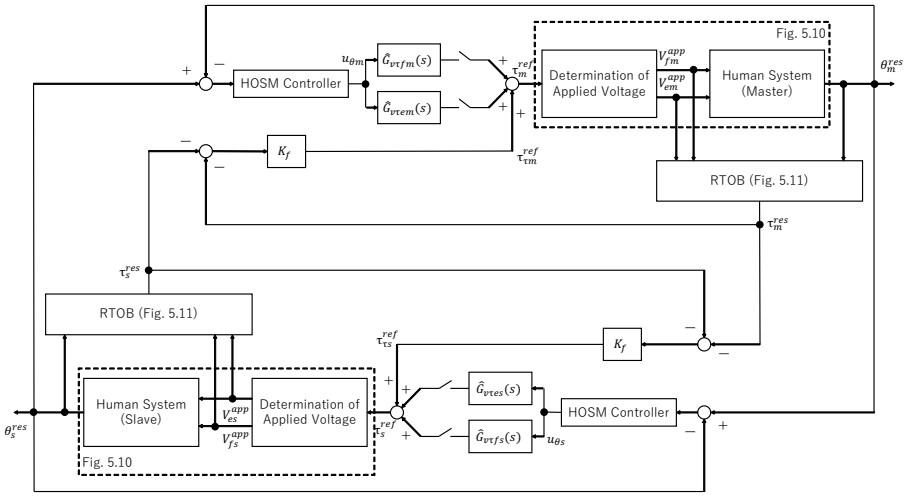

Fig. 5.13 Block diagram of 4ch bilateral control

where K_f is the proportional feedback gain in torque control. In this study, K_f was set to 1.0 for all experiments. Equation (60) can be rewritten by using subscripts m and s as follows:

$$\begin{cases} \tau_{\tau m}^{ref} = -K_f(\tau_s^{res} + \tau_m^{res}), \\ \tau_{\tau s}^{ref} = -K_f(\tau_m^{res} + \tau_s^{res}). \end{cases} \tag{61}$$

The torque reference value from the position controller was obtained in the same way as in case of the position-symmetric method. Therefore, the torque reference value in the 4ch bilateral control is represented by (62) and (63) by adding (58), (59), and (61).

$$\tau_m^{ref} = \begin{cases} \hat{G}_{fm}(s)e^{0.04s}u_{\theta m} \\ \qquad -K_f(\tau_s^{res} + \tau_m^{res}) \quad (u_{\theta m} > 0) \\ \hat{G}_{em}(s)e^{0.04s}u_{\theta m} \\ \qquad -K_f(\tau_s^{res} + \tau_m^{res}) \quad (u_{\theta m} \leq 0), \end{cases} \tag{62}$$

$$\tau_s^{ref} = \begin{cases} \hat{G}_{fs}(s)e^{0.04s}u_{\theta s} \\ \qquad -K_f(\tau_m^{res} + \tau_s^{res}) \quad (u_{\theta s} > 0) \\ \hat{G}_{es}(s)e^{0.04s}u_{\theta s} \\ \qquad -K_f(\tau_m^{res} + \tau_s^{res}) \quad (u_{\theta s} \leq 0). \end{cases} \tag{63}$$

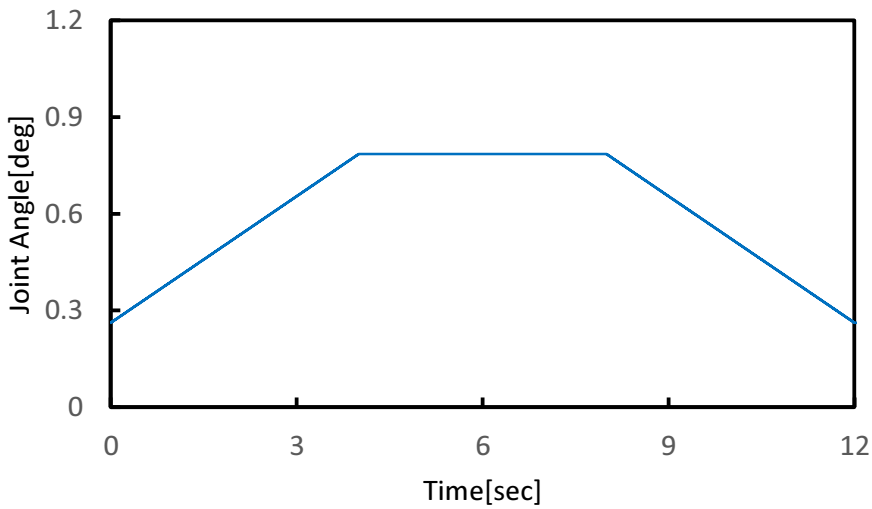

Fig. 5.14 Angular target values in experiment of torque estimation

It should be noted that, as mentioned in the second half of sections 5.2 and 5.3, respectively, the model differs after the torque reference value is entered when using the static model than when using the dynamic model. In this dissertation, the possibility of change in the angle control performance due to differences in the angle control system is eliminated. For this reason, the torque reference value of the angle control was calculated using the dynamic model $\hat{G}(s)e^{0.04s}$ even in the 4ch bilateral control using the static model.

5.2.2.2 Comparison of Estimated Torque Values

Participants wore an angle measurement sensor and grasped a 2.5 kg weight with their arms down. The angle controller was the HOSM controller, where θ^{cmd} and θ^{res} in (53) were the participants' elbow angles, and as shown in Fig. 5.14. Equations (54), (55) can be rewritten as (64), (65).

$$S = (\dot{\theta}^{cmd} - \dot{\theta}^{res}) + \lambda(\theta^{cmd} - \theta^{res}), \tag{64}$$

$$\begin{cases} u_\theta = -\lambda \cdot |S|^\rho \cdot \mathrm{sgn}(S) + u_a \\ \dot{u}_a = -W \cdot \mathrm{sgn}(S), \end{cases} \tag{65}$$

in addition, the applied voltage is represented by the (57).

In this experiment, the real value of the torque exerted by the elbow joint τ^{real} was compared with the exerted torque estimated using RTOB in the static and dynamic models, respectively. Here, the real value of the torque exerted by the elbow joint τ^{real} is as follows:

$$\tau^{real} = g(ML + ml)\sin\theta^{res}, \tag{66}$$

where m, M, l, L, and g are the total weight of the forearm and the tip of the hand, the weight of the object to be grasped, the moment arm of the elbow joint, the length from the elbow joint to the grasp, and the acceleration of gravity, respectively. m was 3.1% of the bodyweight[78], l was 0.1 m[79], and g was 9.8 kgm/s^2.

5.2.2.3 Bilateral Control of Virtual Human–Human

The participants wore an angle measurement device at the elbow joint with their arm up, such that the upper arm was horizontal to the floor. The identification experiment was conducted in the horizontal direction because the exerted torque cannot be measured correctly in the vertical direction owing to gravity. Incidentally, bilateral control using FES in the vertical direction has already been reported.

Exerted torque τ^{ext} and joint angle response values θ^{res} of the virtual human can be expressed by the following equations, respectively:

$$\tau^{ext} = G(s)(V^{app} - V_{th}) - J\ddot{\theta} - \tau^{dis}, \tag{67}$$

$$\theta^{res} = \frac{1}{Js^2}\tau^{ext}. \tag{68}$$

All constant values of the virtual human were assumed to be identical to the values of participant A. In addition, the viscous and elastic frictions were considered to be zero, with reference to previous studies [77].

In this experiment, the angle and torque response of the master (virtual human) and the slave (human) were measured when three kinds of disturbance forces were applied to the master. The torque response values used in the verification were estimated using RTOB, with reference to previous studies[71][72]. The three types of disturbance forces are depicted in Fig. 5.15. These disturbance torques were superpositions of sinusoidal waves of 0.3, 0.5, and 0.8 Hz, and their coefficients were determined randomly.

The experiment was carried out three times with three different external disturbance forces, three different control systems, and two patterns - with and without slave contact, for a total of 18 experiments, each of which lasted 20 s. When the contact experiments, the slave touched obstacles.

5.2.2.4 Bilateral Control of Human–Human

In this experiment, the angle and torque response of the master (human) and the slave (human) were measured. The participants were held in bilateral control without grasping anything for 20 s. I did not provide the master with the command for movement to prevent the slave from predicting the movement simultaneously. The order of the three types of experiments was changed for each pair

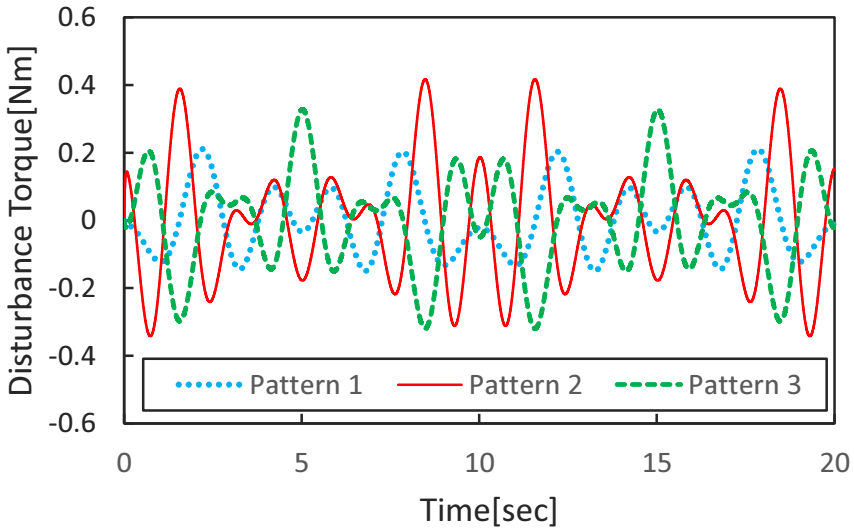

Fig. 5.15 Disturbance torque applied to a virtual person

Table 5.6 RMSE between the real and estimated torque for each participant

Participant	Static model [Nm]	Dynamic model [Nm]
A	1.598	1.276
B	0.442	0.435
C	1.524	1.500
D	0.848	0.780
E	0.254	0.210
F	0.531	0.526
Average	0.866	0.788

to consider the change in performance with habituation. The experiment was carried out three times with three different control systems, two patterns with and without slave contact, for 18 experiments that lasted 20 s each.

5.2.3 Experimental Results

5.2.4 Comparison of Estimated Torque Values

The real value of the exerted torque for participant E, the torque estimate using the static model and the dynamic model are shown in Fig. 5.16. The graphs obtained for only one participant' have been provided herein owing to the dissertation's length limitations. The root mean square error (RMSE) between the real and estimated torque for each participant is shown in Table 5.6.

5.2.4.1 Bilateral Control of Virtual Human–Human

The angle and torque responses when participants C and E were considered as slaves are shown in Figs. 5.17 and 5.18, respectively. The graphs obtained for only a few participants' have been provided

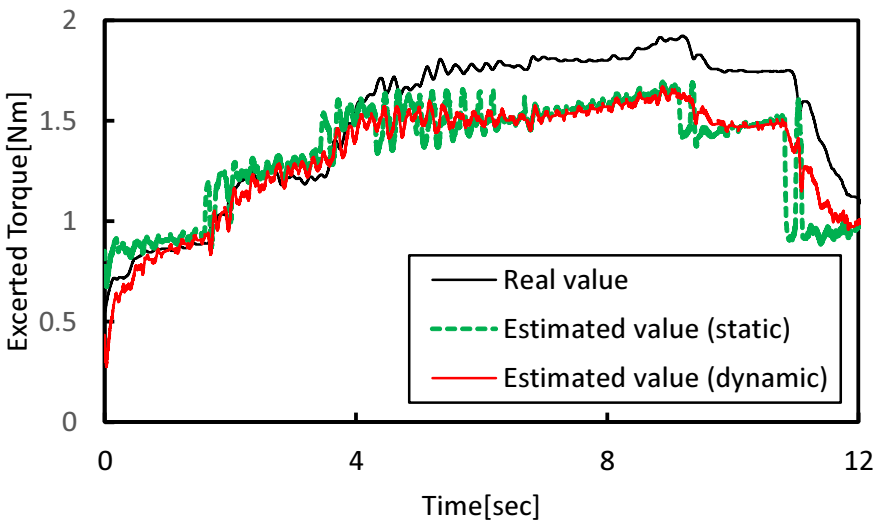

Fig. 5.16 Experimental result of torque estimation of participant E

herein owing to the dissertation's length limitations. The action without contact is plotted in Fig. 5.17, and Fig. 5.18 graphs the action with contact. Moreover, because the contact object was not fixed, the slave's elbow joint still moved at the contact time. However, the amount of change in the joint was reduced owing to limited motion capability. The gray area indicates the instant when the slave touches an obstacle. The errors of the angle and torque responses are defined using the root mean square error (RMSE) as follows

$$RMSE_\theta = \sqrt{\frac{1}{N}\sum_{i=1}^{N}(\theta_i^{cmd} - \theta_i^{res})^2} \tag{69}$$

$$RMSE_t = \sqrt{\frac{1}{N}\sum_{i=1}^{N}(\tau_i^{cmd} + \tau_i^{res})^2}, \tag{70}$$

where N is the number of samples, which is 20,000 in this experiment. The RMSE in each control system for each participant is provided in Table 5.7.

Table 5.7 RMSE of angles and torques in virtual human–human bilateral control

	Position symmetric (Symmetric)				4ch static model approximation (4ch static)				4ch dynamic model approximation (4ch dynamic)			
	Free motion		Contact motion		Free motion		Contact motion		Free motion		Contact motion	
Participant	Angle error [deg]	Torque error [Nm]	Angle error [deg]	Torque error [Nm]	Angle error [deg]	Torque error [Nm]	Angle error [deg]	Torque error [Nm]	Angle error [deg]	Torque error [Nm]	Angle error [deg]	Torque error [Nm]
A	10.08	0.0607	9.81	0.0545	2.11	0.0028	25.03	1.4608	10.41	0.0062	9.62	0.0062
	8.81	0.0550	9.05	0.0559	14.74	1.0583	19.48	1.2842	9.76	0.0078	8.82	0.0070
	9.87	0.0628	8.36	0.0500	16.84	1.1823	19.46	1.2493	9.78	0.0069	9.96	0.0066
B	9.76	0.0758	11.02	0.0811	8.15	2.8823	21.48	4.6713	9.90	0.0077	11.16	0.0080
	10.69	0.1046	9.99	0.1024	6.89	2.6012	11.66	3.3924	9.50	0.0102	10.27	0.0096
	9.04	0.0880	11.36	0.1111	9.05	2.9609	7.40	2.7196	9.97	0.0086	10.41	0.0090
C	10.46	0.1594	8.07	0.1388	5.95	1.4773	25.62	2.7531	9.67	0.0119	10.14	0.0132
	8.89	0.1789	9.22	0.1857	13.56	2.1258	20.17	2.5034	8.45	0.0166	8.87	0.0168
	9.21	0.1847	10.03	0.1900	5.78	1.3724	20.82	2.5066	10.23	0.0160	9.15	0.0156
D	8.04	0.3122	9.29	0.3159	8.46	1.3154	12.37	1.4307	9.06	0.0245	7.92	0.0230
	7.88	0.3963	7.27	0.3877	8.77	1.3324	11.81	1.5576	8.54	0.0254	9.09	0.0273
	10.31	0.3853	9.49	0.3686	7.87	1.2800	20.91	1.7612	8.80	0.0260	8.42	0.0279
E	12.64	0.1678	7.13	0.0998	7.59	1.8874	24.44	3.1427	10.42	0.0069	14.53	0.0144
	7.53	0.2184	7.49	0.1837	16.52	1.8217	24.97	2.2908	12.73	0.0200	5.23	0.0137
	6.56	0.1769	13.95	0.1535	6.20	1.3974	23.59	2.0343	15.18	0.0160	13.75	0.0125
F	4.95	0.3288	5.93	0.3272	4.86	1.6944	15.86	1.5897	11.75	0.0276	3.34	0.0194
	3.13	0.3648	9.70	0.3879	6.79	1.0213	13.76	1.7851	5.31	0.0294	8.94	0.0227
	12.26	0.4005	7.48	0.3983	11.68	1.3580	22.08	1.6104	11.00	0.0300	4.58	0.0299
Average	8.89	0.21	9.15	0.20	8.99	1.60	18.94	2.21	10.03	0.017	9.12	0.016

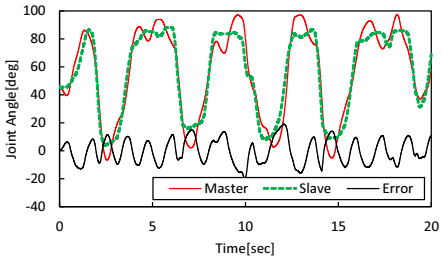

(a)Position response (Symmetric)

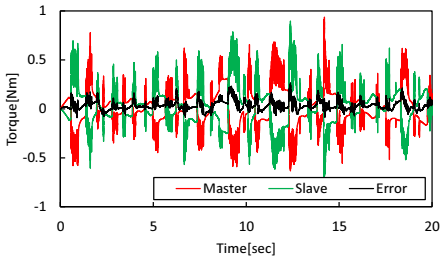

(b)Torque response (Symmetric)

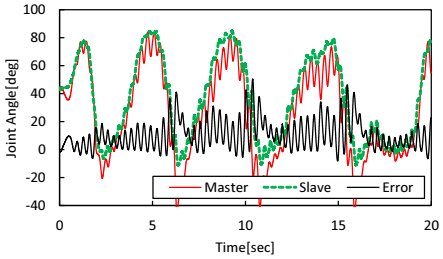

(c)Position response (4ch static)

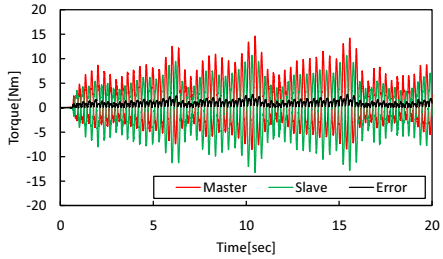

(d)Torque response (4ch static)

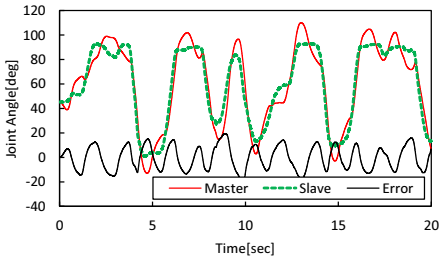

(e)Position response (4ch dynamic)

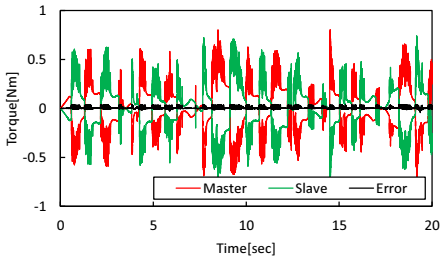

(f)Torque response (4ch dynamic)

Fig. 5.17 Results of bilateral control of a virtual human and participant C (free motion)

5.2.4.2 Bilateral Control of Human–Human

The angular and torque responses when participant A was the master and participant B was its slave, and when participant D was the master and participant C was its slave, are graphed in Figs. 5.19 and 5.20, respectively. Only some participants' graphs are included herein owing to the dissertation's length limitations. Moreover, the RMSE in each control system for each participant is detailed in Table 5.8.

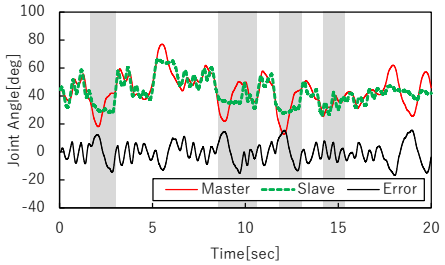

(a)Position response (Symmetric)

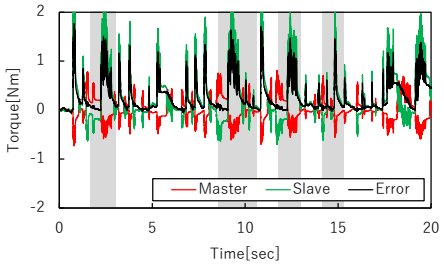

(b)Torque response (Symmetric)

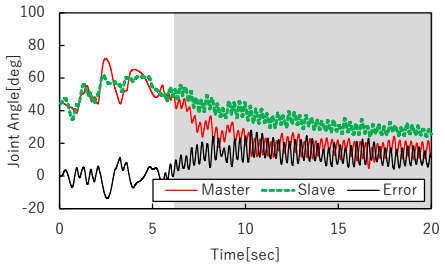

(c)Position response (4ch static)

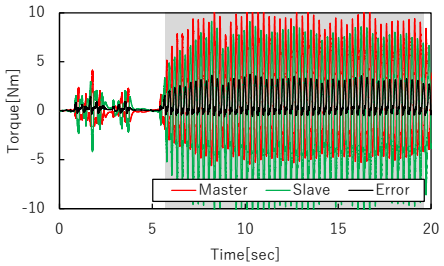

(d)Torque response (4ch static)

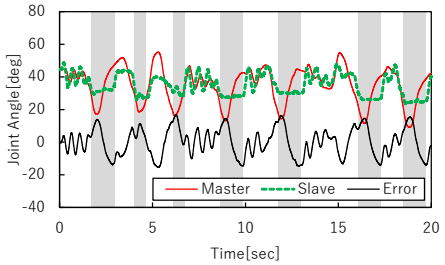

(e)Position response (4ch dynamic)

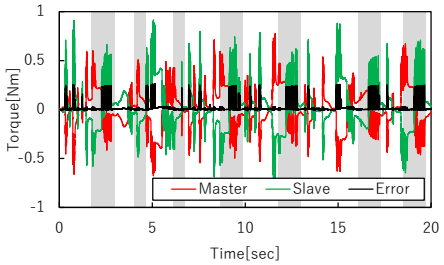

(f)Torque response (4ch dynamic)

Fig. 5.18 Results of bilateral control of a virtual human and participant E (contact motion)

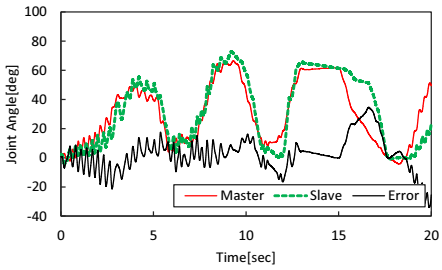

(a)Position response (Symmetric)

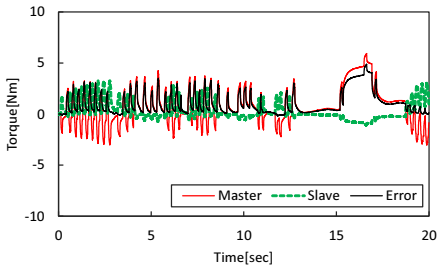

(b)Torque response (Symmetric)

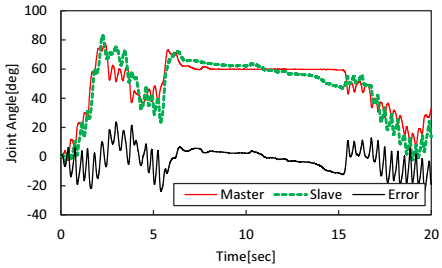

(c)Position response (4ch static)

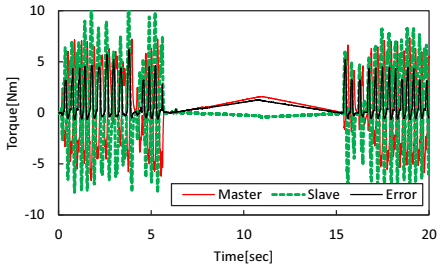

(d)Torque response (4ch static)

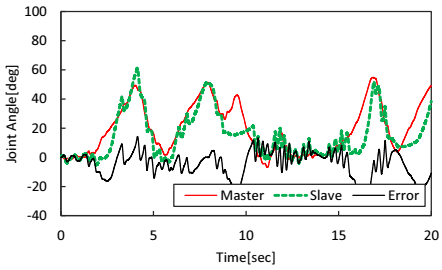

(e)Position response (4ch dynamic)

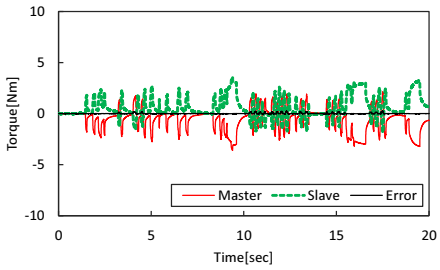

(f)Torque response (4ch dynamic)

Fig. 5.19 Results of bilateral control of participant A (master) and participant B (slave) (free motion)

(a)Position response (Symmetric)

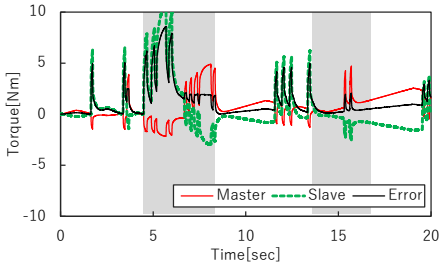

(b)Torque response (Symmetric)

(c)Position response (4ch static)

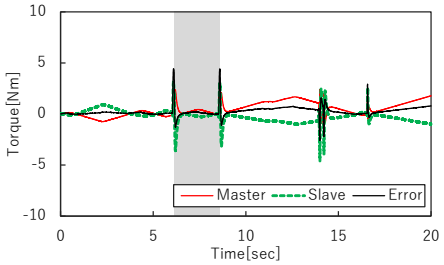

(d)Torque response (4ch static)

(e)Position response (4ch dynamic)

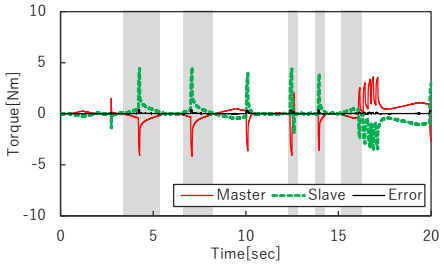

(f)Torque response (4ch dynamic)

Fig. 5.20 Results of bilateral control of participant D (master) and participant C (slave) (contact motion)

Table 5.8 RMSE of angles and torques in human–human bilateral control

	Position symmetric (Symmetric)				4ch static model approximation (4ch static)				4ch dynamic model approximation (4ch dynamic)			
	Free motion		Contact motion		Free motion		Contact motion		Free motion		Contact motion	
Participant	Angle error [deg]	Torque error [Nm]	Angle error [deg]	Torque error [Nm]	Angle error [deg]	Torque error [Nm]	Angle error [deg]	Torque error [Nm]	Angle error [deg]	Torque error [Nm]	Angle error [deg]	Torque error [Nm]
A	19.13	3.76	8.17	2.57	8.36	1.52	17.17	3.66	12.50	0.10	12.41	0.11
	26.94	3.74	20.26	3.25	12.33	1.77	16.25	1.84	7.38	0.07	14.02	0.10
	11.95	1.40	11.85	1.50	21.50	3.23	11.02	1.23	10.03	0.05	15.69	0.04
B	12.14	0.78	14.69	2.22	16.55	1.47	15.42	1.56	14.32	0.08	14.74	0.04
	9.07	0.85	12.59	0.59	21.86	2.26	22.16	0.69	18.30	0.10	18.58	0.04
	10.55	0.90	14.14	2.22	7.48	1.22	8.93	1.49	9.57	0.07	14.56	0.03
C	11.17	1.53	33.55	2.48	10.74	1.73	31.35	3.02	12.79	0.08	22.74	0.12
	13.32	1.42	29.87	2.26	10.56	1.67	31.24	2.72	9.71	0.06	24.86	0.11
	9.21	1.38	37.83	2.91	8.19	1.38	32.43	2.78	11.91	0.08	36.08	0.16
D	31.27	2.39	12.22	2.01	16.31	1.47	21.74	2.26	19.07	0.10	7.13	0.05
	32.71	2.63	17.24	2.97	6.64	0.51	7.27	0.54	26.27	0.11	21.39	0.11
	26.71	2.29	17.07	5.46	17.66	2.47	11.71	1.64	17.53	0.15	7.30	0.04
E	13.35	1.61	32.62	2.09	12.38	2.14	30.17	3.41	13.54	0.03	27.13	0.13
	11.96	1.82	28.13	2.24	13.52	1.37	36.04	2.51	13.99	0.09	21.23	0.08
	6.56	1.30	41.75	2.55	8.61	1.41	35.21	2.31	16.87	0.08	40.68	0.13
F	28.18	2.56	8.87	2.13	12.72	1.85	25.23	2.42	21.76	0.13	2.56	0.02
	27.95	2.31	19.68	2.98	4.66	0.20	9.22	0.77	23.03	0.15	21.24	0.07
	28.65	2.45	15.06	5.76	21.48	2.55	12.87	1.49	19.74	0.19	3.46	0.06
Average	18.38	1.95	20.87	2.68	12.86	1.68	20.86	2.02	15.46	0.10	18.10	0.08

5.2.5 Discussion

In this section, this study aimed to propose and validate the performance of bilateral control using FES based on a dynamic model.

In the torque estimation experiments, the estimation accuracy was better for all participants using the dynamic model. In Fig. 5.16, a real oscillatory value of torque occurs at around 4 sec. This phenomenon was due to chattering near the sliding surface. The high-frequency effect was likely to be suppressed because the body's dynamic characteristics are the delay-time system. In the static model, the high-frequency voltage was multiplied by a constant. On the other hand, in the dynamic model, the effect of high-frequency voltage that occurred in the static model was suppressed. Although the angular response was oscillatory, the torque could be estimated accurately. These results are because the dynamic characteristics were correctly estimated.

Besides, both methods resulted in the estimation errors of approximately 0.3 Nm between 4 and 10 sec. These errors were estimated to be due to the effect of errors in the gain of the model and the real value approximated by (66). Additionally, it has been reported that there is a correlation between the joint angle and gain[39]. Therefore, the exerted torque was larger than the estimated torque between 4 and 10 sec, presumably because the joint angle effect was not taken into account. The purpose of this experiment was to compare the estimation accuracy of the static and dynamic models. Therefore, the errors generated by both models were not issues. In the future, we would like to try to improve the estimation accuracy by introducing an angle-aware model and a sequential estimation algorithm.

Figs. 5.21 and 5.22 show mean RMSEs of angle and torque errors under the bilateral control of virtual human–human and the standard errors of means (SEMs), respectively. The graphs also indicate the results of multiple comparisons with a two-tailed t-test; the significance level was corrected by a Bonferroni method[80] (*i.e.*, $\alpha = 0.01/3$). In experiments with bilateral control of virtual human–human, the angular tracking performance was not significantly different between the position-symmetric and the 4ch bilateral control using a dynamic model approximation. In other words, the addition of torque control did not significantly affect the angle control performance. The poor angle-following performance of the 4ch bilateral control using static model approximation was thought to be due to the degraded accuracy of the estimated reaction force because of modeling errors. As plotted in Fig. 5.17(d), the estimated disturbances oscillate compared to the values represented in Fig. 5.15. This oscillation phenomenon is due to modeling errors that prevent the RTOB from correctly estimating

the reaction torque. It is presumed that this is due to incorrect torque control, thus resulting in RTOB and torque controller generating an input that causes oscillations.

The best torque response results were obtained for 4ch bilateral control using the dynamic model approximation. The torques did not match up in the position-symmetric type because it has no built-in torque control. The proposed method provided the smallest error in the determination of action and reaction force. The RTOB, with dynamic model approximation, correctly estimated the disturbance torque, whereas the action and reaction torques were obtained via torque control. These results indicate that the proposed method could achieve the bilateral control objectives expressed in (1) and (40).

Figs. 5.23 and 5.24 show mean RMSEs of angle and torque errors under the bilateral control of human–human and the SEMs, respectively. The graphs also indicate the results of multiple comparisons with a two-tailed t-test; the significance level was corrected by a Bonferroni method[80] (*i.e.*, $\alpha = 0.01/3$). However, no significant difference in angle response appeared in the bilateral control of human–human. The angle control performance may be similar because the master could not discriminate between the disturbances caused by delay and those originating due to contact. In this study, a simple control system was adopted to verify the superiority of the 4ch bilateral control with dynamic model approximation in terms of performance. A bilateral control system suitable for dead time systems has already been proposed.

By contrast, 4ch bilateral control using a dynamic model has the lowest torque response error. Significant differences were observed when it was compared with the other two methods. This may be because the RTOB correctly estimated the reaction torque in the human–human experiment, and the appropriate torque reference value was output by the torque controller. Therefore, it can be concluded that the 4ch bilateral control using the dynamic model is the control system that best satisfies (1) and (2) in both human–human experiments.

Let me consider the overall results of the experiment. In the latter part of the contact in Figs. 5.18 and 5.20 (the right-hand-side half of each gray area), the slave did not follow when the master bent his elbow for a short time after the slave touched the obstacle. It is assumed that this is because the integral compensation of the angle controller was operating owing to the angle deviation at the time of contact. In addition, the elbow joint is chattering in the first 10 s of Fig. 5.19(a), the first and last 5 s each in (c), and between 10 and 15 s in (e). Both problems are expected to be remedied by incorporating the aforementioned bilateral control to compensate for the dead time. However, these problems are not only related to bilateral control systems but also occur presumably owing to the

poor control performance of FES. Therefore, when using FES, modeling errors were likely to occur owing to tension, involuntary contractions under unconsciousness, and muscle fatigue. To cope with this, a method of sequential model updating has already been reported[39][81].

The HOSM controller was used as the angle controller in this study. Moreover, the gain of the HOSM controller was set to be the same value for all participants. It has been reported that the HOSM controller is extremely robust to disturbances and modeling errors, and previous studies on it have also indicated high control performance with a uniform gain[45]. Furthermore, the gain of the torque controller was also ensured to be the same for all participants. However, in bilateral control, it has been shown that the setting of the position controller and force controller gains is essential[6].

Finally, in bilateral control using FES, it is still unclear whether the most comfortable control goal for the participants is the position synchronization and the establishment of force action-reaction.

5.2.6 Summary

In this section, the position synchronization and force action-reaction can be established through 4ch bilateral control using FES based on a dynamic model was proposed. The significant difference test using a multiple comparisons with a two-tailed t-test; revealed that the proposed method established better angle synchronization and torque action-reaction than its comparative methods. Moreover, it was found that reasonable force control can be achieved by approximating the relationship between the stimulus value and the exerted torque in the bilateral control with the FES using a dynamic model. In this study, a simple angle controller and bilateral control system was implemented. Furthermore, by implementing an advanced bilateral control system to compensate for the dead time, the control performance is expected to improve even further.

5.3 Summary of Chapter 5

In this chapter, bilateral control using FES is discussed, and it is shown that the use of antagonistic muscle stimulation improves control performance in bilateral control of two joints. It is suggested that each joint's force can be transmitted to each joint, indicating that bilateral control with multiple degrees of freedom is possible.

It is also shown that the 4ch bilateral control using the dynamic model can improve the control performance. The dynamic model is relatively simple and requires shorter identification experiments than methods using NNs and other methods. In this dissertation, single DoF control of the elbow joint and 2 DoF control of the elbow and wrist joints were presented.

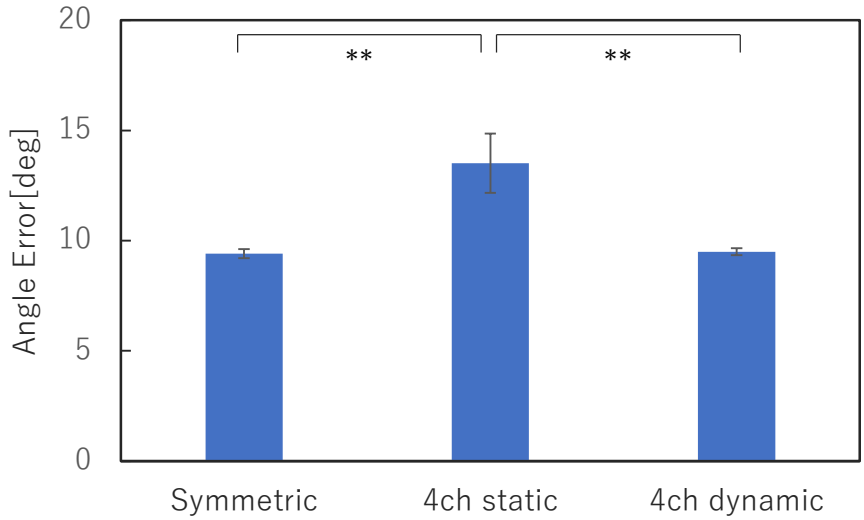

Fig. 5.21 Statistical comparison of angle error in the virtual human–human bilateral control (**: $p < 0.01$)

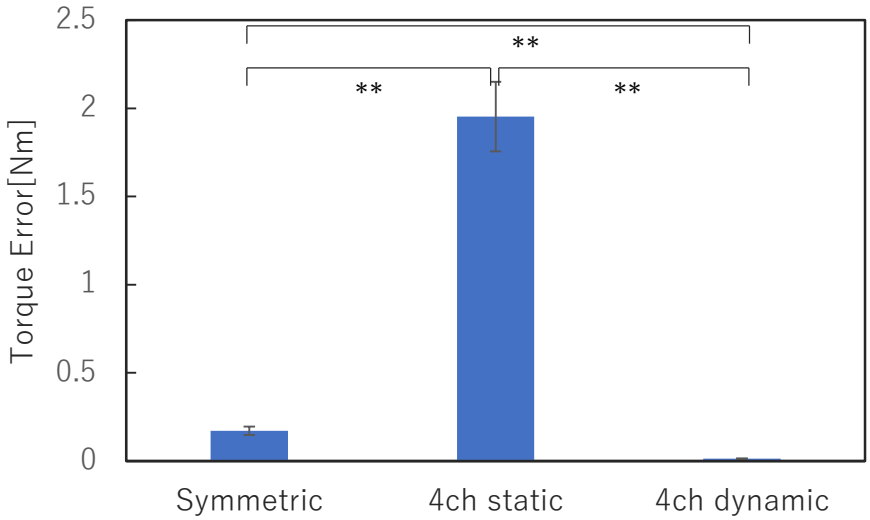

Fig. 5.22 Statistical comparison of torque error in the virtual human–human bilateral control (**: $p < 0.01$)

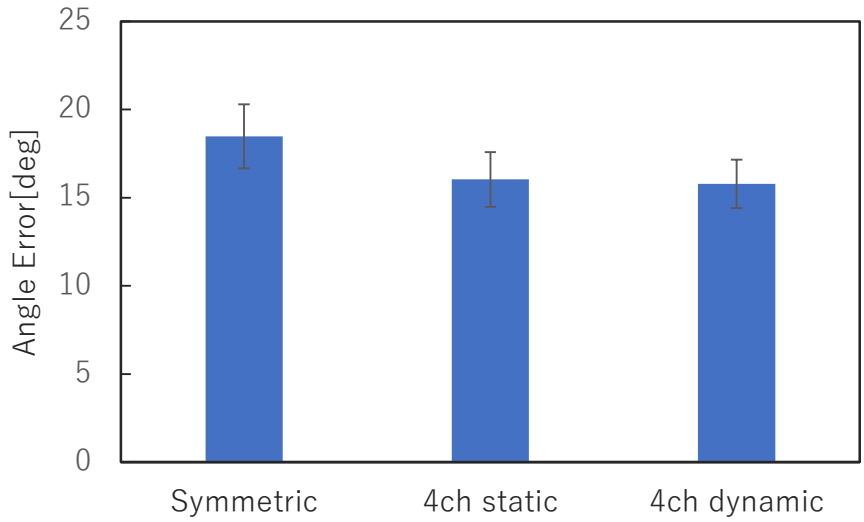

Fig. 5.23 Statistical comparison of angle error in the human–human bilateral control

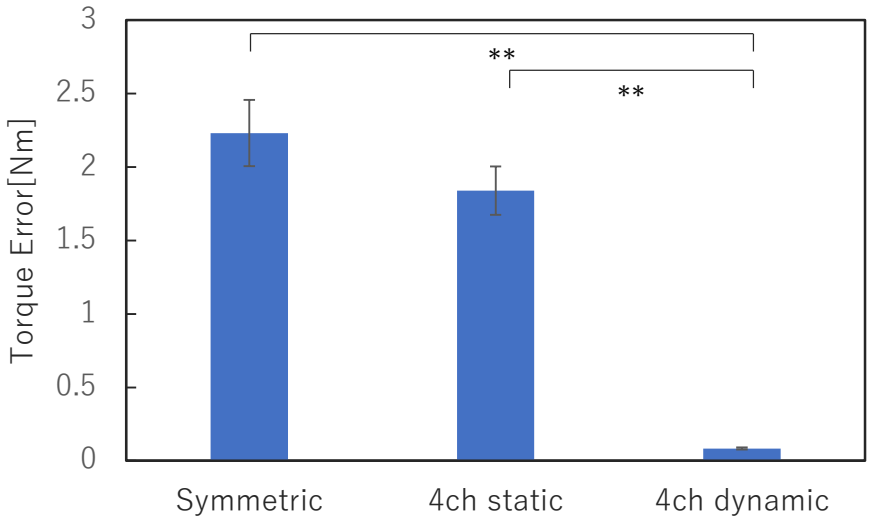

Fig. 5.24 Statistical comparison of torque error in the human–human bilateral control (**: $p < 0.01$)

Chapter 6 CONCLUSION

The system that enables force sensation communication in daily life is expected to spread. However, the current system is too large to be portable. Therefore, this dissertation focuses on bilateral control using FES. While bilateral control has been studied in detail, the FES's control performance is still debatable. Therefore, this dissertation focuses on four aspects of FES control: angular control, modeling, multi-DOFs, and bilateral control.

Firstly, the dynamic characteristics are modeled using the transfer function approximation method with the FFT. The results showed that it could be approximated with a first-order lag system, although it is limited to only the frequency band used in the experiments.

Secondly, the angle control is improved by combining a highly robust HOSM controller and control that compensates for dead time. The results show that frequency modulation and amplitude modulation suppresses the chattering and improves control performance.

Thirdly, the disturbance suppression method's application using antagonist muscle stimulation was shown to improve the control performance of two-joint control. It is also shown that the use of frequency modulation in multi-DOFs control allows controlling a complex arrangement of muscles such as the shoulder joint.

Finally, two types of experiments on bilateral control were conducted using the findings described so far. In the first experiment, bilateral control of two joints using antagonist muscle stimulation was verified. It was shown that antagonist muscle stimulation was effective in bilateral control. In the second experiment, 4ch bilateral control using the estimated dynamic model in FES was verified. In the results, the significant difference test using multiple comparisons with a two-tailed t-test; revealed that the proposed method established better angle synchronization and torque action-reaction than its comparative methods. Moreover, it was found that reasonable force control can be achieved by approximating the relationship between the stimulus value and the exerted torque in the bilateral control with the FES using a dynamic model.

In summary, the control performance when using FES is improved even in a simple system, and it is shown that force sensation transmission can be achieved by bilateral control using FES. The control method in this dissertation needs further consideration. However, it was shown that the control goals of general bilateral control, i.e., establish both position synchronization and force action-reaction can also be achieved in bilateral control using FES. These results will help to construct a force transmitting system using FES.

Acknowledgements

This dissertation summarizes my research conducted in the Kaneko and Sakaino (Motion Control) laboratory. Since April 2014, I received a lot of help from many people for my research. I would like to express my acknowledgment to them.

First of all, I am grateful Associate Professor Dr. Sho Sakaino at University of Tsukuba for his support and tolerance. I was a poor student in his eyes, but he never abandoned me and gave me warm and sometimes harsh guidance. I wanted to be a researcher like him and decided to become a researcher. I admire him for his breadth of vision, depth of knowledge, and perseverance. I could widen my view thanks to him giving me many chances to attend conferences and to meet other researchers.

I am also grateful to Professor Dr. Yasuyoshi Kaneko at Saitama University for his immense support. He accepted me as a supervisor from the master's course. He always took care of me. Without his kindness, I would have been difficult to continue my research.

I am also grateful to Associate Professor Dr. Toshiaki Tsuji at Saitama University to discuss fruitful discussions. He has always had a logical mind and taught me what a researcher should be. He was also very helpful in giving me advice when I was mentally ill.

I am also grateful to the members of my Ph.D. dissertation committee, Professor Dr. Masaya Takasaki and Professor Dr. Kazuhito Ito at Saitama University. Their comments and advice helped me to improve this dissertation.

Associate Professor Dr. Masayuki Hara at Saitama University taught me the difficulties of studying human and how to deal with them. Thanks to him I was able to gain knowledge in areas outside of my expertise.

I am also grateful to Mr. Hiroshi Okawara and Mr. Fujiki Kawahara at Saitama University have brought very useful support for software and hardware. It also helped them learn to have fun and a work ethic.

Assistant Professor Dr. Takahiro Nozaki at Keio University has always accepted me and given me great advice. I asked him in the past, "What is a PhD program?" . He replied, "You'll know the answer to that question in the doctoral program". I think I found my own answer.

I would like to thank the Japan Society for the Promotion of Science (JSPS), which supported me financially.

I am thankful to the members of Sakaino laboratory, Kaneko laboratory, and Tsuji laboratory. Especially, Assistant Professor Dr. Kyo Kutsuzawa at Tohoku University, my colleague, helped me a

lot during my researcher life in the doctoral program. He was my role model in both my research and personal life. Ph.D. program with me, and I am very happy to have him as a colleague.

Finally, I am grateful to my family. My father supported me for eleven years of college. My mother was strict and sometimes kind and supportive of me. My brothers and I would meet each other in a while, and they were my respite.

There are many people I could not mention here. I express my sincere gratitude to everybody who has supported me.

March, 2021 Tomoya Kitamura

Bibliography

[1] D. Prattichizzo, C. Pacchierotti, and G. Rosati: "Cutaneous Force Feedback as a Sensory Subtraction Technique in Haptics," *IEEE Transactions on Haptics*, vol. 5, no. 4, pp. 289-300, 2012.

[2] C. Pacchierotti, D. Prattichizzo, and K. Kuchenbecker: "Cutaneous Feedback of Fingertip Deformation and Vibration for Palpation in Robotic Surgery," *IEEE Transactions on Biomedical Engineering*, vol. 63, no. 2, pp. 278-287, 2015.

[3] Y. Osawa and S. Katsura: "Thermal propagation control using a thermal diffusion equation," *IEEE Transactions on Industrial Electronics*, vol. 65, no. 11, pp. 8809-8817, 2018.

[4] R. Mizuhara, A. Takahashi, and H. Kajimoto: "Experimental evaluation of bilateral control of velocity control system using electric and hydraulic actuators ," *In Proceedings of the 17th International Conference on Virtual-Reality Continuum and its Applications in Industry*, pp. 1–5, 2019.

[5] P. Ramsamy, A. Haffegee, R. Jamieson, and V. Alexandrov: "Using haptics to improve immersion in virtual environments," *In Proceedings of the International Conference on Computational Science*, pp. 603–609, 2006.

[6] S. Sakaino, T. Sato, and K. Ohnishi: "Multi-DOF Micro-Macro Bilateral Controller Using Oblique Coordinate Control," *IEEE Transactions on Industrial Informatics*, vol. 7, no. 3, pp. 446–454, 2011.

[7] D. Takahashi, T. Furuya, S. Sakaino, and T. Tsuji: "Experimental evaluation of bilateral control of velocity control system using electric and hydraulic actuators ," In *Proceedings of the 39th Annual Conference of the IEEE Industrial Electronics Society*, pp. 4118-4123, 2013.

[8] S. Katsura, W. Iida, and K. Ohnishi: "Medical mechatronics-An application to haptic forceps," *Annual Reviews in Control*, vol. 29, pp. 237-245, 2005.

[9] H. Yamada, T. Ni, and D. Zhao: "Construction Telerobot System with Virtual Reality," In *Proceedings of the IEEE Conference on Robotics, Automation, and Mechatronics*, pp. 36-40, 2008.

[10] P. F. Hokayem, F. Peter, and M. W. Spong: "Bilateral teleoperation: An historical survey." *Automatica*, vol. 42, no. 12, pp. 2035-2057, 2006.

[11] T. Tanabe, H. Yano, and H. Iwata: "Evaluation of the Perceptual Characteristics of a Force Induced by Asymmetric Vibrations," *IEEE Transactions on Haptics*, vol.11, no.2, pp.220–231, 2018.

[12] K. Honda and K. Kiguchi: "Control of Human Elbow-Joint-Extension-Motion Change Based on Vibration Stimulation for Upper-Limb Perception-Assist," *IEEE Access*, vol.8, pp. 22697-22708, 2020.

[13] A. Lecuyer, S. Coquillard, A. Kheddar, P. Richard, and P. Coiffet: "Pseudo-haptic feedback: can isometric input devices simulate force feedback?," In *Proceedings of the IEEE International Conference on Virtual Reality*, pp. 83–90, 2000.

[14] P. Lopes, S. You, L. Gheng, S. Marwecki, and P. Baudisch: "Providing Haptics to Walls and Heavy Objects in Virtual Reality by Means of Electrical Muscle Stimulation." In *Proceedings of the Conference on Human Factors in Computing Systems*, pp. 1471–1482, 2017.

[15] P. Lopes, D. Yuksei, F. Guimbretiere, and P. Baudisch: "Muscle-plotter: An Interactive System Based on Electrical Muscle Stimulation that Produces Spatial Output." In *Proceedings of the Annual Symposium on User Interface Software and Technology*, pp. 207–217, 2016.

[16] M. Pfeiffer, S. Schneegass, F. Alt, and M. Rohs: "Let Me Grab This: a Comparison of EMS and Vibration for Haptic Feedback in Free-hand Interaction." In *Proceedings of the Augmented Human International Conference*, article no. 48, 2014.

[17] T. Iwami, H. Miura, K. Hasegawa, A. Nakayama, G. Obinata, K. Miyawaki, and Y. Yanagihara: "A New Bilateral Teleoperator with Force Reflection using Functional Electrical Stimulation." *Journal of the Robotics Society of Japan*, vol. 20, no. 8, pp. 844–851, 2002. (in Japanese)

[18] H. Kajimoto: "Illusion of motion induced by tendon electrical stimulation," In *World Haptics Conference (WHC), 2013*, pp. 555-558, 2013.

[19] T. Ishikawa, T. Tsuji, and Y. Kurita: "Wearable Pseudo-Haptic Interaction by Using Electrical Muscle Stimulation," In *Haptic Interaction*, Springer Japan, pp. 135-140, 2015.

[20] E. B. Marsolais, and R. Kobetic: "Functional Walking in Paralyzed Patients by Means of Electrical Stimulation," *Clinical Orthopaedics, and Related Research*, vol. 175, pp. 30-36, 1983.

[21] B. T. Smith, M. J. Mulcahey, and R. R. Betz: "Development of an Upper Extremity FES System for Individuals with C4 Tetraplegia," *IEEE Transactions on Rehabilitation Engineering*, vol. 4, no. 4, pp. 264-270, 2002.

[22] H. Hummelsheim, M. L. Maier-Loth, and C. Eickhof: "The Functional Value of Electrical Muscle Stimulation for The Rehabilitation of The Hand in Stroke Patients," *Scandinavian Journal of Rehabilitation Medicine*, vol. 29, no. 1 pp. 3-10, 1997.

[23] S. Khamis, R. Martikaro, S. Wientroub, Y. Hemo, and S. Hayek: "A functional electrical stimulation system improves knee control in crouch gait." *Journal of children's orthopaedics*, vol. 9,

no. 2. pp. 137-143, 2015.

[24] T. Watanabe, Y. Tagawa, E. Nagasue, and N. Shiba, "Surface Electrical Stimulation to Realize Task Oriented Hand Motion," In *Proceedings of the IEEE Conference on Medicine and Biology Society*, pp. 662-665, 2009.

[25] E. Tamaki, T. Miyaki, and J. Rekimoto: "Possessed Hand: Techniques for Controlling Human Hands Using Electrical Muscles Stimuli," *CHI2011, 2010.*

[26] K. Kurosawa, R. Futami, T. Watanabe, and N. Hoshimiya: "Joint Angle Control by FES Using a Feedback Error Learning Controller," *IEEE Transactions on Neural Systems and Rehabilitation Engineering*, vol. 13, no. 3, pp. 359-371, 2005.

[27] A. V. Hill and Sec. R. S., "The Heat of Shortening and the Dynamic Constants of Muscle," In *Proceedings of the Royal Society B*, vol. 126, no. 843, pp. 136–195, 1938.

[28] F. E. Zajac, "Muscle and Tendon Properties Models Scaling and Application to Biomechanics and Motor," *Critical Reviews in Biomedical Engineering*, vol. 17, no. 4, pp. 359–411, 1989.

[29] F. E. Zajac and M. E. Gordon, "Determining Muscle's Force and Action in Multi-Articular Movement," *Exercise and Sport Sciences Reviews*, vol. 17, no. 1, pp. 187–230, 1989.

[30] J. Ding, S. A. Binder-Macledo, and A. S. Wexler: "Two-step, Predictive, Isometric Force Model Tested on Data From Human and Rat Muscles," *Journal of Applied Physiology*, vol. 85, no. 6, pp. 2176–2189, 1998.

[31] J. Ding, A. S. Wexler, and S. A. Binder-Macledo: "Mathematical Models for Fatigue Minimization During Functional Electrical Stimulation," *Journal of Electromyography and Kinesiology*, vol. 13, no. 6, pp. 575–588, 2003.

[32] J. Ding, A. S. Wexler, and S. A. Binder-Macledo: "A Mathematical Model That Predicts the Force Frequency Relationship of Human Skeletal Muscle," *Muscle and Nerve: Official Journal of the American Association of Electrodiagnostic Medicine*, vol. 26, no. 4, pp. 477–485, 2002.

[33] A. B. Hmed, T. Bakir, A. Sakly, and S. Binczak: "A New Mathematical Force Model that Predicts the Force-pulse Amplitude Relationship of Human Skeletal Muscle," In *Proceedings of the 40th Annual International Conference of the IEEE Engineering in Medicine and Biology Society*, pp. 3485–3488, 2018.

[34] A. B. Hmed, T. Bakir, Y. M. Garnier, A. Sakly, R. Lepers, and S. Binczak: "An Approach to a Muscle Force Model with Force-pulse Amplitude Relationship of Human Quadriceps Muscles," In *Computers in Biology and Medicine*, pp. 218–228, 2018.

[35] M. Berniker, A. Jarc, K. Kording, and M. Tresch, "A Probabilistic Analysis of Muscle Force

Uncertainty for Control ," *IEEE Transactions on Biomedical Engineering*, vol. 63, no. 11, pp. 2359–2367, 2016.

[36] Q. Wei, D. K. Pai, and M. C. Tresch, "Uncertainty in limb configuration makes minimal contribution to errors between observed and predicted forces in a musculoskeletal model of the rat hindlimb," *IEEE Transactions on Biomedical Engineering*, vol. 65, no. 2, pp. 469–476, 2018.

[37] Z. Li, M. Hayashibe, C. Fattal, and D. Guiraud: "Muscle Fatigue Tracking with Evoked EMG Via Recurrent Neural Network: Toward Personalized Neuroprosthetics." *IEEE Computational Intelligence Magazine* vol. 9, no. 2, pp. 38–46, 2014.

[38] Z. Li, D. Guiraud, D. Andreu, M. Benoussaad, C. Fattal, and M. Hayashibe: "Real-time Estimation of FES-induced Joint Torque with Evoked EMG," *Journal of NeuroEngineering and Rehabilitation*, vol. 13, no, 60, 2016.

[39] M. Ferrarin, and A. Pedotti: "The Relationship Between Electrical Stimulus and Joint Torque: a Dynamic Model," *IEEE Transactions on Rehabilitation Engineering*, vol. 8, no. 3, pp. 342–352, 2000.

[40] I. M. Yassin, A. Zabidi, R. Jailani, N. M. Tahir, and M. S. A. M. Ali: "NARX Muscle Model Based on Functional Electrical Stimulation (FES) Using Polynomial Estimators and Singular Value Decomposition (SVD)," In *Proceedings of the 2015 IEEE Conference on System, Process and Control*, pp. 168–172, 2015.

[41] I. M. Yassin, R. Jailani, M. S. A. M. Ali, R. Baharom, A. Huzaifah, A. Hassan, and Z. I. Rizman: "Comparison Between Cascade Forward and Multi-layer Perceptron Neural Networks for NARX Functional Electrical Stimulation (FES)-based Muscle Model," *International Journal on Advanced Science, Engineering and Information Technology*, vol. 7, no. 1, pp. 215–221, 2017.

[42] K. J. Hunt, R. P. Jaime, and H. Gollee: "Robust Control of Electrically-stimulated Muscle Using Polynomial H∞ Design," *Control Engineering Practice*, vol. 9, no. 3, pp. 313–328, 1988.

[43] H. Gollee, K. J. Hunt, and D. E. Wood: "New Results in Feedback Control of Unsupported Standing in Paraplegia," *IEEE Transactions on Neural Systems and Rehabilitation Engineering*, vol. 12, no. 1, pp. 73–80, 2004.

[44] A. P. L. Bô, L. O. da Fonseca, and A. C. C. de Sousa: "FES-induced Co-activation of Antagonist Muscles for Upper Limb Control and Disturbance Rejection," *Medical Engineering and Physics*, Vol. 38, No. 11, pp. 1176–1184, 2016.

[45] A. Farhoud and A. Erfanian, "Fully Automatic Control of Paraplegic FES Pedaling Using Higher-order Sliding Mode and Fuzzy Logic Control," *IEEE Transactions on Neural Systems and Reha-*

bilitation Engineering, Vol. 22, No. 3, pp. 533–542, 2014.

[46] G. C. Chang, J. J. Lub, G. D. Liao, J. S. Lai, C. K. Cheng, B. L. Kuo, and T. S. Kuo: "A Neuro-control System for the Knee Joint Position Control with Quadriceps Stimulation," *IEEE Transactions on Rehabilitation Engineering*, vol. 5, no. 1, pp. 2–11, 1997.

[47] K. Kurosawa, R. Futami, T. Watanabe, and N. Hoshimiya: "Joint Angle Control by FES Using a Feedback Error Learning Controller," *IEEE Transactions on Neural Systems and Rehabilitation Engineering*, vol. 13, no. 3, pp. 359–371, 2005.

[48] A. Ajoudani, and A. Erfanian: "A Neuro-sliding-mode Control with Adaptive Modeling of Uncertainty for Control of Movement in Paralyzed Limbs Using Functional Electrical Stimulation," *IEEE Transactions on Biomedical Engineering*, vol. 56, no. 7, pp. 1771–1780, 2009.

[49] W. D. Chang, R. C. Hwang, and J. G. Hsieh: "Application of an Auto-tuning Neuron to Sliding Mode Control," *IEEE Transactions on Systems, Man, and Cybernetics, Part C (Applications and Reviews)*, vol. 32, no. 4, pp. 517–522, 2002.

[50] N. Sharma, C. M. Gregory, M. Johnson, and W. E. Dixon: "Closed-loop Neural Network-based NMES Control for Human Limb Tracking," *IEEE Transactions on Control Systems Technology*, vol. 20, no. 3, pp. 712–725, 2012.

[51] H. R. Kobravi and A. Erfanian, "Decentralized Adaptive Robust Control Based on Sliding Mode and Nonlinear Compensator for the Control of Ankle Movement Using Functional Electrical Stimulation of Agonist-antagonist Muscles," *Journal of Neural Engineering*, vol. 6, no. 4, 046007 (10pp), 2009.

[52] V. Nekoukar and A. Erfanian, "Adaptive Fuzzy Terminal Sliding Mode Control for a Class of MIMO Uncertain Nonlinear Systems," *Fuzzy Sets and Systems*, vol. 179, no. 1, pp. 34–49, 2011.

[53] V. Nekoukar and A. Erfanian, "A Decentralized Modular Control Framework for Robust Control of FES-activated Walker-assisted Paraplegic Walking Using Terminal Sliding Mode and Fuzzy Logic Control," *IEEE Transactions on Biomedical Engineering*, vol. 59, no. 10, pp. 2818–2827, 2012.

[54] M. Ferrarin, F. Palazzo, and R. Riener: "Model-based Control of FES-induced Single Joint Movements," *IEEE Transactions on Neural systems and rehabilitation engineering*, vol. 9, no. 3, pp. 245–257, 2001.

[55] N. Kirsch, N. Alibeji, and N. Sharma: "Nonlinear Model Predictive Control of Functional Electrical Stimulation," *Journal of Control Engineering Practice*, vol. 58, pp. 319–331, 2017.

[56] C. A. Smith, and A. B. Corripio, *Principles and practice of automatic process control.* New York:

Wiley, 1985.

[57] W. Perruquetti, and J. P. Barbot, *Sliding Mode Control in Engineering.* New York: Marcel Dekker, 2002

[58] O. Camacho, R. Rojas, and W. Garcia-Gabin, "Some long time delay sliding mode control approaches." *ISA transactions* vol. 46, no. 1, pp. 95-101, 2007.

[59] O. Camacho, C. Smith, and W. Moreno: "Development of an internal model sliding mode controller."*Industrial Engineering Chemistry Research*, vol. 41, pp. 568-573, 2003.

[60] J. Dideriksen, K. Leerskov, M. Czyzewska, and R. Rasmussen: "Relation Between the Frequency of Short-Pulse Electrical Stimulation of Afferent Nerve Fibers and Evoked Muscle Force," *IEEE Transactions on Biomedical Engineering*, Vol. 64, No. 11, pp. 2737–2745, 2017.

[61] D. B. Popović and M. B. Popović, "Automatic Determination of the Optimal Shape of a Surface Electrode: Selective Stimulation." *Journal of Neuroscience Methods*, vol. 178, no. 1, pp. 174–181, 2009.

[62] C. E. Bouton, A. Shaikhouni, N. V. Annetta, M. A. Bockbrader, D. A. Friedenberg, D. M. Nieson, G. Sharma, P. B. Sederberg, B. C. Glenn, W. J. Mysiw, A. G. Morgan, M. Deogaonkar, and A. R. Rezai: "Restoring Cortical Control of Functional Movement in a Human with Quadriplegia." *Nature* vol. 533, pp. 247–250, 2016.

[63] N. M. Malešević, L. Z. P. Maneski, V. Ilic, N. Jorgovanović, G. Bijelić, T. Keller, and D. B. Popović: "A Multi-pad Electrode Based Functional Electrical Stimulation System for Restoration of Grasp." *Journal of Neuroengineering and Rehabilitation*, vol. 9, no. 66, 2012.

[64] T. Keller, M. Lawrence, A. Kuhn, and M. Morari: "New Multi-channel Transcutaneous Electrical Stimulation Technology for Rehabilitation," In *Proceedings of the 28th Annual International Conference of the IEEE Engineering in Medicine and Biology Society*, pp. 194–197, 2006.

[65] K. Gibo, T. Takahashi, and R. Futami: "Reconstruction of Finger Function by Functional Electrical Stimulation Based on Interference Potential Current.", In *Proceeding of the 253th SICE Tohoku Chapter Workshops*, 253-3, 2009.(in Japanese)

[66] E. M. Schearer, Y. W. Liao, E. J. Perreault, M. C. Tresch, W. D. Memberg, R. F. Kirsch, and K. M. Lynch: "Semiparametric Identification of Human Arm Dynamics for Flexible Control of a Functional Electrical Stimulation Neuroprosthesis." *IEEE Transactions on Neural Systems and Rehabilitation Engineering*, vol. 24, no. 12, pp. 1405–1415, 2016.

[67] J. Kameyama, Y. Handa, N. Hoshimiya, and M. Sakurai: "Restoration of Shoulder Movement in Quadriplegic and Hemiplegic Patients by Functional Electrical Stimulation Using Percutaneous

Multiple Electrodes." *The Tohoku Journal of Experimental Medicine*, vol. 187, no. 4, pp. 329–337, 1999.

[68] G. Yamaguchi, N. Yoshida, Y. Tomita, and S. Honda: "A Functional Electrical Stimulation System for Shoulder, Elbow and Hand Articulations in a Horizontal Movement.", *Journal of Japan Ergonomics Society*, vol. 33, no. 1, pp. 21–25, 1997.(in Japanese)

[69] K. Taniguchi, Y. Yu, T. Noma, H. Yamanaka, I. Fukuda, S. Matsumoto, M. Shimodozono, and K. Kawahira: "Training Condition Research on Selective DOF Constrainable Rehabilitation Unit with Shrinkable Electrical and Vibratory Stimulation Timing and Duration Control System for Hemiplegic Shoulder-flexion and Elbow-extension." In *Proceedings of the IEEE International Conference on Robotics and Biomimetics*, pp. 45–50, 2016.

[70] R. S. Razavian, B. Ghannadi, N. Mehrabi, M. Charlet, and J. McPhee, "Feedback Control of Functional Electrical Stimulation for 2-D Arm Reaching Movements," *IEEE Transactions on Neural Systems and Rehabilitation Engineering*, vol. 26, no. 10, pp. 2033–2043, 2018.

[71] W. Iida and K. Ohnishi: "Reproducibility and Operationality in Bilateral Teleoperation," In *Proceedings of the IEEE International Workshop on Advanced Motion Control, 2004*, pp. 217–222, 2004.

[72] K. Tanida, T. Okano, T. Murakami, and K. Ohnishi: "Control Structure Determination of Bilateral System based on Reproducibility and Operationality," *IEEJ Journal of Industry Applications*, vol. 8, no. 5, pp. 767–778, 2019.

[73] Z. Li, M. Hayashibe, C. Fattal, and D. Guiraud: "Muscle Fatigue Tracking with Evoked EMG Via Recurrent Neural Network: Toward Personalized Neuroprosthetics." *IEEE Computational Intelligence Magazine* vol. 9, no. 2, pp. 38–46, 2014.

[74] Z. Li, D. Guiraud, D. Andreu, M. Benoussaad, C. Fattal, and M. Hayashibe: "Real-time Estimation of FES-induced Joint Torque with Evoked EMG," *Journal of NeuroEngineering and Rehabilitation*, vol. 13, no, 60, 2016.

[75] K. Matsui, Y. Hishii, K. Maegaki, Y. Yamashita, M. Uemura, H. Hirai, and F. Miyazaki: "Equilibrium-point Control of Human Elbow-joint Movement Under Isometric Environment by Using Multichannel Functional Electrical Stimulation," *Frontiers in Neuroscience*, vol 8, no. 164, pp. 1–9, 2014.

[76] T. Murakami, Y. Fangming, and K. Ohnishi: "Torque sensorless control in multidegree-of-freedom manipulator," *IEEE Transactions on Industrial Electronics*, vol. 40, no. 2, pp. 259-265, 1993.

[77] T. Yamazaki, S. Sakaino, and T. Tsuji: "Estimation and Kinetic Modeling of Human Arm using

Wearable Robot Arm," *IEEJ Transactions on Industry Applications*, vol. 136, no. 4, pp. 254–262, 2016.

[78] M. Russell, and R. J. Merritt, *ASPEN nutrition support practice manual.* American Society for Parenteral and Enteral Nutrition, 2005.

[79] E. Nakano, H. Imamizu, R. Osu, Y. Uno, H. Gomi, T. Yoshikawa, and M. Kawato: "Quantitative Examinations of Internal Representations for Arm Trajectory Planning: Minimum Commanded Torque Change Model," *Journal of Neurophysiology Published*, vol. 81, no. 5, pp.2140-2155, 1999.

[80] J. M. Bland and D. G. Altman: "Multiple significance tests: the Bonferroni method," *BMJ*, vol. 310, pp. 170, 1995.

[81] O. Brend, C. Freeman, and M. French: "Multiple-Model Adaptive Control of Functional Electrical Stimulation," *IEEE Transactions on Control Systems Technology*, vol. 23, no. 5, pp. 1901–1913, 2015.

List of Achievements

Journals (First Author)

[1] **T. Kitamura**, S. Sakaino, and T. Tsuji: "Bilateral Control of Human Upper Limbs Using Functional Electrical Stimulation Based on a Dynamic Model Approximation" *IEEJ Journal of Industry Applications*, 2021. (Accepted Publication)

[2] **T. Kitamura**, N. Mizukami, H. Mizoguchi, S. Sakaino, T. Tsuji: "Bilateral Control in the Vertical Direction Using Functional Electrical Stimulation" *IEEJ Journal of Industry Applications*, Vol. 5, No. 5, pp. 398-404, 2016.

Journals (Co-author)

[1] S. Sakaino, **T. Kitamura**, N. Mizukami, and T. Tsuji. " "High-Precision Control for Functional Electrical Stimulation Utilizing a High-Resolution Encoder." *IEEJ Journal of Industry Applications*, 2021.

[2] Y. Hasegawa, **T. Kitamura**, S. Sakaino, T. Tsuji. "Bilateral Control of Elbow and Shoulder Joints Using Functional Electrical Stimulation Between Humans and Robots." *IEEE Access*, Vol. 8, pp. 15792-15799, 2020.

International Conferences (First Author)

[1] **T. Kitamura**, Y. Hasegawa, S. Sakaino, T. Tsuji: "Control Using High-carrier Frequency PWM in Functional Electrical Stimulation" *Proc. of the 45th Annual Conference of the IEEE Industrial Electronics Society*, 2019.

[2] **T. Kitamura**, Y. Hasegawa, S. Sakaino, T. Tsuji: "Estimation of Relationship between Stimulation Current and Exerted Force Considering Muscle Length" *Proc. of the IEEJ International Workshop on Sensing, Actuation, Motion Control, and Optimization*, SS3-1, 2019.

[3] **T. Kitamura**, Y. Hasegawa, S. Sakaino, T. Tsuji: "Estimation of Relationship between Stimulation Current and Force Exerted during Isometric Contraction" *Proc. of the 44th Annual Conference of the IEEE Industrial Electronics Society*, pp. 5080-5085, 2018.

[4] **T. Kitamura**, N. Mizukami, H. Mizoguchi, S. Sakaino, T. Tsuji: "Control with Adjusted Pulse Frequency and Amplitude in Functional Electrical Stimulation" *Proc. of the IEEE 40th Annual International Conference of the Engineering in Medicine and Biology Society*, pp. 2064-2067, 2018.

[5] **T. Kitamura**, N. Mizukami, H. Mizoguchi, S. Sakaino, T. Tsuji: "Chattering Reduction of Functional Electrical Stimulation with the Smith Compensator" *Proc. of the 43rd International Conference on Industrial Electronics, Control and Instrumentation*, pp. 7577-7582, 2017.

[6] **T. Kitamura**, N. Mizukami, S. Sakaino, T. Tsuji: "Bilateral Control of Two-Link Human Arms Using Antagonist Muscle Stimulation" *Proc. of the IEEJ international workshop on Sensing, Actuation, Motion Control, and Optimization*, SS1-3, 2017.

[7] **T. Kitamura**, N. Mizukami, S. Sakaino, T. Tsuji: "Bilateral Control Using Functional Electrical Stimulation with Reaction Torque Observer" *Proc. of the 2016 IEEE 14th International Workshop on Advanced Motion Control*, pp. 160-166, 2016.

[8] **T. Kitamura**, S. Sakaino, T. Tsuji: "Bilateral Control Using Functional Electrical Stimulation" *Proc. of 41th International Conference on Industrial Electronics, Control and Instrumentation*, pp. 2336-2341, 2015.

International Conferences (Co-author)

[1] Y. Hasegawa, **T. Kitamura**, S. Sakaino, T. Tsuji: "Bilateral Control of Two Finger Joints Using Functional Electrical Stimulation" *Proc. of the 44th Annual Conference of the IEEE Industrial Electronics Society*, pp. 5433-5438, 2018.

[2] N. Mizukami, **T. Kitamura**, S. Sakaino, T. Tsuji: "Fundamental Examination for Motor Point Identification of Functional Electrical Stimulation" *Proc. of the IEEJ International Workshop on Sensing, Actuation, Motion Control, and Optimization*, V3-8, 2018.

[3] H. Mizoguchi, **T. Kitamura**, S. Sakaino, T. Tsuji: "Bilateral Control Using Functional Electrical Stimulation Considering Muscle Length" *Proc. of the IEEJ International Workshop on Sensing, Actuation, Motion Control, and Optimization*, TT8-6, 2016.

[4] S. Sakaino, **T. Kitamura**, T. Tsuji: "A New Possibility of Bilateral Control -Functional Electrical Stimulation-" *Proc. of the IEEJ International Workshop on Sensing, Actuation, Motion Control, and Optimization*, ISI-3, 2016.

Domestic Conferences (First Author)

[1] **T. Kitamura**, H. Mizoguchi, S. Sakaino, T. Tsuji:"Control of Two Links Between the Shoulder and Elbow using Noninvasive Functional Electrical Stimulation, " *Proc. of the SICE Life Engineering Symposium*, 2018.(in Japanese)

[2] **T. Kitamura**, S. Sakaino, T. Tsuji: "Verification of the Relationship between Mobility when using Functional Electrical Stimulation and Individual Differences among Subjects", *Proc. of the Robotics and Mechatronics Conference*, 1A1-J16, 2018.(in Japanese)

[3] **T. Kitamura**, N. Mizukami, S. Sakaino, T. Tsuji, "Verification of Bilateral Control of Two-Link Human Arms Using Antagonist Muscle Stimulation," *Proc. of the IEEJ Society of Mechatronics Control and Motion Control*, MEC-16-038, 2016.(in Japanese)

[4] **T. Kitamura**, N. Mizukami, H. Mizoguchi, S. Sakaino, T. Tsuji: "Bilateral Control using FES with Higher Order Sliding Mode Control, " *Proc. of the Annual Conference of the Robotics Society of Japan*, 3F2-05, 2016.(in Japanese)

Domestic Conferences (Co-author)

[1] Y. Hasegawa, **T. Kitamura**, S. Sakaino, T. Tsuji:" Bilateral Control of Elbow and Shoulder Joints Using Functional Electrical Stimulation Between Human and Robot, " *Proc. of the IEEJ Section C Conference*, GS8-2, 2019.(in Japanese)

[2] Y. Nishiwaki, Y. Hasegawa, **T. Kitamura**, H. Mizoguchi, N. Mizukami, S. Sakaino, T. Tsuji:"Investigation of Correlation between Impedance and Muscle Contractility in Functional Electrical Stimulation, " *Proc. of the Robotics and Mechatronics Conference*, 2019.(in Japanese)

[3] Y. Hasegawa, **T. Kitamura**, H. Mizoguchi, N. Mizukami, S. Sakaino, T. Tsuji:"Closed-loop Control of Index Finger using Functional Electrical Stimulation, " *Proc. of the Robotics and Mechatronics Conference*, 1A1-J15, 2018.(in Japanese)

[4] H. Mizoguchi, **T. Kitamura**, S. Sakaino ,T. Tsuji: "Study of shoulder control using noninvasive functional electrical stimulation, " *Proc. of the IEEJ Society of Mechatronics Control and Motion Control*, MEC-17-005, 2017.(in Japanese)

[5] T. Adachi, **T. Kitamura**, N. Mizukami, H. Mizoguchi, S. Sakaino, T. Tsuji: "Nonlinear Modeling of Muscles in Functional Electrical Stimulation Using Machine Learning, " *Proc. of the Robotics and Mechatronics Conference*, 2A2-J02, 2017.(in Japanese)

[6] N. Mizukami, **T. Kitamura**, H. Mizoguchi, S. Sakaino, T. Tsuji: "Comparison of Bilateral Control Systems Using Functional Electrical Stimulation, " *Proc. of the Annual Conference of the SICE SI*, 2A2-2, 2016.(in Japanese)

[7] N. Mizukami, **T. Kitamura**, S. Sakaino, T. Tsuji: "Bilateral Control between Human and Robot Using Functional Electrical Stimulation, " *Proc. of the Robotics and Mechatronics Conference*, 1P1-19a1, 2016.(in Japanese)

Awards

[1] **T. Kitamura**, 『IES Student Paper and Travel Assistance (IES-SPTA) Award』, The Technical Organizing Committee of the IEEE IECON 2017, 2017

[2] **T. Kitamura**, 『Student Recognition』, Saitama University, 2016.

[3] **T. Kitamura**, 『Best Presentation Recognition』, The Technical Organizing Committee of the IEEE IECON 2015, 2015.